Università degli Studi di Catania

Dottorato di Ricerca in Scienza dei Materiali
XXVI Ciclo

Gabriella Zappalà

Assembly and characterization of molecular films for energetics and electronics.

Tutor: Prof. A. Licciardello
Coordinatore: Prof.ssa M. G. Grimaldi

Tesi di Dottorato di Ricerca

Dicembre 2013

Ai miei genitori

"Learn from yesterday, live for today, hope for tomorrow.
The important thing is to not stop questioning"

Albert Einstein, ***Relativity: The Special and the General Theory***

Riassunto

Nell'ambito della ricerca scientifica, un crescente interesse viene rivolto all'ottenimento di dispositivi molecolari in grado di sostituire quelli macroscopici attualmente impiegati. Affinché ciò sia possibile è necessario uno studio approfondito dei fenomeni alla base dei processi di funzionamento dei diversi componenti e delle metodologie che possano permetterne l'assemblaggio. In questo contento si inserisce il presente lavoro di tesi di dottorato, il cui scopo è stato l'assemblaggio e la caratterizzazione di sistemi molecolari applicabili nell'ambito dell'elettronica e dell'energetica.

I sistemi studiati sono stati preparati seguendo un approccio *bottom-up*, ed in particolare è stato sfruttato il processo di *self-assembling*, che si basa sul chemisorbimento di molecole aventi funzionalità specifiche per la superficie considerata. Nel caso di superfici di oro sono state utilizzate molecole caratterizzate da un gruppo tiolico, mentre nel caso di superfici di ossidi si è scelto di applicare una metodologia sviluppata all'interno del nostro gruppo di ricerca, la metodologia dello zirconio fosfato-fosfonato (ZP) che sfrutta l'interazione di un gruppo fosfonico con gli ioni zirconio (precedentemente legati alla superficie), per cui sono state scelte molecole che aventi un gruppo fosfonico come gruppo attivo nei confronti della superficie.

La prima parte del lavoro è stata dedicata alla preparazione e caratterizzazione di fili molecolari a base di complessi politerpiridinici del ferro ancorati su substrati di oro. Essi sono stati ottenuti sfruttando un processo iterativo che coinvolge una serie di reazioni di complessazione tra un metallo (nel caso specifico Fe^{II}) e un legante contenente una doppia funzionalità terpiridinica. È stata condotta una caratterizzazione sia chimica, mediante spettroscopia di fotoelettroni (XPS) e spettrometria di massa di ioni secondari con analizzatore a tempo di volo (ToF-SIMS), sia strutturale tramite spettroscopia *near edge X-ray absorption fine structure* (NEXAFS). L'attenzione è stata poi in particolare rivolta allo studio delle proprietà di conduzione molecolare di tali sistemi mediante microscopia a forza atomica con punta conduttiva (*conductive atomic force microscopy*, C-AFM).

La seconda parte del lavoro è stata focalizzata sullo sviluppo di metodologie utili per la funzionalizzazione di substrati di ossidi utilizzabili nell'ambito dell'energetica molecolare. Come detto, la funzionalizzazione di tali substrati è stata ottenuta applicando la metodologia "ZP". Sono stati condotti studi riguardanti il ricoprimento e la stabilità dei monostrati ancorati, sfruttando un derivato fosfonato della rodamina B. Quindi tale metodologia è stata estesa a substrati di TiO_2 (nella forma di anatasio), in quanto esso è attualmente il substrato maggiormente utilizzato nella costruzione di celle fotoelettrochimiche. Sono state preparate diverse tipologie di film su tali superfici, e –tra l'altro - è stata verificata la possibilità di formare un bistrato auto assemblato formato da un complesso dendrimerico del Ru(II), che funge da sensibilizzatore, e da un poliossometallato capace di fungere da catalizzatore per lo *splitting* foto indotto dell'acqua. I diversi campioni sono stati caratterizzati tramite indagine ToF-SIMS e UV-visibile.
Infine è stato affrontato il problema generale dell'ottenimento di profili di profondità molecolari di sistemi polimerici. Al fine di studiare l'applicabilità del metodo su sistemi multistrato a base polimerica, sono stati preparati multistrati polielettrolitici mediante deposizione *layer- by-layer*. Tali campioni sono stati caratterizzati tramite *cluster-SIMS* dinamico in modalità *dual beam* e sono stati studiati gli effetti della natura e dello spessore degli strati polimerici sull'ottenimento di profili di profondità molecolari. I profili di profondità di questi sistemi ottenuti hanno evidenziato che la possibilità di ottenere un buon profilo dipende dall'ordine in cui sono depositati gli strati contenenti polimeri aventi un comportamento radiochimico diverso. In particolare , si è scoperto che la presenza di uno strato che tende ad accumulare "danno da radiazione" ha un effetto negativo anche sulla profilabilità degli strati sottostanti. Tale problema può essere superato introducendo un *radical scavenger* (ossido nitrico) nella camera di analisi durante l'acquisizione dei profili di profondità. Nell'ambito di tale ricerca il *cluster*-SIMS è stato applicato allo studio di sistemi di interesse nel campo dell'elettronica molecolare. In particolare, è stato possibile evidenziare, dai profili di profondità ottenuti, fenomeni di separazione di fase lungo la profondità in in sistemi costituiti da miscele binarie di oligotiofeni.

Table of contents

Introduction

The problematics related with the current trends in miniaturization of techonological devices and the consequent search for suitable materials and methods have, since some years, an important impact in materials science. The transition from “micro” to “nano” materials offers several advantages. One of them is the increase of surface area, with the consequence that typical bulk properties become governed by surface properties. Products of micro- and nano-technology provide several advantages over conventional macroscopic structures, including lower power consumption, higher efficiency, and many others interesting features that are depending on the properties of materials at the micro- and nanometer scale. Nanotechnology is the engineering of functional systems at the molecular scale in order to develop precise machine and components with sizes comparable with the molecular ones (0.1-100nm). Research in nanotechnology and in nanoscience has given very promising results also in terms of industrial and commercial applications in many areas, including – among others - energy production, storage and conversion, production of new materials, health-related applications and information technology. A branch of nanoscience and nanotechnology is dedicated to the obtaining of molecular devices, which can be defined as chemical systems structurally organized and functionally integrated, consisting of the union of different molecular components having different properties.

In order to obtain nanodevices the classical top down approach (typical, for example, of many microelectronics-related technologies), needs to be replaced, or at least integrated, with a bottom up approach in order to fabricate nanostructures with well controlled properties, such as molecular machines for specific applications.

The way for the bottom-up approach is based on chemistry, either “conventional” or supramolecular. In particular it is possible to form self assembled structures thanks to “the spontaneous association of molecules

under equilibrium conditions into stable, structurally well-defined aggregates joined by non-covalent bonds”[1].

In this respect, part of research is focused on the development of new molecular building blocks that can improve the efficiency and the stability of the built nanomachine and on to the development of the suitable assembling methods. In this context supramolecular chemistry plays an important role because it allows to form supramolecular entities, “supramolecules”, which possess new properties, thanks to the combination of molecular chemistry with non-covalent interactions. The properties of the supramolecular entities are not necessarily the sum of the properties of the individual assembled molecules. In fact, the widely accepted definition of supramolecular chemistry was given by Jean -Marie Lehn: "Supramolecular chemistry is the chemistry of the intermolecular bond, covering the structures and functions of the entities formed by the association of two or more chemical species."[2]

As mentioned above, realization of nanostructured devices using the bottom-up approach is required in nanotechnology, and supramolecular chemistry allows building of functional materials starting from molecular components that self-assemble via chemical bonds, using the principles of molecular recognition.

Moreover the fabrication of devices through the bottom-up approach generally needs to integrate the supramolecular system in a solid device, which doesn’t act as a simple support, but generally plays an active role in the device (for example as electrode in an electronic device). In this context the role of the surface becomes important in order to obtain a good control of the system properties, so that it is necessary not only to develop methods for the preparation and modification of molecular and supramolecular surfaces, but also to develop suitable characterization techniques allowing a fine monitoring of surface properties, including chemical composition, morphology and structure.

Many methods have been employed for surface engineering, and in particular some of them are based on the modification of existing layer, while others rely on addition of new layers onto the surface by formation of molecular thin films. According to the kind of system to be prepared, it is possible to use

different techniques, including, among others, spin coating, [3] Langmuir-Blogdett deposition,[4] self assembly. [5]

For the to the characterization of thin films and surfaces, several techniques are available. Among them, scanning probe techniques, and in particular Atomic Force Microscopy, are very useful since they allow a precise study of the morphology of the surface, in a nanoscale dimension, as the lateral resolution is typically of the order of 20 nm (and in some special cases it can be pushed down to atomic resolution) while the vertical resolution can be of the order of 0.1 nm. Nevertheless, AFM doesn't give significant amount of chemical information, although some information in this direction can be sometimes obtained. For this reason, morphological studies have to be coupled with other techniques able to provide extensive chemical information. Among them, time-of-flight secondary ions mass spectrometry (ToF-SIMS) allows chemical characterization of the surface with very high sensitivity and good lateral resolution, allowing not only the detection and three dimensional mapping of all the elements, including hydrogen, but also providing a large amount of molecular information on the species present at the surface and, with some limitations, along the depth of molecular films.

The present thesis work is focused on the preparation and characterization of functional thin films for energetics and molecular electronics. In this framework, some preparation methods have been developed, and the systems of interest have been studied by using different techniques such as time-of-flight secondary ion mass spectrometry (ToF-SIMS), conductive atomic force microscopy (C-AFM) and UV-visible spectroscopy. The thesis is divided in three main sections.

Chapter 1 deals with self-assembled supramolecular wires of interest for molecular electronics. They have been prepared and characterized both from the compositional/structural point of view and from the point of view of their electrical properties. For the latter purpose, conductive-AFM measurements were carried out in order to understand the electrical characteristics at the nanometre scale and the underlying electron transport mechanisms.

The second chapter deals with a method for functionalizing oxide surfaces, and in particular TiO_2 surfaces, suitable for building-up dye sensitized electrodes

exploitable in solar energy conversion applications. In particular, a stable way of dye anchoring has been demonstrated for such surfaces, and it has been applied to the preparation of surface-anchored monolayers of different kind of molecular and supramolecular dyes. Also, the method has been employed for the formation of a molecular bilayer that could be applied in photoinduced water splitting devices.

Chapter 3 is dedicated to the problem of in-depth characterization of molecular layers, which is an open topic of large interest in many technological fields, including molecular electronics and organic-based energy conversion devices. In particular, a SIMS method (NO-assisted cluster-SIMS) has been studied, that gives promising results in this direction. With the aim of studying the applicability of the method to polymer-based multilayers, well-controlled layered systems have been prepared by means of layer-by-layer polyelectrolyte deposition. Moreover, the cluster SIMS technique was used in the study of in-depth phase separation oligothiophene based blends.

Finally, in order to make more fluid the presentation and discussion or the results, many experimental details were described in a dedicated Appendix section.

References

[1] Whitesides, G.M., Mathias J.P., Seto C.T., Science. **1991,** *254,* 1312-1319.

[2] Jean- Marie Lehn , *Supramolecular chemistry- scope and perspectives molecules-supermolecules- molecular devices*. Nobel lecture, December 8, **1987**

[3] D. W. Schubert, *Polym. Bull*., **1997**, *38*, 177-184

[4] I.R. Peterson, *J. Phys. D* , **1990,** *23*, 379–95

[5] Ralph G.; Whitesides, George M. *Chem. Rev.* **2005** *105,* 1103–1170

1 Nanoscale electrical investigation molecular wires

1.1 Molecular electronics

According to Moore's law the number of transistors per square centimetre of silicon doubles every 18 months.[1] Miniaturization of silicon-based structures has several limits that make this law impractical. In particular the limitation is due to the top-down approach used to miniaturize the electronic components, that is the use of techniques such as electron beam lithography and micro-contact printing, in which the lateral dimension that can be obtained is in the order of hundred nanometres. By contrast, a top-down approach can be used, starting from molecular building blocks to form self-assembled structures with a nanometric dimension.

It is clear since several years that molecular electronics can be a valid alternative to the silicon technology, and to reach this goal not only is necessary to use molecules with exceptional electronic properties, but also to integrate them into an appropriate electronic circuit with an efficient method.

Already in 1959 the eminent physicist Richard Feynman opened the discussion of obtaining extremely small devices in his lecture entitled "There's plenty of room at the bottom".[2] Scientific knowledge was not adequate at the time, but thanks to the progresses achieved in the '90s, it is now a fact that a large community of scientists is working on the use of single molecules as electronic components.

In a single-molecule electronic device electrodes must be connected by a system indicated as a "conductive molecular wire", that is a molecular system able to transfer a signal transferring excitation energy, or moving holes or electrons. The use of organic molecular wire offers many advantages; the first is the high level of control of the structural and electronic properties that can be easily obtained. Moreover, several conjugated molecules can be built so that they can self-assemble into supra-molecular structures suitable for charge transport [3] and thereby they can possibly be exploited to assemble molecular wires into electronic circuits. In this context supramolecular interactions play

an important rule and it has already been shown that they can be used to control the optical and charge transport properties of conjugated molecular wires. [4-6]
One of the first study in single-molecule conduction was made by Gimzewski and Joachim who measured the electrical conductance of a single fullerene C_{60} molecule. [7] Other pioneer experiments were carried out by Reed et al.,[8] who measure the electrical resistance of a single benzenedithiol molecule, and by Metzger et al.,[9] who demonstrated the single-molecule rectification. Since these early studies, a high level of knowledge has been achieved in molecular electronics, both in the practical problem of building single molecules device and characterizing them and in the fundamental understanding of the electrical mechanisms involved.

1.1.1 Molecular junction

In the context of the emergence of molecular electronics, the study of charge transport through molecular wires has become an important research topic.
In order to obtain information about molecular conduction it is necessary to construct a molecular junction, i.e. a system in which two metal electrodes are connected with molecules. In a so built device, the conductivity is simply determined by measuring the current-voltage (I-V) characteristics.

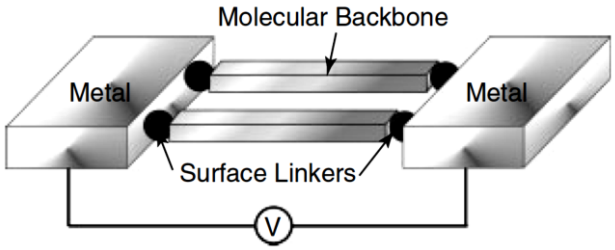

Figure 1. Schematic rapresentation of a metal-molecule-metal junction.[10]

Molecular junctions can be formed using several methods, [11-15] that allow to form them in a reproducible way, and to enable studies of conduction properties as a function of molecular length [16-18] applied voltage,[19] temperature,[20-21] ecc…
The most difficult step in the construction of a molecular junction is the application of the second electrode, and several methods have been developed, including the evaporation of a metallic counter-electrode onto the organic film, mechanical break junction,[22-23] mercury drop measurements,[24-25] scanning probe microscopy (SPM), including conducive atomic force microscopy (C-AFM). [26-30]

1.1.2 Self assembling

The most common strategy to form a molecular film on a substrate is the self-assembling technique, which is the spontaneous formation of complex structures from molecular building blocks. Self-assembled monolayers, SAMs, are molecular aggregates that form when surfactant molecules spontaneously adsorb on surfaces. Molecules suitable to form SAMs should have a chemical functionality, the “head group”, able to react chemically with the substrate and a second one, the “tail group”, which is conveniently chosen in order to give a new functionality to the surface. The “backbone” of the molecule (or “spacer”), connects tail and head groups and generally provides stability to the self-assembled film thanks to the interactions with the backbones of the other molecules. (Figure 2).

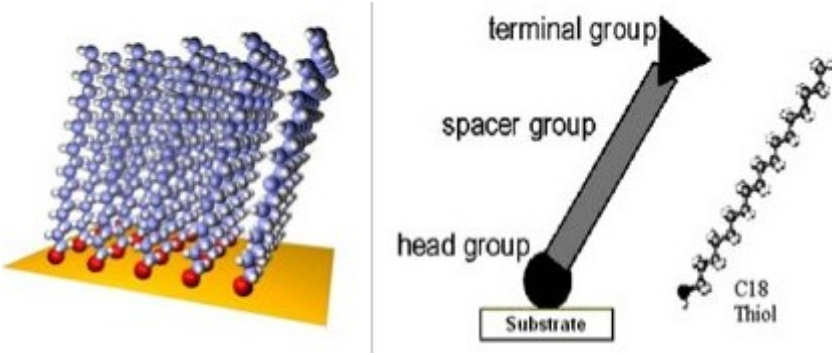

Figure 2. Schematic diagram of an SAM on a substrate.

SAMs are generally easy to prepare, they do not require specialized equipment in their preparation and they can form nanometre-scale objects (for example, thin films, nanowires, nanodomains, and other nanostructures). Moreover, by modifying the "tail group" of the surfactant, surface properties can be easily tuned. For these reasons SAMs can be considered as ideal model systems in many fields. [31-33]

Alkanethiols on metals are the most extensively studied class of SAMs.[34-41] The high affinity of thiols for the surfaces of noble and coinage metals makes possible to generate well-defined organic surfaces (Figure 3) with useful chemical functionalities at the exposed interface.[42]

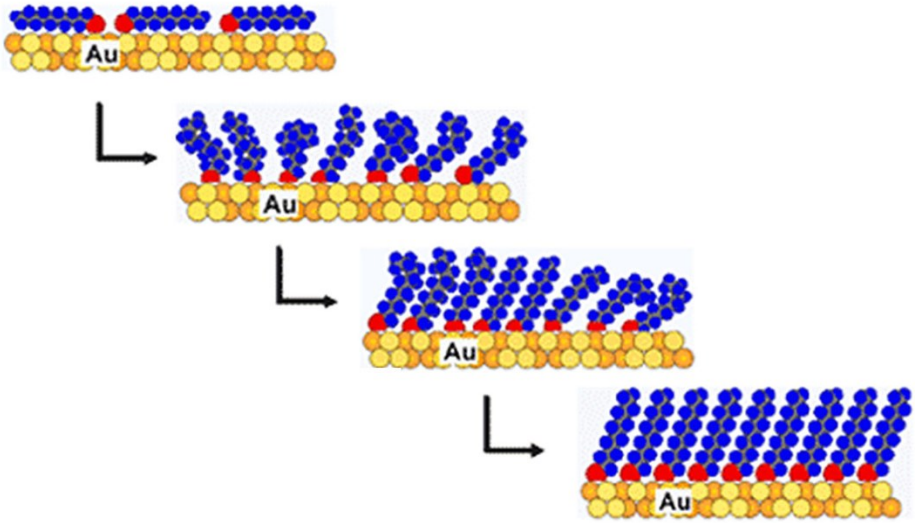

Figure 3. Formation of well-defined SAM film on gold surface. [35]

The most common protocol for preparing SAMs on gold and other materials is by immersion of a freshly prepared or clean substrate into a diluted (millimolar) solution of thiols in ethanol for ~12-18 h at room temperature. This procedure resulted from a combination of studies planned to optimize the reproducibility of the SAMs.[43] It is possible to obtain dense coverage of adsorbates quickly (milliseconds to minutes) from millimolar solutions, but, in order to maximize the density of molecules and minimize the defects in the SAM, a slow reorganization process is required (hours). A very wide number of experimental factors can affect the structure of the resulting SAM and the rate of its formation, such as solvent, temperature, adsorbate concentration, immersion time, purity of the adsorbate, concentration of oxygen in solution, cleanliness of the substrate, and structure of the adsorbate itself.[44]

Thiol monolayers comprising a well-defined mixture of molecular structures are called “mixed” SAMs. There are different methods for synthesizing mixed SAMs, the most common being coadsorption from solutions containing mixtures of thiols and adsorption of asymmetric disulphides or asymmetric dialkylsulfides. Mixed SAMs provide a useful methodology for incorporating

into a SAM a molecular species that for some reason (steric hindrance, presence of charges) cannot form directly a well-organized assembly.

1.1.3 Charge transport mechanism

The charge transport mechanism of a molecular wire can be understood looking at the dependence between its electrical resistance and its length. It is well known that, if the wire is short enough, electrons can tunnel between the two electrodes; while in the case of longer wires electrons are transported thanks to a hopping mechanism.
If a tunnelling mechanism occurs, electrons traverse a potential barrier and propagate on the other side without changing their phase. The tunneling mechanism is often ‘‘non-resonant’’ in that the tunnelling electron energies are not precisely matched with the molecular orbital energies; however, the frontier molecular orbitals still assist the tunnelling process (i.e., they lower the junction resistance) by lowering the effective tunnelling barrier [45].

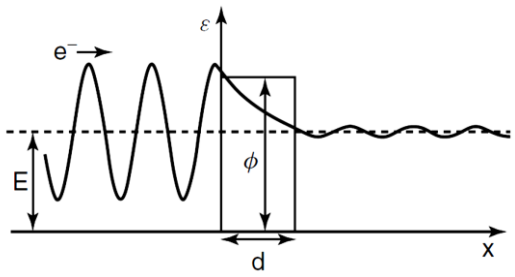

Figure 4. Transmission of electron wavefunction thtough a potential barrier. [10]

For this kind of mechanism, resistance R is connected to the wire length L by the equation:

$$R=R_0 \exp(\beta L)$$

where R_0 is the effective contact resistance and β is a structure dependent attenuation factor. According to this equation, it is possible to find the value of

R_0 and β from a semi log plot of R versus molecular length. Efficient tunnelling is characterized by low values of β, in the range of 2.0-5.0 nm^{-1} in the case of delocalized π electrons and between 7.0 and 10.0 nm^{-1} in the case of a saturated chain. R_0 is depending by the type of metal and the kind of connection between surface and molecules.
In conjugated molecular wires longer then few nanometres tunnelling mechanism cannot occur; the charge conduction occurs through a serie of discrete steps, involving a initial charge injection in the molecular orbitals of wire, the field-induced drift of the charge carrier down the length of the molecule, and finally the extraction of the charge into the receiving contact.

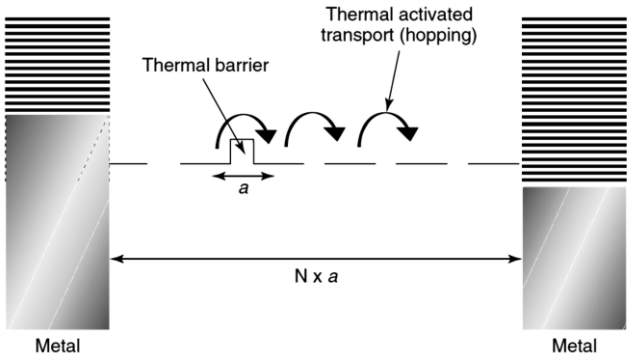

Figure 5. Schematic energy diagram for incoherent hopping through N sites [10]

The hopping mechanism is thermally activated and can be described using an equation that follows a classical Arrhenius behaviour:

$$R=R_0 \exp(E_a/kT)$$

In which E_a is an activation energy and k is the Boltzmann constant. In tunnelling regime, as said before, there is an exponential dependence between R and molecular length; in case of hopping mechanism on the contrary there is a linear correlation in the low bias regime, and this different behaviour allows a charge transport over longer distances.

From the above it is clear that electron conduction mechanism depends on several factors including electronic structure, molecular length, temperature, applied bias. For these reasons, a deep understanding of the electrical behaviour of a molecular junction involves both experimental and theoretical studies.
There are several examples reported in recent years. Selzer et al [46-47] studied the thermal dependence of the electrical behaviour in nitro-substituted oligo-phenylene-ethylene (OPE), and they show that there is a transition from a temperature-independent behaviour at low temperature to a temperature-dependent behaviour at high temperature, that is a transition from a tunnelling mechanism to a hopping one.
More recently, Frisbie et al. [20] published a study on oligophenyleneimine (OPI) in which the electrical behaviour of molecular wires with different length was studied by using conductive AFM. They show that for short wires there is a tunnelling transport mechanism, and that there is a transition to a hopping mechanism for wires longer than 4 nm, as supported by the dependence of electrical characteristics as function of length, temperature, and electric field.

1.1.4 Conductive-AFM

Conductive probe atomic force microscopy is a variant of the "classical" atomic force microscopy, in which a tip with a conductive coating is used as second electrode. This tip is brought into contact with surface with a known applied force. In order to measure I-V characteristics a voltage between the sample and the tip is applied and the resulting current is measured. The resistance is calculated from the inverse of the slope of the I-V obtained curve at small voltages, where the correlation is generally linear.

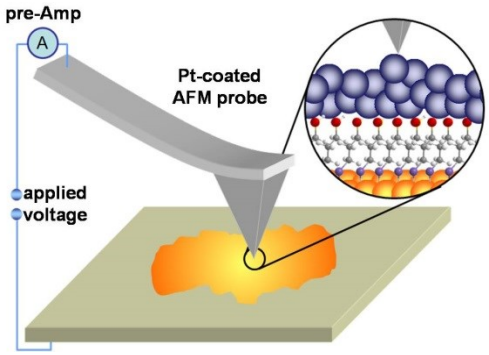

Figure 6. Schematic rapresentation of a set up for conductive AFM.

Two configuration can be used, the horizontal one and the vertical one. The first one allows measuring the current between the AFM tip and a metallic contact on insulating substrate. The second one is used with conductive substrates and it is well suited for studying the electrical properties of ultrathin films, such as self-assembled monolayers. (Figure 7)

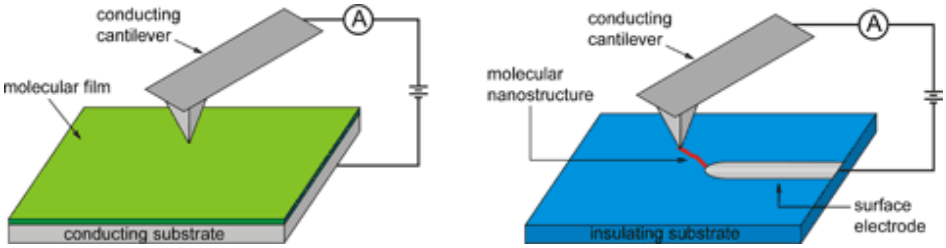

Figure 7. Schematic representation of the arrangement used for C-AFM measurements in vertical configuration (left) and in horizontal configuration (right). [26]

C-AFM is useful also for imaging: by applying a constant voltage between the tip and the substrate and by scanning the surface, it is possible to record the current as a function of the position of the tip, so obtaining a map of the local sample conductivity.

1.1.5 Supramolecular wires.

Supramolecular chemistry can be very useful in obtaining a wide range of system with different properties. In this particular context, polymetallic (supramolecular) complexes can be used as models for the study of electron transport mechanism in a molecular junction. Generally, supramolacular polymers can be obtained from the complexation of metal ions and ditopic ligands. Although the toxicity of some metals can be seen as a drawback, this strategy for obtaining molecular wires has several advantages, such as the high specificity and directionality (provided that suitable ligands are choosen).

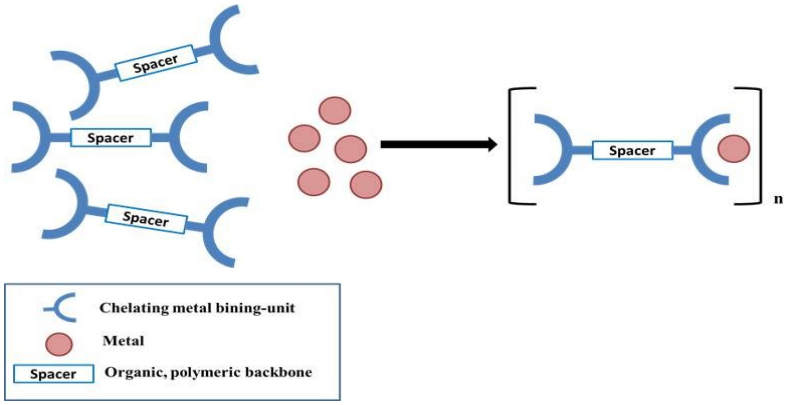

Figure 8. Schematic representation of the metallo-supramolecular polymerization process.

With the aim of building functional complexes, that show luminescence, and/or have interesting electrochemical properties, or display photoinduced energy- and electron-transfer processes, the choice of suitable bridging ligands is crucial. In fact, according to their coordinating sites, they contribute to determine the spectroscopic and redox properties of the active metal-based units; moreover, their chemical nature controls the electronic communication between the metal-based units. As a consequence the choice of appropriate building blocks makes possible to tailor the supramolecular polymer properties by combining the characteristic features of a metal ligand complex (such as

electrochemical, optical, magnetic properties) to the ones of polymers (processability, mechanical properties, solubility, etc..).
Among many ligands, terpyridine derivatives are widely used as building blocks in supramolecular and macromolecular chemistry. In particular 2,2':6',2''-terpyridines derivatives (tpy) are tridentate ligands which can complex a variety of transition metal ions with a high binding constant, forming structures with very interesting optical, magnetic and electrochemical properties. [48]

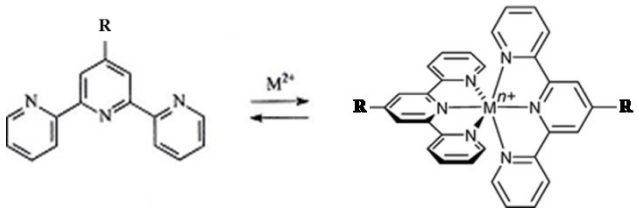

Figure 9. Example of terpyridine-based metal complex.

To understand the photophysical properties of these compounds many studies have been made by looking at the photo-induced electron transfer reactivity, [49-51] in order to extend their use in optoelectronic devices, e.g. as dye sensitizers [52] Their application in electronics has been hampered by a relative lack of knowledge on their charge transport behavior in the solid state. For this reason several electrochemical studies were made in order to explore the redox conduction properties of polymers bearing terpyridine complexes in the side chains. [53-54] Since the structural versatility of the coordination compounds allows for the fabrication of well-defined architectures, such as quasi-1D structures, they are also being considered as possible building blocks for the fabrication of conductive molecular wires.[55-56] Stepwise coordination reactions involving terpyridine functions have been successfully exploited to connect the molecular wires to solid surfaces as gold, [57-58] silicon,[59] and oxides,[60-61] and to lengthen the wires up to tens of nanometers. [62-65]

1.2 Results and discussion

In order to prepare ordered molecular wires using a bottom-up approach, it is first necessary to form a stable platform on the substrate. It is well known that using a system made by a mixture of a terpyridine derivative (4-[2,2':6',2''-terpyridin]-4'-yl-benzenethiol, MPTP) and benzenthiol (MB), it is possible to obtain a well ordered monolayer on gold. In such a film, in which the MPTP acts as the functional component and the MB as a lateral spacer, the two components are perfectly interconnected, due to the strong lateral interaction between the MB and the head group side of the MPTP. [66-67]
Starting from this kind of platform, molecular wires can be constructed exploiting the affinity of terpyridine with transition metals and using a bifunctional terpyridine ligand, such as the 4',4''''-(1,4-phenylene)bis(2,2':6',2'-terpyridine) (TPT).
To prepare the self-assembled platform, Au(111) substrates were incubated in a mixed solution of MB and MPTP in a 1:1 ratio. After rinsing, the stepwise construction of the molecular layers was carried out by dipping Au-MB/MPTP sample in (i) a solution of Fe(II) salt and then in (ii) a solution of TPT ligand. Steps (i) and (ii) were repeated iteratively in order to grow multilayers, and each iteration represents a coordination step, adding one Fe-TPT unit to the molecular nanowire.[62]

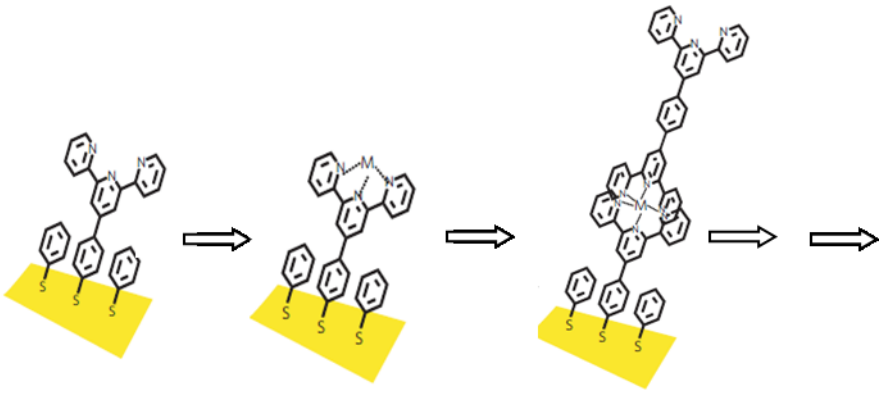

Figure 10. Schematic representation of the iterative growth of the nFeTPT multilayers

In the following samples will be indicated as nFeTPT, where n is the nominal number of complex layers, i.e. the number of preparative coordination steps.

1.2.1 ToF SIMS characterization

Time-of-Flight Secondary ion Mass Spectrometry (ToF SIMS) measurements were carried out in order to verify the success of each step of reaction. Indeed the technique gives information on the uppermost surface layers, with high sensitivity, high mass resolution and, in *static* mode, with very low surface damage. This makes ToF-SIMS well suited for providing molecular information from surfaces, even those – such as molecular ones – that are very sensitive to the damage induced by the ion beam acting as a probe in SIMS .

Figure 11 shows a typical spectrum obtained for samples after the formation of the first layer MPTP-Fe-TPT. It is possible to observe some characteristic fragments, including the quasi-molecular ion at 936 Da ($C_{57}H_{38}N_9SFe^+$), the MPTP and TPT protonated ions ($C_{21}H_{14}N_3S$ at 341 Da and $C_{36}H_{24}N_6$ at 541 Da, respectively), the MPTP-Fe ion (396 Da) and the TPT-Fe ion (596 Da). This is an evidence that using this approach it is possible to form bisterpyridine-Fe complex, and consequently to grow multilayers.

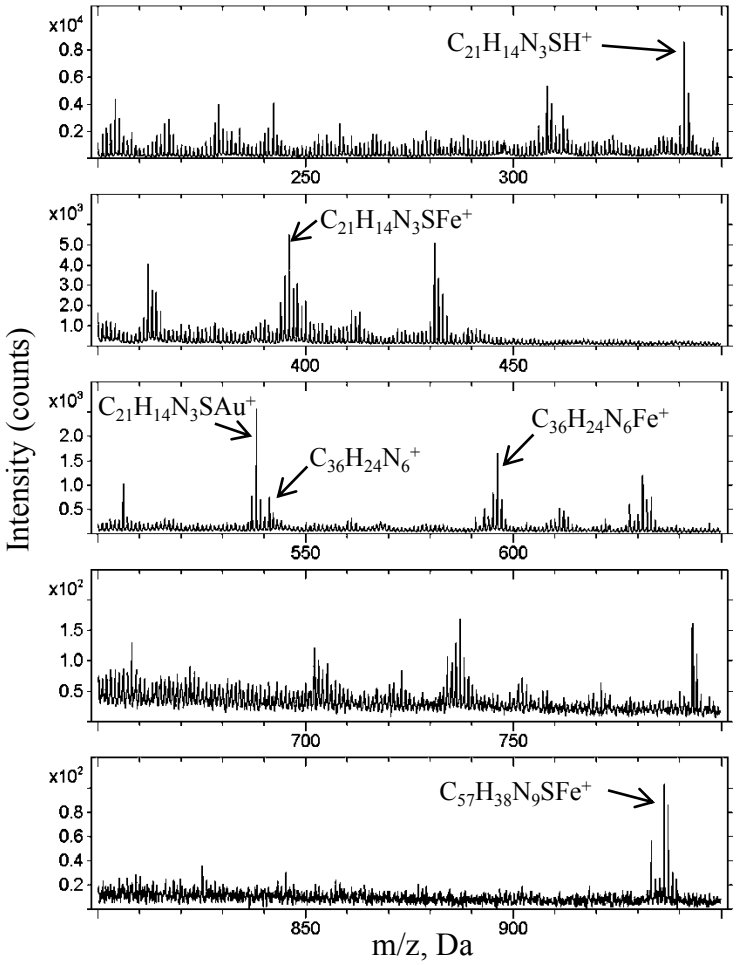

Figure 11. Typical ToF-SIMS spectrum of a 1-monolayer FePTP sample on MPTP.

1.2.2 UV-Vis characterization

Tof-SIMS measurements provide a qualitative information about the formation of the complex at the surface, but in order to verify the multilayer growth and to have a quantitative estimation of it, it is necessary to use other techniques. For that purpose multilayers were grown on semitransparent gold substrates (evaporated on quartz) in order to monitor changes in surface plasmon band of gold using UV-Visible measurements, since this is strongly sensitive to the thickness of adsorbed molecular layers.[68-69]

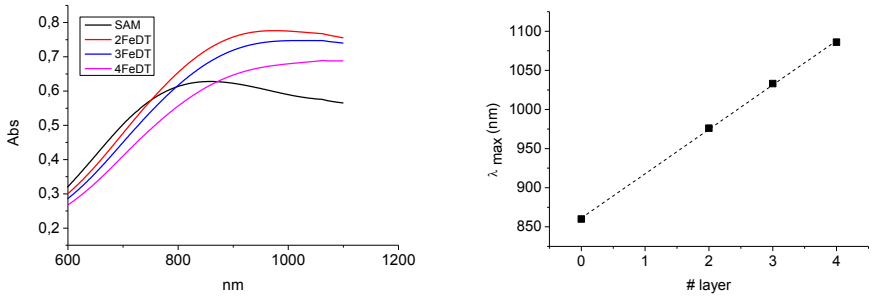

Figure 12. a) gold plasmon band of nFeTPT layers; b) gold plasmon band maximum as a function of number of layers.

Figure 12 shows clearly that the maximum of the band related to the plasmon moves linearly toward higher wavelengths with the increasing of the number of layers, as expected from literature, and this is an evidence of the success of the multilayers growth.

1.2.3 XPS analysis

In order to increase the chemical information about the surface and to get additional information on the multilayer growth, X-Ray photoelectron spectroscopy (XPS) measurements with synchrotron radiation were carried out for MB-MPTP monolayer and for each nFeTPT layer. Such measurements

were done by in collaboration with Prof. Michael Zharnikov's group (Angewandte Physikalische Chemie, Universität Heidelberg).
Figure 13a shows the Au $4f_{7/2}$ XP spectra acquired at a photon energy of 580 eV; it is possible to observe that the intensity of the substrate signal decreases upon the successive addition of the TPT units due to the increasing attenuation of the photoelectron signal by the growing overlayer. This trend confirms the linear growth of iron-based multilayers.
Looking at the C 1s XP spectra, Figure 13b, (acquired at a photon energy of 350 eV) and at N 1s XP spectra, Figure 14a, (acquired at a photon energy of 580 eV), it is also possible to observe that nFeTPT films exhibit only one emission at a BE of 285.0-285.1 eV related to the carbon atoms in the TPT units, and only one emission at a BE of ~399.7 eV related to the nitrogen atoms in the terpyridine moieties. [70-71] In both cases the signal is saturated because of the strong self-attenuation; therefore there are no intensity differences between the spectra. The spectrum of the MB/MPTP template differs a little bit from the other spectra because of the contribution of the MB molecules and effect of the substrate.

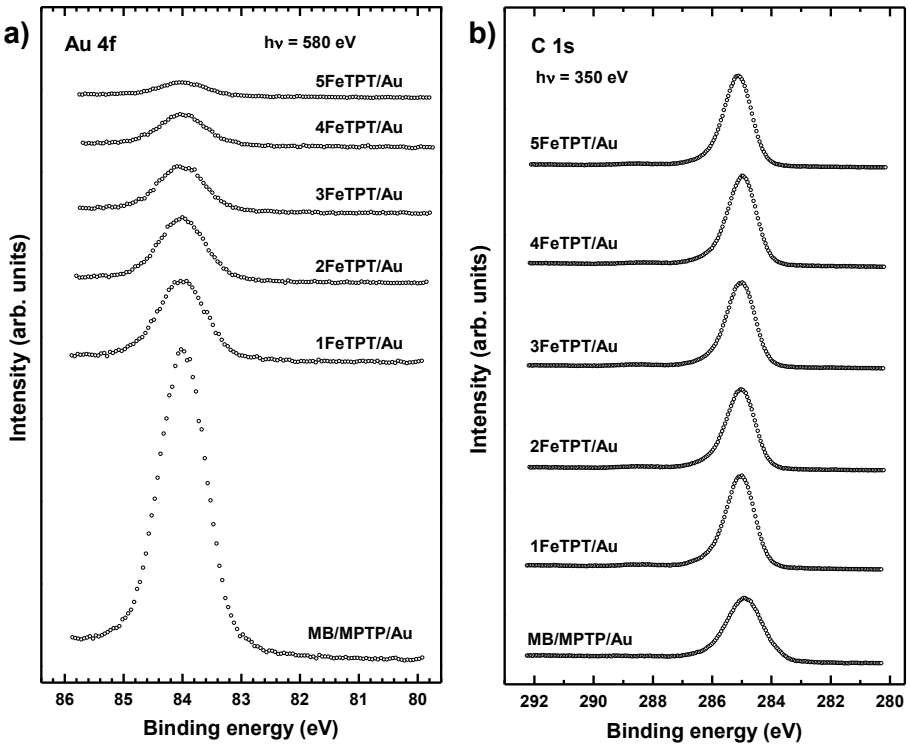

Figure 13. a) Au 4f7/2 XP spectra of the MB/MPTP and nFeTPT films acquired at a photon energy of 580 eV; b) C 1s XP spectra of the MB/MPTP and *n*FeTPT films were acquired at a photon energy of 350 eV

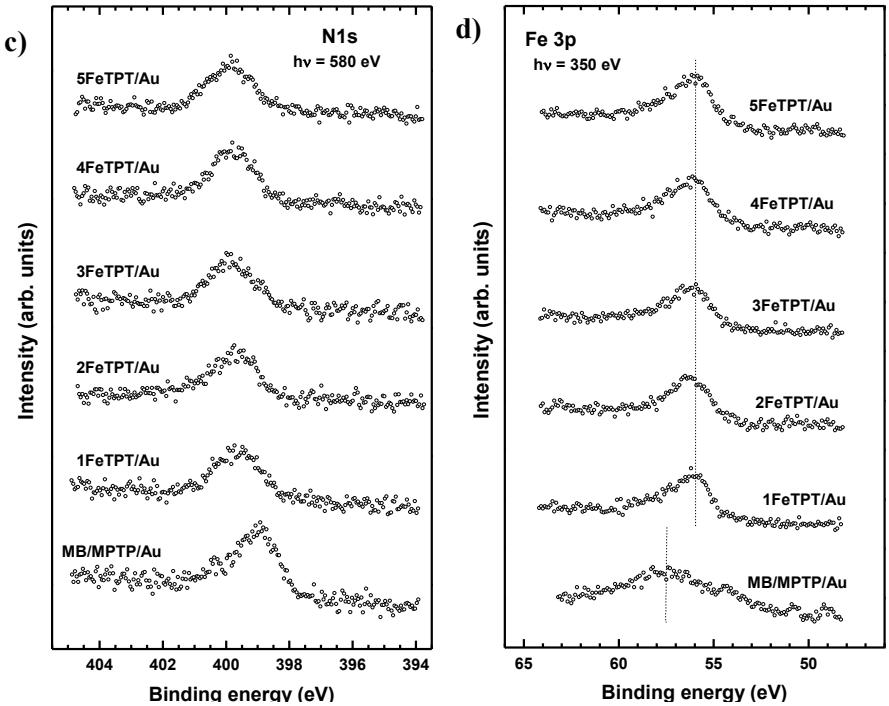

Figure 14. a) N 1s XP spectra of the MB/MPTP and nFeTPT films were acquired at a photon energy of 580 eV; b) Fe 3p XP spectra of the MB/MPTP and nFeTPT films were acquired at a photon energy of 580 eV

From the Fe 3p XP spectra shown in Figure 14b (acquired at a photon energy of 580 eV) it is possible to observe that *n*FeTPT films exhibit pronounced Fe $3p_{3/2,1/2}$ doublet at a BE of ~56.0 eV assigned to the bridging Fe atoms. The signal is saturated because of the strong self-attenuation; therefore, there are no intensity differences between the spectra. As expected, due to the small thickness of the organic layer, the spectrum of the MB/MPTP template exhibits a Au $5p_{1/2}$ emission at ~57.4 eV,[72] in the same region of the Fe 3p band.

1.2.4 NEXAFS analysis

In order to obtain structural information of the MB/MPTP and *n*FeTPT films, NEXAFS investigation has been carried out, again in collaboration with Prof. Michael Zharnikov.

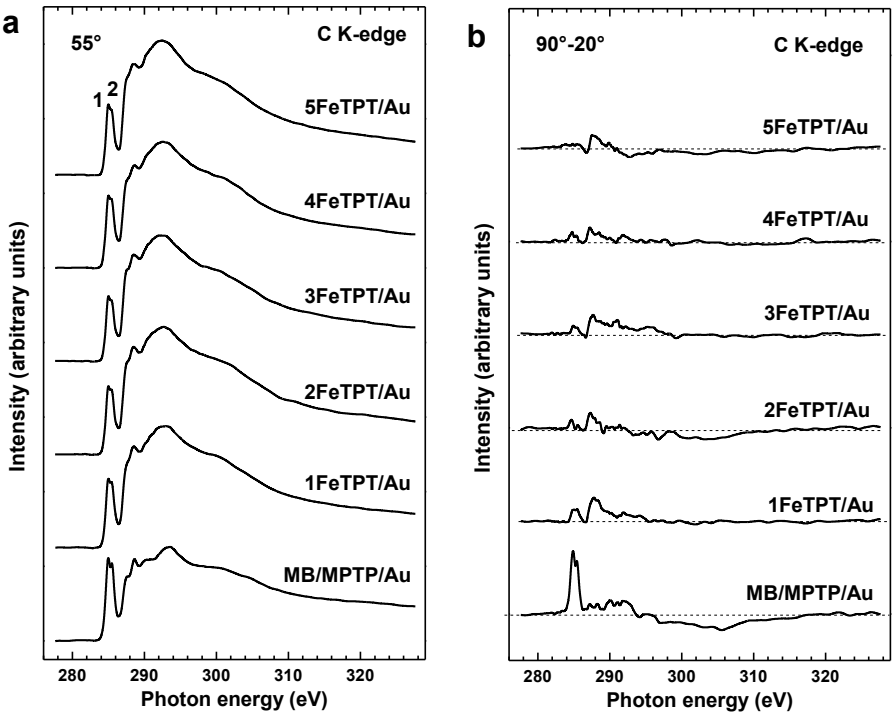

Figure 15. a) C K-edge NEXAFS spectra of the MB/MPTP and nFeTPT films acquired at an X-ray incidence angle of 55°; b) Difference between the C K-edge spectra of the MB/MPTP and *n*FeTPT films collected at normal (90°) and grazing (20°) angles of X-ray incidence for the above samples.

Figure 15a shows the C K-edge NEXAFS spectra of the MB/MPTP and *n*FeTPT films acquired at an X-ray incidence angle of 55°. The spectra of the *n*FeTPT films exhibit the characteristic double peak due to the C 1s→π* transition of the pyridine ring carbon at 285.0 eV (1) and 285.5 eV (2),

observed also for pyridine-substituted self-assembled monolayers. The weight of the resonance 1 is larger in the spectrum of the MB/MPTP template since it overlaps with the π_1* resonance from the MB moieties. In order to evidence the features associated with angular dependence, it is shown (Figure 154b) the difference between the C K-edge spectra of the MB/MPTP and *n*FeTPT films collected at normal (90°) and grazing (20°) angles of X-ray incidence for the above samples. This difference is representative of the linear dichroism in X-ray absorption, and the positive peaks at the positions of the resonances 1 and 2 suggest predominant upright orientation of the MPTP and MB moieties in the case of the MB/MPTP template and *n*FeTPT chains in the case of the *n*FeTPT films. The difference peaks are especially strong in the spectrum of the MB/MPTP template due to the contribution of the BT moieties, which seem to have pronounced upright orientation.

The N K-edge NEXAFS spectra of the MB/MPTP and *n*FeTPT films acquired at an X-ray incidence angle of 55° are reported in Figure 16. The spectra of the *n*FeTPT films exhibit the characteristic π*-like resonances of terpyridine at 398.7.0 eV, and the difference between the C K-edge spectra of the MB/MPTP and *n*FeTPT films collected at normal (90°) and grazing (20°) angles of X-ray incidence for the above samples and the positive peaks at the positions of the absorption resonance at 398.7.0 eV suggest predominant upright orientation of the MPTP moieties in the case of the MB/MPTP template and the *n*FeTPT chains in the case of the *n*FeTPT films.

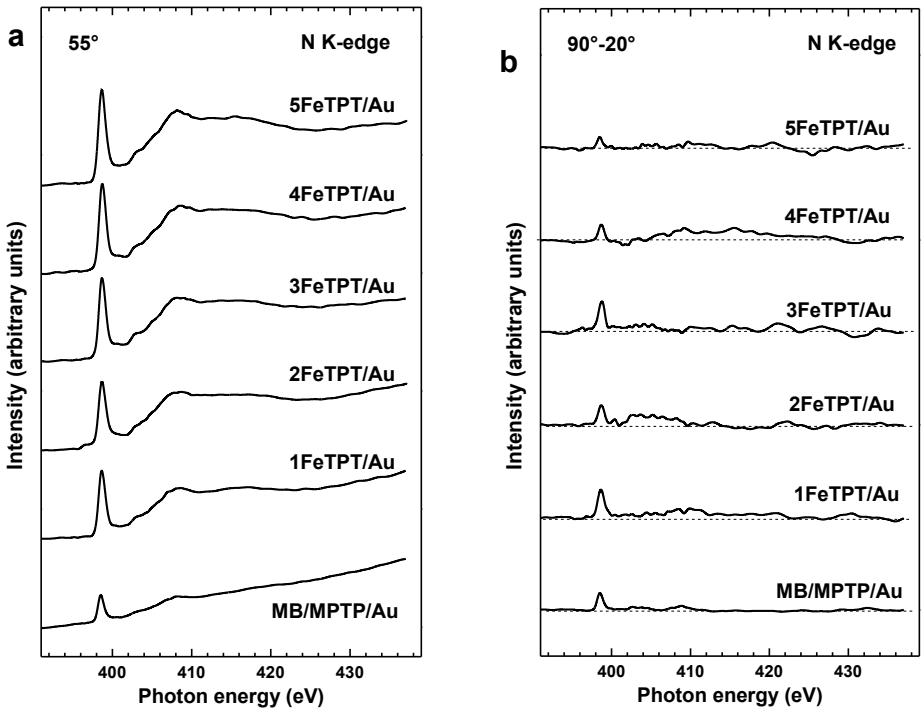

Figure 16. a) N K-edge NEXAFS spectra of the MB/MPTP and nFeTPT films acquired at an X-ray incidence angle of 55°; Difference between the C K-edge spectra of the MB/MPTP and *n*FeTPT films collected at normal (90°) and grazing (20°) angles of X-ray incidence for the above samples.

1.2.5 C-AFM measurements

The data reported above demonstrate the ability of building, on gold substrates, well ordered and contamination free self assembled FeTPT multilayers, that can be regarded as an assembly of molecular wires with upright orientation with respect to the surface plane. Electrical properties of this kind of systems have already been investigated by using the macroscopic mercury-drop technique.[Errore. Il segnalibro non è definito.] Here we focused our attention on the study of the nanoscale charge transport mechanism across the wires by using the

Conductive Atomic Force Microscopy. Measurements were performed at Institut de Science et d'Ingénierie Supramoléculaires (ISIS), Stasbourg, in collaboration with the group of Prof. Paolo Samorì, during some stage periods. C-AFM measurements were carried out using a Digital Instruments Dimension 3100 AFM with a Nanoscope IV controller, using Pt/Ir coated silicon cantilevers with a nominal spring costant of 0.2 N/m. Measurements were acquired in contact mode and one hundred junction were established on each molecular layer. The I-V current-voltage data were first treated by discarding both the zero-current plots (see example of Figure 17a) and the saturated ones (Figure 17b), being originated from bad contacts or by direct contact of the C-AFM tip with the gold substrate, respectively . The statistics of the I-V measurements are reported in Table 1.

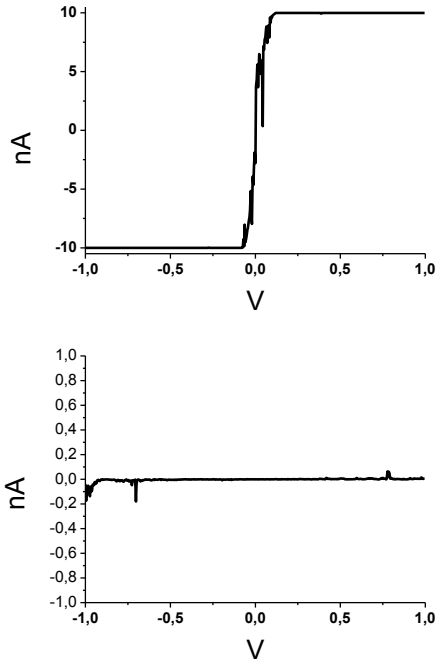

Figure 17. A typical saturated plot (left) and a typical zero-current plot(right).

	n of junctions	n of good junctions	% of working junctions
MB-MPTP	111	48	43
1 FeTPT	139	65	47
2 FeTPT	100	53	53
3 FeTPT	210	56	27
4 FeTPT	91	30	33

Table 1. Statistical evaluation of the current-voltage measurements.

The further treatment of the "good" experimental I-V data is illustrated in Figure 18 in the case of MB/MPTP sample. The procedure is performed as follows: working curves are averaged (red curve) and a linear fitting of this curve in low bias regime is obtained (green line), with the aim of obtaining information about the resistance value.

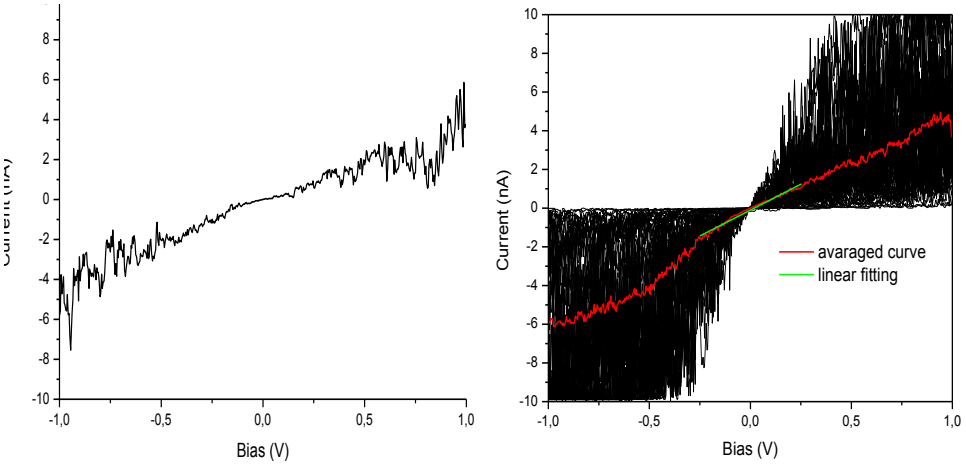

Figure 18. A typical working I-V (on the left); all the working curves obtained for a sample (in black), the average curve (in red) and its linear fit in the low bias region (in green) (on the right).

Such kind of operation is performed for each nFeTPT layer and the obtained average curves are finally plotted as shown in Figure 19.

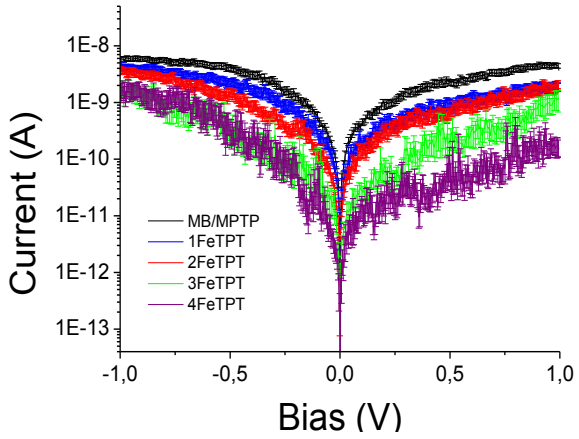

Figure 19. Current-voltage characteristics of nFeTPT layers.

It is easily observed that current decreases with the increasing number of layers. In particular, Figure 20 reports the dependency of the current at a determined bias value as a function of the thickness of the multilayer (which is proportional to the length of the wires) and a linear decrease is obtained. The same behavior is observed by plotting the resistance values: a linear increase is observed with increasing thickness, that is typical of ohmic conductors.

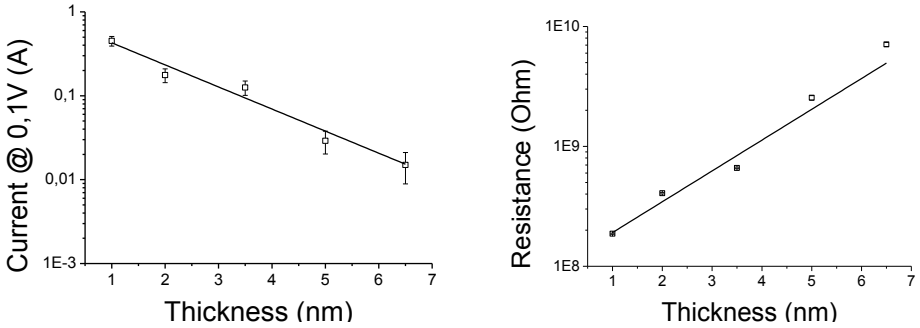

Figure 20. Dependence of current (left) and resistance (right) on the layer thickness.

From this kind of plots it is possible to determine the efficiency of electron tunneling through molecular bonds. In fact, by using the equation $I = I_0 e^{-\beta L}$ for the current values at a fixed voltage and the equation $R = R_0 e^{\beta L}$ for low bias resistances it is possible to determine a β value, that is a structure dependent attenuation factor.[29] In our case β was estimated to be of 0.058 ± 0.006 $Å^{-1}$ by a linear fitting of both the two plots of Figure 20, being the same order of magnitude of the one measured with the Hg drop technique (0.028 $Å^{-1}$). [62]

The small discrepancy between the two values is due to the different methods by which I-V curves are carried out: with the Hg-drop method an area in the order of mm^2 is in contact, while with the C-AFM just a few molecules are contacted, with an area in the order of nm^2, and that causes differences in sensitivity to defects at domain boundaries.

Moreover there is a different degree of deformation of the film between the two methods; in particular it occurs in the case of Hg-drop measurements, in which there is no control of the applied force, while it is avoided in the case of C-AFM, in which the force applied is well controlled.

Similar decay coefficients were also estimated on analogous bis(terpyridine)-based wires by measuring thermodynamic parameters of electron transfer through electrochemical methods.[73-74]

Weak dependences on the wire lengths are typically considered being a signature of a hopping mechanism, i.e. a series of electron transmission events between redox units, even though some cases of long-range tunneling have been reported. [56]

In the case of organic conjugated molecular wires it was shown that a transition of mechanism from direct tunneling ($\beta > \sim 0.1$ Å^{-1}) to hopping ($\beta < \sim 0.1$ Å^{-1}) occurs when going from small (less than 3-4 nm) to longer wires. [62] In our case the data fit with a single straight line, which gives a single low attenuation coefficient even at the smallest lengths, and that means that no transition seems to be present.

To better understand the transport mechanism it is also necessary to characterize the electric field dependency of the I-V characteristics.[75] By applying a bias across a junction, the electronic structure can be perturbed and this phenomenon can generate changes in conduction mechanism. In particular looking at plots of log I versus electric field (E) it is possible to observe two different behavior regimes: if curves nearly collapse on top of one another, this means that an hopping transport occurs, because it is field driven; if curves remain distinctly separated, thus a tunneling transport occurs because it is voltage driven. In our case the plots of log I versus electric field (E) (Figure 21) reveal that curves collapse on top of one another. This result indicates that transport is field driven, rather than voltage driven, and that a hopping mechanism occurs when charges are pushed along the molecules by electric field.

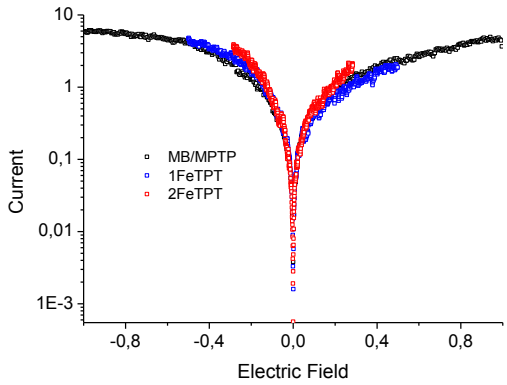

Figure 21. Current vs. electric field dependence for successive short wires

Moreover, by plotting the current versus the inverse of the wire length, as shown in Figure 22, we found a linear dependence, that is again consistent with a hopping mechanism.[76-77]

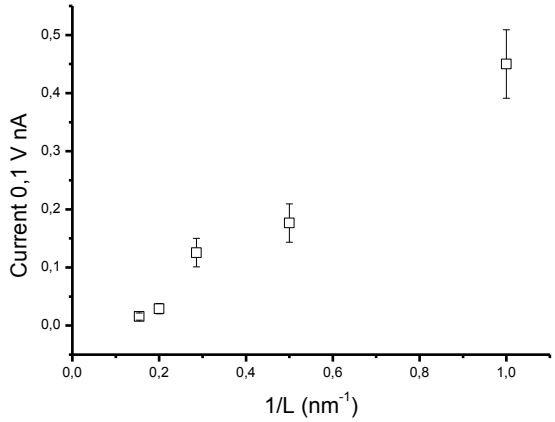

Figure 22. Dependence of the current on the inverse of the length.

In order to see if there is a change in transport regime as a function of the voltage a log-log plot of the I-V characteristics was obtained and it is reported in Figure 23.

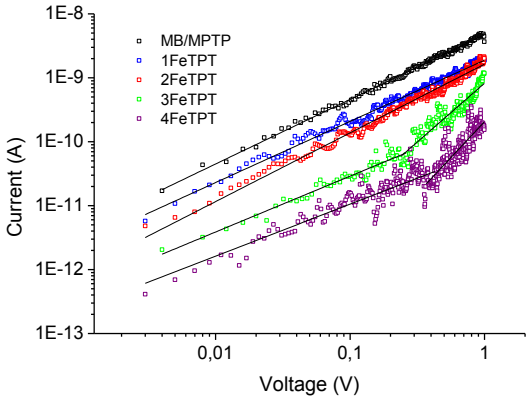

Figure 23. logI – logV plots of successive layers, from MB/MPTP to 4FeTPT. The black straight lines are linear fits whose slope values are marked beside.

For shorter wires, from MB/MPTP to 2FeTPT (3.5 nm) the plots are linear in all the examined bias range with a slope of about 1, indicating Ohmic conduction. Longer 3FeTPT and 4FeTPT wires, instead, exhibit a second regime at voltages higher than 0.4 V and 0.5 V respectively, with the current roughly following a quadratic dependence on the bias, and the mechanism probably switches to the so called Space Charge Limited Current (SCLC) regime. [78]

Consistently an inflection region can be observed for the longer wires 3 and 4FeTPT in $\ln(I/V^2)$ vs. $1/V$ plots which have already been ascribed to the transitional regime (SCLC) between Ohmic hopping and field emission.(Figure 24).

No negatively sloped line is visible in these graphs but an inflection point can be observed for the longer wires 3 and 4FeTPT, likely corresponding to the transitional regime (SCLC) between ohmic hopping and field emission.

SCLC predicts that the current density (J) at a given electric field (E) decreases with increasing layer thickness (L) according to a power law: $J(E) \propto L^{-l}$, where $l = 1$ in the trap-free space charge transport regime. In our case a slope $l > 1$ is found when plotting the current at fixed electric field for different

thickness, consistent with the appearance of more defects/trapping with increasing the number of coordination sites.[79-81]

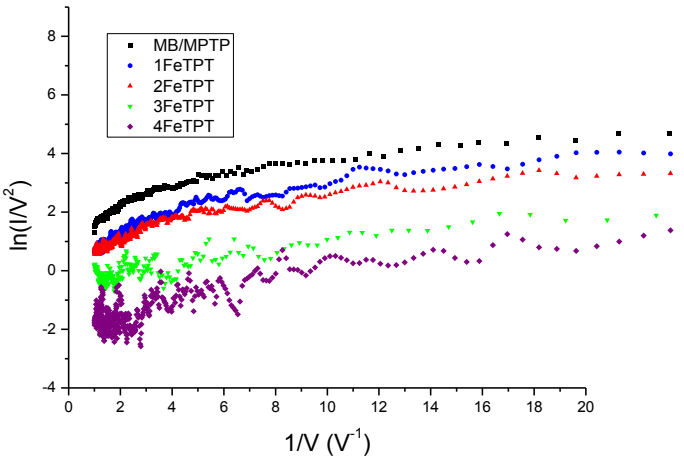

Figure 24. Fowler-Nordheim plot for the successive coordination layers.

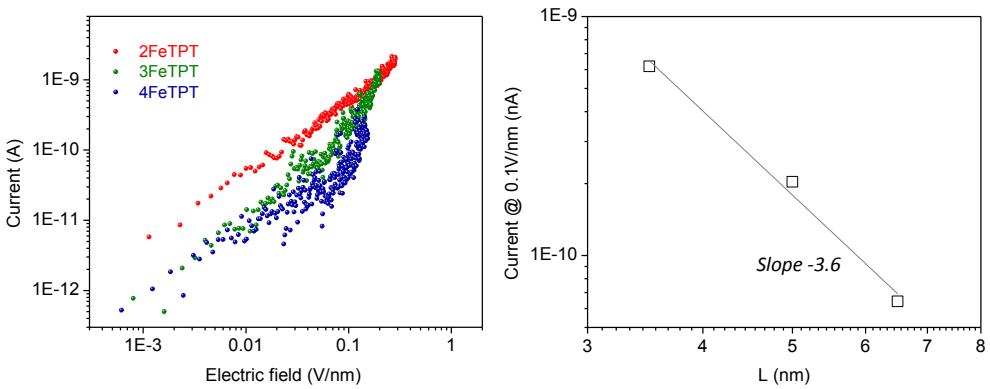

Figure 25. Thickness dependence of space charge limited current

1.2.6 Theoretical calculations

In order to characterize the parameters influencing the transport mechanism, electronic structure calculations on different models of the wire were performed by Prof. Troisi's group (University of Warwick). The main results of these calculation are resumed in the following.

As in all Fe(II) compounds, the hopping mechanism is possible via oxidation of one of the sites to Fe(III), i.e. via hole hopping. The important parameters for charge transport are therefore the electronic coupling between the iron centres and the reorganization energy. The degeneracy of the three highest occupied orbitals of Fe(II) complex (often indicated as t_{2g} assuming an perfectly octahedral ligand field) is lifted by the presence of the neighboring iron complex. The highest occupied orbital, the one that would be occupied by a hole, has a very strong d_{xy} character (assuming that z is the direction connecting the iron centres). The coupling between d_{xy} orbitals of neighboring Fe atoms is extremely small (less than 0.15 meV, the resolution of the electronic structure calculation). The computed reorganization energy for the hole hopping reaction is slightly affected by the choice of the model (with or without counterion) and it is evaluated between 60 meV (without counterion) and 170-1140 meV (with HSO_4^- counterion, possibly more accurately representing the experimental system). Under the condition of reorganization energy much larger than electronic coupling, resonant tunnelling is essentially impossible and the only viable mechanism is hopping between sites. The calculation illustrates (i) that is it not possible to neglect vibronic coupling in these type of complexes,[82] and (ii) that the coupling between iron sites is so weak that resonant tunnelling is also very difficult. In fact, any tiny alternation of the orbital levels (e.g. due to the counterions) will completely destroy the resonance between the metal sites. A modified hopping mechanism may involve the promotion of the hole on the Fe complex from the d_{xy} orbital to next energetically available d-orbital on the same centre, which is only 121 meV away and more strongly coupled with its neighbour (the coupling between these orbitals derived from the energy splitting is 54 meV).

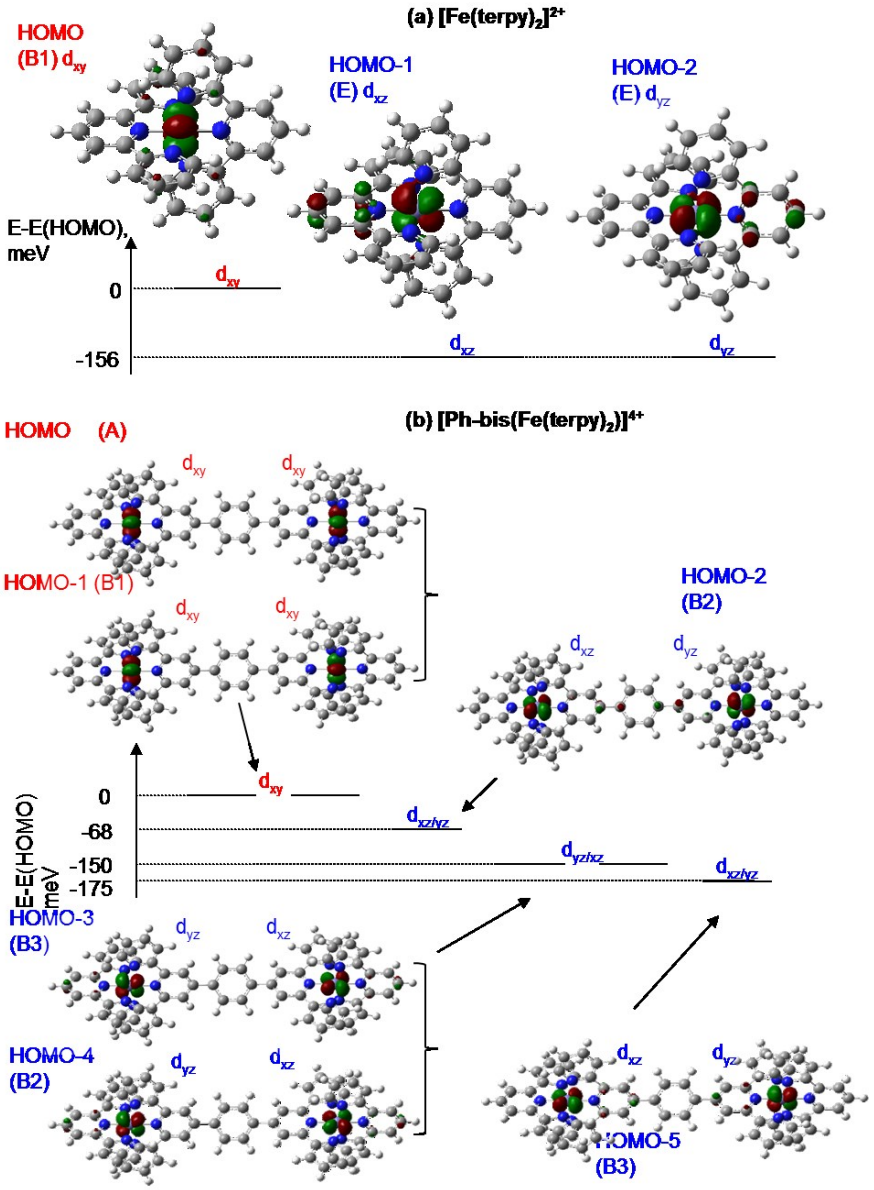

Figure 26. Highest occupied d-orbitals of (a) [Fe(terpy)2]2+ and (b) [(Ph)-bis(Fe(terpy)2)]4+. Irreducible symmetry representations of the molecular orbitals are in parentheses. The main atomic d orbitals contributing to these MO are also indicated.

1.3 Conclusions

In conclusion, Fe-bis(terpyridine) multilayers have been grown on gold surfaces via a self-assembling stepwise method involving direct coordination reactions at the sample surface in order to study their electrical behaviour using the conductive AFM technique.
The formation and growth of the molecular films have been demonstrated by ToF-SIMS, XPS and UV-Vis spectroscopy. Moreover structural information was obtained by means of NEXAFS spectroscopy. From all these data it is quite clear that the molecular wires grow well ordered and contamination free, and that they are oriented upright with respect to the substrate surface.
The C-AFM results show β decay values as low as the ones measured by using macroscopic Hg-drop junctions, providing unambiguous evidence for the existence of a hopping charge transport mechanism.
In the case of shorter wires, less that 3.5 nm long, the electrical data indicate an ohmic conduction mechanism. On the contrary longer wires (more than 4nm) exhibit a transition in transport mechanism at certain voltages, to a regime in which the current is roughly following a quadratic dependence on the bias, indicative of a space charge limited current (SCLC) regime.
The theoretical calculations performed on different models of the wire rule out the existence of resonant tunnelling mechanisms while fully support a charge transport mechanism dominated by charge hopping.

1.4 References

[1] Moore, G.E. Cramming more components onto integrated circuits. *Electronics*, **1965,** *38*, 114–117.

[2] Feynman, R.P. (1960) There's plenty of room at the bottom. *Eng. Sci.*, **23**, 22–36.

[3] Hoeben, F.J.M., Jonkheijm, P., Meijer, E.W., and Schenning, A.P.H.J. *Chem. Rev.*, **2005,** *105*, 1491–1546.

[4] Grozema, F.C., Houarner-Rassin, C., Prins, P., Siebbeles, L.D.A., and Anderson, H.L. *J. Am. Chem. Soc.*, **2007**, *129*, 13370–13371.

[5]Frampton, M.J. and Anderson, H.L. *Angew. Chem. Int. Ed. Engl.*, **2007**, *46*, 1028–1064.

[6]Cacilli, F., Wilson, J.S., Michels, J.J., Daniel, C., Silva, C., Friend, R.H., Severin, N., Samori, P., Rabe, J.P., O'Connell, M.J., Taylor, P.N., and Anderson, H.L. *Nat. Mater.*, **2002**, *1*, 160–164.

[7]Joachim, C., Gimzewski, J.K., Schlitter, P.R., and Chavy, C. *Phys. Rev. Lett.*, **1995**, *74*, 2102–2105.

[8]Reed, M.A., Zhou, C., Muller, C.J., Burgin, T.P., and Tour, J.M. *Science*, **1997**, *278*, 252–254.

[9] Metzger, R.M., Chen, B., Hopfner, U., Lakshmikantham, M.V., Vuillaume, D., Kawai, T., Wu, X., Tachibana, H., Hughes, T.V., Sakurai, H., Baldwin, J.W., Hosch, C., Cava, M.P., Brehmer, L., and Ashwell, G.J. *J. Am. Chem. Soc.*, **1997**, *119*, 10455–10466.

[10] Laurens D. A. Siebbeles and Ferdinand C. Grozema **.** *Charge and Exciton Transport through Molecular Wires.* **2011,** Wiley-VCH.

[11] Mantooth, B.A. and Weiss, P.S. *Proc. IEEE*, **2003,** *91*, 1785–1802.

[12]Wang, W.Y., Lee, T.H. and Reed, M.A. *Proc. IEEE*, **2005,** *93*, 1815–1824.

[13]Fang Chen, Joshua Hihath, Zhifeng Huang, Xiulan Li, and N.J. Tao. *Annu. Rev. Phys. Chem.*, **2007**, *58*, 535–564.

[14]Selzer, Y. and Allara, D.L. *Annu. Rev. Phys. Chem.*, **2006**, *57*, 593–623.

[15] McCreery, R.L. *Chem. Mater.*, **2004**, *16*, 4477–4496.

[16]Liu H., Wang N., Zhao J., Guo Y., Yin X., Boey F.Y., Zhang H. *ChemPhysChem*, **2008**, *9*, 1416–1424.

[17]Kim B., Beebe J.M., Jun Y., Zhu X.Y., Frisbie C.D. *J. Am. Chem. Soc.*, **2006**, *128*, 4970–4971.

[18] Engelkes, V.B., Beebe, J.M. and Frisbie, C.D. *J. Am. Chem. Soc.*, **2004**, *126*, 14287–14296

[19] Lakshmi, S., Dutta, S. and Pati, S.K. *J. Phys. Chem. C*, **2008**, *112*, 14718–14730.

[20] Choi, S.H., Kim, B.-S. and Frisbie, C.D. *Science*, **2008**, *320*, 1482–1486.

[21] Selzer, Y., Cabassl, M.A., Mayer, T.S. and Allara, D.L. *Nanotechnology*, **2004***, 15*, S483–S488.

[22] Grueter, L. Gonzalez, M.T., Huber, R., Calame, M., Schoenenberger, C., *Small* **2005**, *1*, 1067-1070

[23] Gonzalez, M.T., Wu, S., Huber, R., van der Molen, S.J., Schoenenberger, C., Calame, M., *Nanoletters* **2006**, *6*, 2238-2242.

[24]Slowinski, K. and M. Majda, J. Phys. Chem. B, **1999**, *103*, 8544-8551

[25] Holmin, R.E., Haag, R. Chabinyc, M.L., Ismagilov, R.F., Cohen, A.E., Terfort, A., Rampi, M.A., Whitesides, G. M., ., *J. Am. Chem. Soc*. **2001**, *123*, 5075

[26] Mativetsky, J. M.; Palma, M.; Samorì, P. *Top. Curr. Chem.* **2008**, *285*, 157-202.

[27] Pingree, L. S. C.; Reid, O. G.; Ginger, D. S. *Adv. Mater.* **2009**, *21*, 19-28.

[28]Kelley, T. W.; Granstrom, E. L.; Frisbie, C. D. *Adv. Mater.* **1999**, *11*, 261-264.

[29]Wold, D.J., Haag, R., Rampi, M.A. and Frisbie, C.D. *J. Phys. Chem. B*, **2002**, *106*, 2813–2816.

[30]Beebe, J.M., Kim, B.-S., Frisbie, C.D. and Kushmerick, J.G. *ACS Nano*, **2008**, *2*, 827–832.

[31]Ulman, *A. Chem. Rev*. **1996**, 96, 1533-1554.

[32] Bishop, A.R.; Nuzzo, R.G. *Current Opinion in Colloid and Interface Science* **1996**, *1*, 127-136.

[33] Dubois, L.H.; Nuzzo, R.G. *Annu. Rev. Phys. Chem*. **1992**, *43*, 437-463.

[34] Poirier, G. E.; Pylant, *E. D. Science (Washington, D.C.)* **1996**, *272*, 1145-1148.

[35] Nuzzo, R. G.; Allara, D. L. J. Am. Chem. Soc. 1983, 105, 4481.

[36] Porter, M. D.; Bright, T. B.; Allara, D. L.; Chidsey, C. E. D. J. Am. Chem. Soc. 1987, 109, 3559. d) Dubois, L. H.; Nuzzo, R. G. Annu. Rev. Phys. Chem. 1992, 43, 437.

[37] Bain, C. D.; Evall, J.; Whitesides, G. M. J. Am. Chem. Soc. 1989, 111, 7155.

[38] Bain, C. D.; Whitesides, G. M. Science (Washington, D.C.) 1988, 240, 62.

[39] Biebuyck, H. A.; Bain, C. D.; Whitesides, G. M. Langmuir 1994, 10, 1825.

[40] Laibinis, P. E.; Whitesides, G. M.; Allara, D. L.; Tao, Y. T.; Parikh, A. N.; Nuzzo, R. G. J. Am. Chem. Soc. 1991, 113, 7152.

[41] Dubois, L. H.; Zegarski, B. R.; Nuzzo, R. G. J. Chem. Phys. 1993, 98, 678.

[42] Laibinis, P. E.; Whitesides, G. M. *J. Am. Chem. Soc*. **1992**, *114*, 1990-1995.

[43] Bain, C. D.; Troughton, E. B.; Tao, Y. T.; Evall, J.; Whitesides, G. M.; Nuzzo, R. G. *J. Am. Chem. Soc*. **1989**, *111*, 321-335.

[44]Self-Assembled Monolayers of Thiolates Chemical Reviews, 2005, Vol. 105, No. 4 1111

[45] Xu, B. and Tao, N.J. *Science*, **2003**, *301*, 1221–1223

[46] Selzer, Y., Cabassi, M.A., Mayer, T.S. and Allara, D.L. *J. Am. Chem. Soc.*, **2004**, *126*, 4052–4053.

[47]Selzer Y., Cai L., Cabassi M.A., Yao Y., Tour J.M., Mayer T.S., and Allara D.L. *Nano Lett.*, **2005**, *5*, 61–65.

[48] Schubert, U. S.; Winter, A.; Newkome, G. R. *Terpyridine-based materials: For Catalytic, Optoelectronic and Life Science Applications*. Wiley-VCH Verlag GmbH & Co. KGaA: Weinheim, Germany, 2011.

[49] De Cola, L.; Belser, P. *Coord. Chem. Rev.* **1998**, *177*, 301-346.

[50] Balzani, V.; Juris, A. *Coord. Chem. Rev.* **2001**, *211*, 97-115.

[51] Wild, A., Winter, A., Schlutter, F., Schubert, U. S. *Chem. Soc. Rev.* **2011**, *40*, 1459-511.

[52]Nazeeruddin, M. K., Pechy, P., Renouard, T., Zakeeruddin, S. M., Humphry-Baker, R., Comte, P., Liska, P., Cevey, L., Costa, E., Shklover, V., Spiccia, L., Deacon, G. B., Bignozzi, C. A., Gratzel. *J. Am. Chem. Soc.* **2001**, *123*, 1613.

[53] Hurrell, H. C., Abruna, H. D. *Inorg. Chem.* **1990**, *29,* 736-741.

[54] Hjelm, J., Handel, R. W., Hagfeldt, A., Constable, E. C., Housecroft, C. E., Forster, R. J. *Electrochem. Comm.* **2004**, *6*, 193-200.

[55] Nishihara, H., Kanaizuka, K., Nishimori, Y., Yamanoi, Y. *Coord. Chem. Rev.* **2007**, *251*, 2674-2687.

[56] Sedghi, G., Esdaile, L. J., Anderson, H. L., Martin, S., Bethell, D., Higgins, S. J., Nichols, R. J. *Adv. Mater.* **2012**, *24*, 653-657.

[57] Kurita, T., Nishimori, Y., Toshimitsu, F., Muratsugu, S., Kume, S.; Nishihara, H. *J. Am. Chem. Soc.* **2010**, *132*, 4524-4525.

[58] Kosbar, L., Srinivasan, C., Afzali, A., Graham, T., Copel, M., Krusin-Elbaum, L.. *Langmuir* **2006**, *22*, 7631-7638.

[59] Maeda, H., Sakamoto, R., Nishimori, Y., Sendo, J., Toshimitsu, F., Yamanoi, Y., Nishihara, H. *Chem. Comm.* **2011**, *47*, 8644.8646

[60] Terada, K.-i., Nakamura, H., Kanaizuka, K., Haga, M.-a., Asai, Y., Ishida, T. *ACS Nano* **2012**, *6*, 1988–1999.

[61] Spampinato, V., Tuccitto, N., Quici, S., Calabrese, V., Marletta, G., Torrisi, A., Licciardello, A. *Langmuir* **2010**, *26*, 8400-6.

[62] Tuccitto, N., Ferri, V., Cavazzini, M., Quici, S., Zhavnerko, G., Licciardello, A., Rampi, M. A. *Nat. Mater.* **2009**, *8*, 41-46.

[63] Tuccitto, N., Delfanti, I., Torrisi, V., Scandola, F., Chiorboli, C., Stepanenko, V., Würthner, F., Licciardello, A. *Phys. Chem. Chem. Phys.* **2009**, *11*, 4033-4038.

[64] Mondal, P. C.; Yekkoni Lakshmanan, J.; Hamoudi, H.; Zharnikov, M.; Gupta, T. *J. Phys. Chem. C* **2011**, *115*, 16398-16404.

[65] Gupta, T.; Mondal, P. C.; Kumar, A.; Jeyachandran, Y. L.; Zharnikov, M. *Adv. Funct. Mater.* **2013**, *23*, 4227-4235.

[66] Auditore, A.; Tuccitto, N.; Marzanni, G.; Quici, S.; Puntoriero, F.; Campagna, S.; Licciardello, A. *Chem. Comm.* **2003**, *19*, 2494-2495.

[67] Auditore, A.; Tuccitto, N.; Quici, S.; Marzanni, G.; Puntoriero, F.; Campagna, S.; Licciardello, A. *App. Surf. Sci.* **2004**, *231-232*, 314-317.

[68] Doron-Mor, I.; Cohen, H.; Barkay, Z.; Shanzer, A.; Vaskevich, A.; Rubinstein, I. *Chem. Eur. J.* **2005**, *11*, 5555-62.

[69] Kalyuzhny, G.; Vaskevich, A.; Schneeweiss, M. A.; Rubinstein, I. *Chem. Eur. J.* **2002**, *8*, 3850.

[70]Hamoudi, H.; Döring, K.; Chesneau, F.; Lang, H.; Zharnikov, M. *J. Phys. Chem. C* **2012**, *116*, 861-870.

[71] Darlatt, E.; Traulsen, C. H.-H.; Poppenberg, J. s.; Richter, S.; Kühn, J.; Schalley, C. A.; Unger, W. E. S. *J. Electron Spectrosc. Relat. Phenom.* **2012**, *185*, 85- 89.

[72] Moulder, J. F.; Stickle, W. E.; Sobol, P. E.; Bomben, K. D. *Handbook of X-ray Photoelectron Spectroscopy*. Perkin-Elmer Corp.: Eden Prairie: MN, 1992.

[73] Sakamoto, R.; Katagiri, S.; Maeda, H.; Nishihara, H. *Coord. Chem. Rev.* **2013**, *257*, 1493-1506.

[74] Nishimori, Y.; Kanaizuka, K.; Kurita, T.; Nagatsu, T.; Segawa, Y.; Toshimitsu, F.; Muratsugu, S.; Utsuno, M.; Kume, S.; Murata, M.; Nishihara, H. *Chem. Asian J.* **2009**, *4*, 1361-1367.

[75] Lakshmi, S. , Dutta, S., Pati, S.K. *J. Phys. Chem. C*. **2008**, *112*, 14718-14730.

[76] Segal, D.; Nitzan, A.; Davis, W. B.; Wasielewski, M. R.; Ratner, M. A. *J. Phys. Chem. B* **2000**, *104*, 3817-3829.

[77] Nitzan, A. *Annu. Rev. Phys. Chem.* **2001**, *52*, 681-750.

[78] Engelkes, V.B., Beebe, J.M. and Frisbie, C.D. *J. Phys. Chem. B*, **2005**, *109*, 16801–16810.

[79] Steyrleuthner, R.; Schubert, M.; Jaiser, F.; Blakesley, J. C.; Chen, Z.; Facchetti, A.; Neher, D. *Adv. Mater.* **2010**, *22*, 2799-2803.

[80] Joung, D.; Chunder, A.; Zhai, L.; Khondaker, S. I. *Appl. Phys. Lett.* **2010**, *97*, 093105.

[81] Steyrleuthner, R.; Bange, S.; Neher, D. *J. Appl. Phys.* **2009**, *105*, 064509.

[82] Terada, K.-i.; Nakamura, H.; Kanaizuka, K.; Haga, M.-a.; Asai, Y.; Ishida, T. *ACS Nano* **2012**, *6*, 1988–1999.

2 Oxide surface engineering

This chapter is devoted to the description of the results of functionalization approaches of oxide surfaces, that are of interest, among others, in the preparation of dye-sensitized semiconductor transparent electrodes suitable in solar energy conversion applications. The description of the experimental results will be preceded by a short excursus on some key points about solar energy conversion and on the state-of-the art in the field of surface functionalization of oxides by self-assembling techniques.

2.1 Solar energy conversion: the molecular approach.

Nowadays, a very important research field is related to the energetic problem, the general aim being that of replacing the fossil based fuels with renewable energies, with a particular interest to solar energy. [1-2] Among other energy forms, solar energy has the advantage of a high potential for power generation: solar radiation amounts to 3.8 million EJ/year, which is approximately 10000 times more than human current energy needs.[3] In particular, present research is focused in finding an efficient way to convert this enormous quantity of energy in an exploitable form. Indeed, although commercial photovoltaics are available, they produce electricity only when illuminated, and one of the problems is that this energy it cannot be stored efficiently.
As it often happens, a guideline is given by nature: it is well known that vegetables are able to convert sunlight in substances with more chemical energy than the reactants trough the photosynthesis process, and researchers have studied several system able to mimic this phenomenon, by using an approach known as artificial photosynthesis.[4] Several papers have been published, that describe photochemical approaches to produce high energy content substances, or fuels, from simple reactants such as water or CO2.[5-10] in an analogous way to that which is occurring in green plant, algal and

cyanobacterial photosynthesis. Among several possibilities, dye-sensitized solar cells, DSSCs, have emerged as promising devices since they are simple, cheap and they are capable of converting sunlight into electricity through a photoelectrochemical process.
The use of sensitization effect for solar energy conversion has been known for a long time,[11] but only in 1991, when B. O'Reagan and M. Grätzel published the use of nanocrystalline and mesoporous TiO2 film,[12] the use of DSSC underwent a great breakthrough. Starting with the paper of 1991, this field has grown very fast and all the aspects of these solar cells have been investigated. [13-17] Some of the advantageous features of DSSCs can be exploited in other possible approaches of solar energy conversion and storage, and in particular in the context of photocatalytic solar water splitting, that involves the use of dye-sensitization coupled with the use of a catalysts for water oxidation and reduction.

2.1.1 Water splitting dye sensitized solar cells

Dye-sensitized solar cells (DSSC) are semiconductor photovoltaic devices that convert solar radiation into electric current. The ones use for electricity production (like the Graetzel-type cells) generally have the following configuration:

- a transparent anode made of a glass sheet treated with a transparent conductive oxide layer;
- an oxide layer (typically,mesoporousTiO_2) deposited on the anode ;
- a dye monolayer covalently bonded to the oxide surface to enhance light absorption;
- an electrolyte containing a redox mediator able to regenerate the dye;
- a cathode made of a glass sheet coated with a catalyst (typically, platinum to facilitate electron collection.

The working principle of this kind of cell is based on the fact that the sunlight is harvested by the dye, that reach an excited-state capable of inject an electron

into the semiconductor conducting band. The oxidized dye is then regenerated by the redox mediator and the injected electron percolates through the semiconductor film, it reaches the conducting glass and it flows through the external circuit to the counter electrode. Finally the counter electrode regenerates the oxidized specie of the mediator using electrons from the external circuit.[18] In this kind of scheme (**Errore. L'origine riferimento non è stata trovata.**) any permanent chemical change for dye-sensitized solar cells it is not expected, and for this reason the estimated lifetime of these devices is of the order 20 years.[19] However the practical lifetime of DSSC devices is shortened by adverse side phenomena affecting their durability, including degradation of the interfaces, desorbtion of the dye, side reactions of the dye with the redox mediator. Moreover, the efficiency of these devices if still considered not sufficient, and many studies are directed to its improvement.

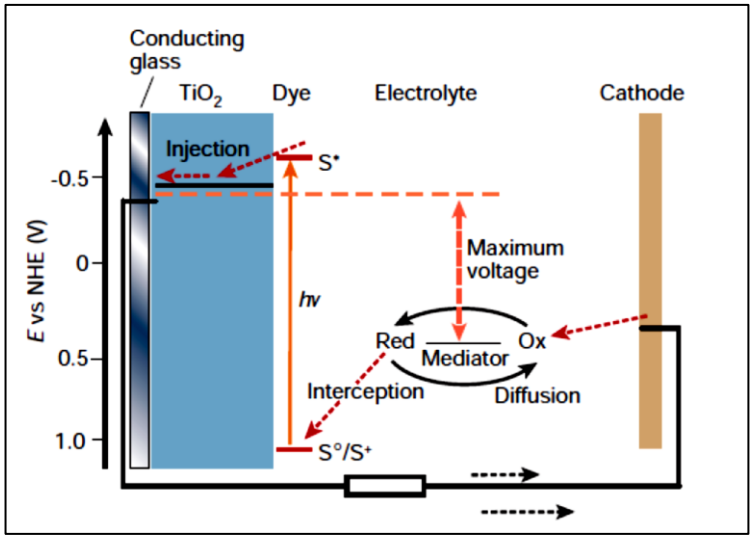

Figure 27. General scheme of a typical dye-sensitized photoelectrochemical cell. [19]

In order to obtain an efficient dye sensitized solar cell it is necessary that the dye is able to absorb the sunlight, to use its energy for generating an excited state, to inject electron into the semiconductor conducting band. Moreover, the

original oxidation state of the dye must be easily regenerated by a redox mediator. Since several years research is focused in synthesis of new dyes. [20-23]

The first DSSC in which the absorption in the UV-visible region μ was >10% (a good value is considered about 44%) [24] employed as dye-sensitizer the cis-di(isothiocyanate)bis-(2,2'-bipyridyl-4,4'-dicarboxylic acid) ruthenium(II) complex [referred as N3].[25] Later on, the complex mer-tri(isothiocyanate) (2,2',2''-terpyridyl-4,4',4''-tricarboxylic acid) ruthenium(II), [black-dye] was prepared and also successfully used as sensitizer.[26] The good performance of these dyes allowed researchers to use them as models for molecular engineering of new dyes.

Until now the most studied dyes are high potential porphyrins and ruthenium complexes based on 2,2'-bipyridine derivative ligands. [27-29] In particular $[Ru(bpy)_3]^{2+}$ is one of the first dyes that has been used also for testing the production of hydrogen [30] and oxygen [31] from water. It was first chosen for several reasons: it absorbs below 500nm with a high ε (M^{-1} cm^{-1}) and it has a sufficient long lifetime of the excited state(~600 ns).[32] Most important, the internal quantum yield for formation of the exited state is nearly unity, i.e. virtually all the excited molecules are useful for the electron transfer reaction.[33] Several papers were reported showing its efficiency in water splitting. [34-36]

The use of this dye has also several disadvantages, including the limited wavelength range of its absorption band in the UV-Vis region. A possible solution has been reported by Campagna et al, [37] who showed a new dendrimeric ruthenium complex with an ε higher that of $[Ru(bpy)3]^{2+}$ and a larger range of absorption in the UV-visible region.(Figure 28)

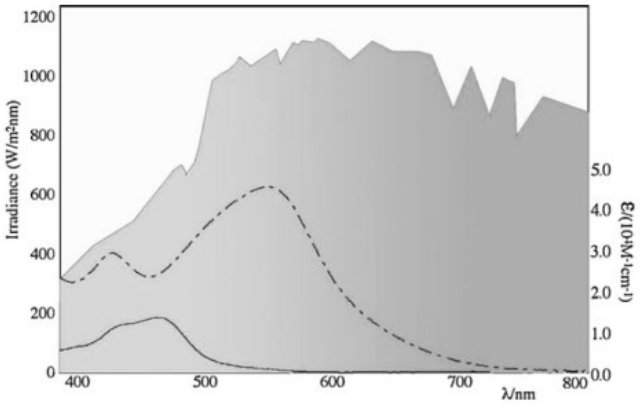

Figure 28. absorption spectra of mono-complex(solid line), dendrimeric-complex (lineatratteggiata) respect to the sun emission.

These differences can affect positively the efficiency of a dye-sensitized solar device, by increasing - for example - the oxygen evalution yield, as demonstrated in some test experiments. [38]

In order to use a dye-sensitized device the photo-induced water splitting, two other components are necessary with respect to a conventional DSSC (Graetzel-type) cell: a proton reduction catalyst that uses the reducing equivalents to store energy in the form of reduced material, including hydrogen, hydrocarbons, or other fuels. An example is platinum, that has a low overpotential (activation energy) and a rapid turnover for proton reduction to hydrogen gas, but it is a rare and expensive element.

A water oxidation catalyst, that uses oxidizing equivalents to oxidize water to oxygen gas and hydrogen ions. The search for artificial water oxidation catalysts that are useful in artificial photosynthesis is very active. A scheme for the oxidation process is given below, where P indicates the photosensitizer molecule, SA is an electron acceptor (the semiconductor electrode in a real cell, substituted by a sacrificial acceptor molecule in test experiments performed in homogeneous solution phase) and WOC is the water oxidation catalyst.

- $P + h\nu \rightarrow {}^*P$
- ${}^*P + SA \rightarrow P^+ + SA^-$
- $4P^+ + WOC \rightarrow P + WOC^{4+}$
- $WOC^{4+} + 2H_2O \rightarrow WOC + O_2 + 4H^+$

Catalyst role is very important because it determines the efficiency of the entire process. In particular, it must be able to accumulate four positive charges and to transfer them to water in order to make possible its oxidation. In literature there are a few examples of WOCs, the first of them reported by Mallouk et all,[34] who showed the efficiency of IrO2 nanoparticles. They showed that the oxidized photosensitizer, $[Ru(bpy)_3]^{3+}$, is reduced with the formation of Ir^{IV} on the surface of nanoparticles. Nevertheless, the successive electron transfer between $[Ru(bpy)_3]^{3+}$and Ir^{IV} is too slow and makes the process inefficient due to the low speed of turnover of the catalyst.

Polyoxometallates recently turned out to be another promising class of possible WOCs. They are completely inorganic molecules with several μ-hydroxo/oxobridge bonds, as in natural water oxidation catalyst.[38-40] Their well defined structure makes it possible to use them in several applications,[42] and they are good candidates for water oxidation also because of their stability in the oxidizing conditions required by the process.[43] The first work about the use of POM as a catalyst was reported in 2004 by Howells et all,[44] although they were unable to study the mechanism because the structure of the used POM was unknown. The first structural characterization of a POM was that of $[Ru_4(\mu\text{-}O)_4(\mu\text{-}OH)_2(H2O)_4(\gamma\text{-}SiW_{10}O_{36})_2]^{10-}$; and its catalytic activity was first demontrated by in dark conditions. [45]

Its efficiency in presence of a photosensitizer was then demostrated independently by Hill et al [46] and Sartorel et al [47], who showed that in presence of POM and $[Ru(bpy)_3]^{3+}$water oxidation is about 102 times faster than the same reaction without catalyst. Also, the working mechanism of the catalyst has been proposed on the basis of a test experiment with a sacrificial acceptor: the $[Ru(bpy)_3]^{2+}$ dye absorbs light and it transfers one electron (i.e. is oxidized) to the sacrificial molecule (S_2O_8); the formed Ru^{III}complex then oxidizes one of the metallic centers of the POM, becoming again Ru^{II}. When

all the four metals of POM are oxidized, it can split water into O_2 and H^+, but with a yield of 9%, that is low respect to the theoretical limit of 25%.

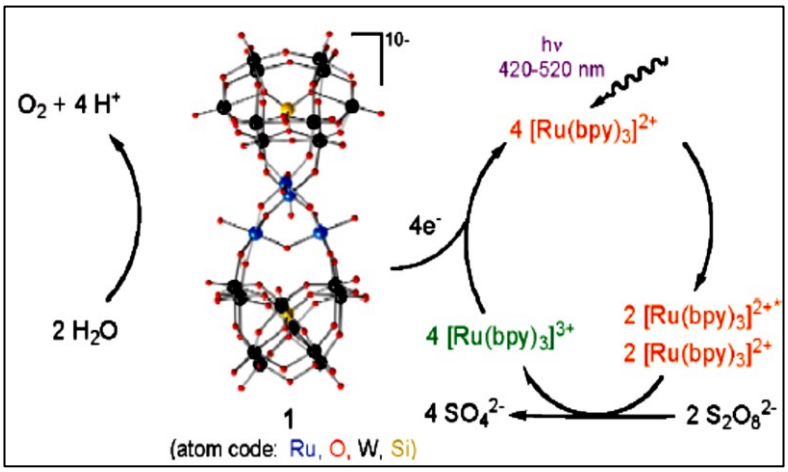

Figure 29. Light-Induced Catalytic Water Oxidation by Tetraruthenium Polyoxometalate 1 using [Ru(bpy)3]2+ as a Photosensitizer and Persulfate as a Sacrificial Electron Acceptor. [46]

It must be pointed out that in a real cell for water splitting the role of electron acceptor should be played by a solid semiconducting electrode. This suggests that, in addition to the right choice of the dye/catalyst couple, also the "communication" (i.e. a good efficiency of the electron transfer, coupled with a low efficiency of charge recombination mechanisms) the between the dye and the electrode is a critical issue. This highlights the importance of a proper attachment (anchoring) of the dye molecule to the semiconductor substrate. Among several kinds of substrate, TiO_2 is probably the most exploited as transparent semiconductor in dye-sensitized devices. Since the '70s it is well known that TiO_2 has important photocatalytic properties, including the Honda-Fujishima effect: when an anodic potential is applied to a TiO_2 cristal in water under sunlight, a development of oxygen at the TiO_2 electrode and of hydrogen at the counter electrode occur. TiO_2 exists in three different allotropic forms,

that have different structure and as a consequence different properties. The anatase form has a distorted tetragonal structure, the brookite form is orthorhombic and the rutile form is tetragonal. Among them anatase form presents an higher electronic mobility, a lower dielectric costant and a Fermi level a little bit higher. Moreover its conduction band has an energy level that is compatible with almost all the photosensitizers generally available, and this makes easier and faster the electron transfer process. This kind of semiconductor offers the possibility to transfer in an efficient way the electrons to the external circuit, preventing the back electron transfer. This feature is is usually explained in two possible ways. A first explanation is related with the large band gap of the semiconductor. Due to it, electron injection occurs directly to the conduction band of TiO_2 and localized Ti(III) states are formed on the surface. By means of thermal decay processes they reach the lower level of the conduction band but, because of the large band gap the process of their transport across the external circuit is more favoured than the back electron transfer.

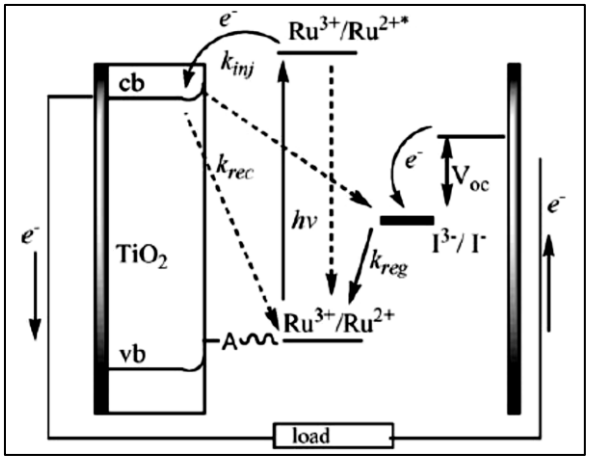

Figure 30. Schematic representation of processes that occur in a ruthenium based solar cell

An alternative explanation involves the different nature of the orbitals involved in the formation of the conduction band and of the valence band of TiO_2, the 3d and 2p metal orbitals respectively. Accordingly, there is a very low probability that the electron can relax to the valence band and then back transferred to the oxidized dye.
Since redox reactions involved in this process occur at the surface, nanocrystallinity of the semiconductor layer plays an important role on the electron injection and transport.[19] This is the reason why TiO_2 is used as nanoporous film, typically obtained by deposition and subsequent sintering of TiO_2 nanoparticles on a conductive solid electrode.

2.1.2 Self assembling on oxide substrates

Although in many practical appications the adsorption of the dye to the semiconducting oxide is obtained by simple physisorbtion, it would be highly desirable to anchor it in a stable way. Among others, this should increase the durability of dye-sensitized semiconductor electrodes for solar energy applications. Moreover, the anchoring strategies be developed in this context are of more general interest, as they can be exploited in different fields, from sensors to biocompatibily, just to cite some of them. Several anchoring strategies have been proposed to functionalize oxide materials. Substituted silanes, for example, are widely used, in particular for functionalising silicon dioxide. With silanes it is possible to form very compact monolayers, due to the formation of a covalent bond upon reaction of the between the silane molecules and the M-OH groups presents at the oxide surface.[48] The silane group can be introduced as head group in the molecule to be anchored to the surface or, more often, it brings a proper tail group (i.e. a functional group that is connected to the silane moiety through a proper backbone) that can undergo a further coupling reaction with the molecule to be linked to the surface. In many cases, in the silane based methodology, the formation of M-O-Si bonds is accompanied by the formation of Si-O-Si “horizontal” bonds between

adjacent molecules.[49] This cross-linking characteristic can have a positive effect in the stability of the film. However, silane functionalization has several disadvantages: since the formation of the film depends on hydrolysis of the silane,[50-51] it is necessary to control strictly, temperature and water content. In particular it is known that a small amount of water leads to an incomplete film, [52-53] while –by contrast – with an excess of water the rate and extent of hydrolysis will be too high and self–condensation will occur with possible uncontrolled formation of multilayers on the surface. [54]

For these reasons other techniques have been developed, introducing the use of carboxylic and phosphonic acid groups, especially in functionalising titania surfaces. It is known that phosphonate linkage to a TiO2 surface is stronger and more stable than the carboxylate one in organic solvent. [55-59] The main difference between these two kind of organic acids is the different number of coordination sites (two in carboxylates and three in phosphonates), that lead to different anchoring structure. Moreover, a different chemical stability (for example towards hydrolysis) should be expected for the two kinds of ester bonds that are formed with the surficial hydroxyl groups.

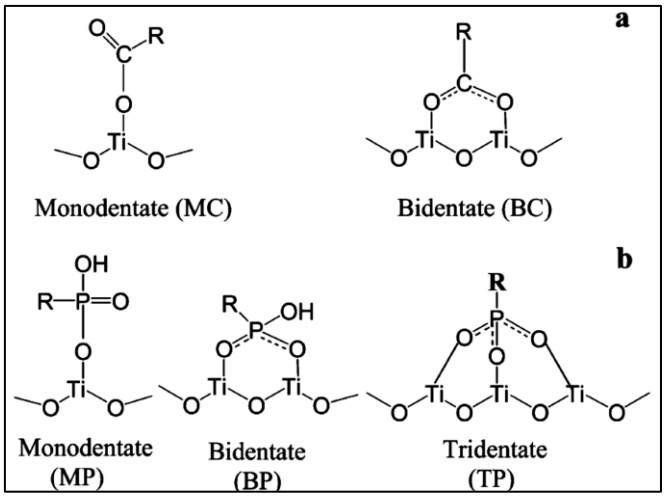

Figure 31.Structures of the possible surface attachment of carboxylic (a) and phosphonic (b) groups on TiO2 surface. [60]

These differences leads to a different stability of the formed film. In fact, it is known that in the case of carboxylic acids, the obtained monolayers are often weakly bound to the surface and they can be easily removed, sometimes by simple rinsing in solvents.[61] A general problem in both cases (using phosphonic or carboxylic acids) is, however, that the strength of the obtained linkage is strongly dependent on the nature of the oxide. It is possible to overcome this problem by changing the chemical composition of outermost surface layers, in order to increase the stability of the bonds with phosphonic or carboxylic groups. Such an approach, at least in principle, has the advantage to make the stability of the anchoring independent on the nature of the oxide surface. A method that exploits this kind of approach is based on the properties of zirconium phosphates and phosphonates.

It is well known in solid state chemistry that interactions between metals and phosphonic groups lead to a large variety of materials, including the l'α-zirconium phosphate $Zr(O_3POH)$, that has a lamellar structure (studied by

Clearfield [62]) in which all the inorganic layers have an hexagonal arrangement of zirconium ions, as well as phosphoric groups (that are situated above and below plane of zirconium atoms).

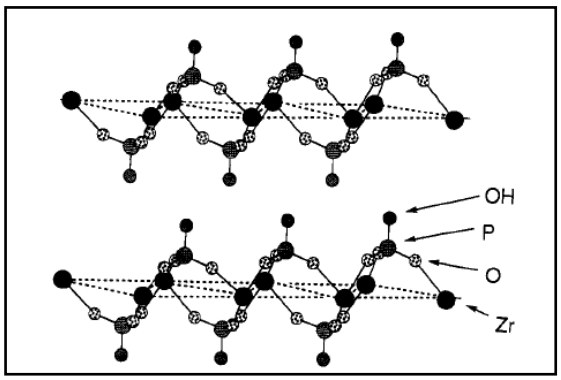

Figure 32. Structure of α-Zr(O3POH)

A similar structure was determined for compounds in which organic ligands are present. The increasing interest in studies related to zirconium-phosphonate derivatives is due to the possibility to obtain them at room temperature, in water, and because they offer the possibility to build several kind of supramolecular structures. The same kind of chemistry can be exploited for surface functionalization.

One of the first examples was reported by Mallouk and co-workers. They anchored onto an oxide surface a bifunctional molecule containing a silanole group (that can react with the surface as described previously) and a phosphonic group that can subsequently interact with a zirconium ion. In turn, the surface obtained in such a way can react with a foshate- or phosphonate-containing molecule, and this kind of approach can be used for growing multilayers if bifunctional molecules are used.

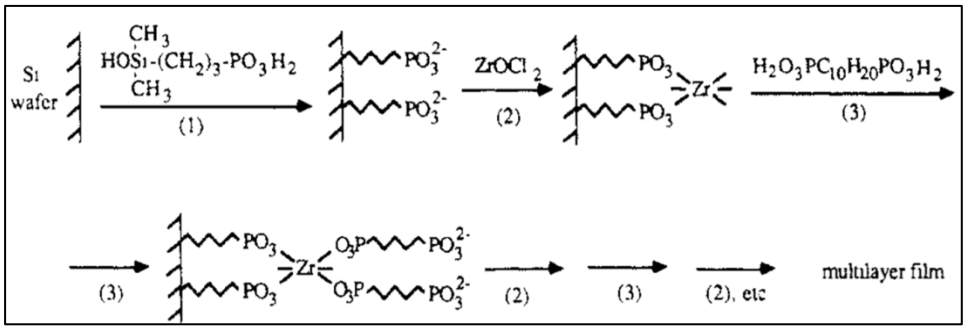

Figure 33. Reaction scheme for Mallouk's group proposed strategy.

However the Mallouk's approach still relies on surface silanization, so that it doesn't solve the problems connected with the use silanes, some of them mentioned at the beginning of this paragraph. For this reasons Kohli and Blanchard, [63-65] proposed a different approach in which the surface is directly modified by a phosphorylation oprocedure. In order to apply this strategy (Figure 34) three reaction steps are necessary: i) immersion of the substrate in an oxidising ("piranha") solution (3:1 H_2SO_4:H_2O_2) with the main aim of increasing the amount of hydroxyl groups at the surface; ii) the phosphorylation of hydroxyl groups by $POCl_3$ and collidine in anhydrous acetonitrile; iii) the reaction of phosphoric present at the surfane with a zirconium salt aqueous solution.

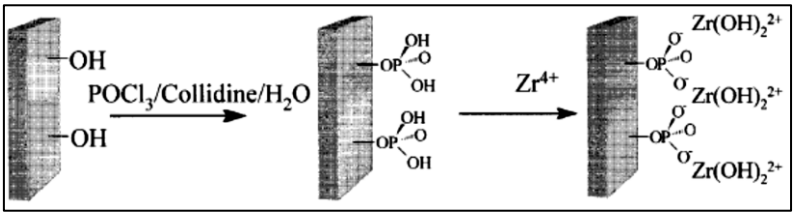

Figure 34. Reaction scheme for Kohli and Blancard proposed strategy.

Finally the Blanchard method was modified by Morotti et al [66] and Spampinato at al,[67] by using neat $POCl_3$ during the phosphorylation step.

In the following we show the results obtained in functionalization of oxide surfaces by applying the zirconium phosphate-phosphonate procedure (henceforth ZP procedure) oxide surfaces with particular focus on titanium oxide substrates. The results on quartz substrates are reported as well, as these substrates constituted the model systems we used for developing the functionalization and characterization protocols.

2.2 Results and discussions

2.2.1 Zirconium phosphate-phosphonate anchoring (ZP method) on on quartz surfaces.

Quartz substrates were treated for 15 minutes in UV-O_3 and rinsed in pure water. This procedure enriches the with OH groups and, at the same time strongly reduces organic contamination of the surface. Subsequently, the zirconium-phosphonate (ZP) methodology was applied: samples were immersed in $POCl_3$ then rinsed with water, and finally immersed in a $ZrCl_2O$ solution (10^{-4} M, water) for 15 minutes (Figure 35).

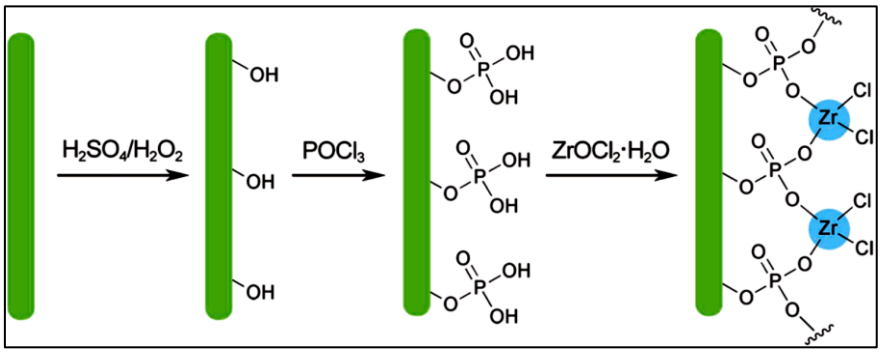

Figure 35. Reaction scheme for oxide surface priming and formation of a ZP layer.

The surface obtained in this way is ready for the subsequent anchoring of molecules bringing a phosphonate head group. The feasibility of the method has been already demonstrated [68] that by means of XPS and ToF-SIMS measurements. However there is a lack of knowledge on degree of the surface covering and on the stability of the anchoring of the organic molecules in comparison with other methods. For this reason we developed a method that is able to give some answers in both directions. The method, initially developed

for quartz substrate, has been then extended to titania substrates, as it will be shown in the next paragraphs.

Simply, the method uses the anchoring of a strongly light absorbing molecule, that can be detected, even in monolayer concentration, in UV-Vis absorbtion spectroscopy. The molecule of choice was a rhodamine B derivative: Rhodamine B belongs to a family of molecules known as xanthenic dyes. Because of its peculiar structure it exists in solution as a mixture of several forms in equilibrium between them, the main of which are the zwitterionic coloured form and the colourless lactone form. [69]

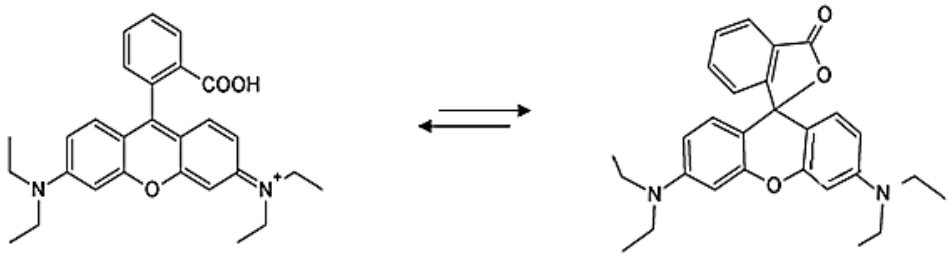

Figure 36. Tautomeric equilibrium of rhodamine B.

The equilibrium constant depends both on the solvent (high polar solvents favour the opened form)[70] and on the temperature.[71] In polar solvents, therefore, being the carboxylated form the prevalent one, the solution appears red-violet coloured with a high molar extinction coefficient (ε= 106000 L mol^{-1} cm^{-1}) and shows high quantum yield of fluorescence, because the rigidity of the molecular structure prevents the non radiative decay pathways. These optical properties of rhodamine B make it well suited for studying when present as a mono- or submonolayer.
In order to make the rodamine B molecule suitable for self-assembly on the zirconium phosphate-modified oxide surface, it has been modified by insertion a phosphonic group. (Figure 37). The synthesis of this derivative was performed in collaboration with the group of prof. M.E. Amato and it will be the subject of a separate publication.

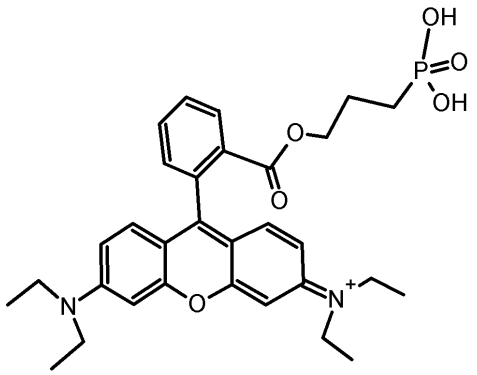

Figure 37. Structures of the phosphonate rhodamine derivative.

Surface anchoring was performed by the immersion for 24 hours of the ZP-modified substrate in a rhodamineB derivative solution (~10^{-4} M in $CHCl_3$).

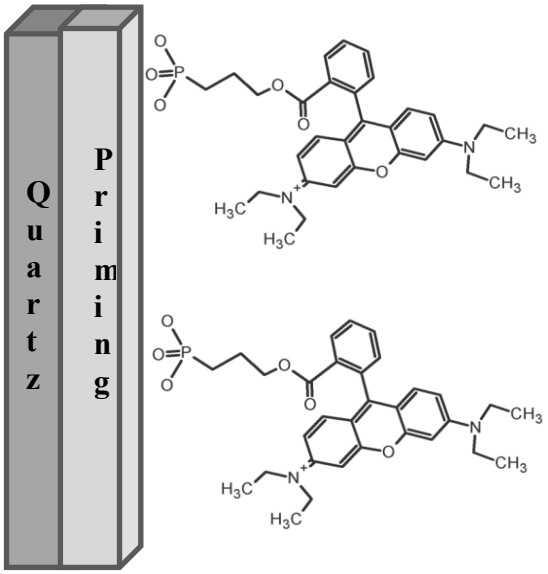

Figure 38. Schematic representation of a SAM of rhodamine B on ZP-modified quartz.

2.2.1.1 ToF SIMS characterization

Surfaces obtained after each modification step were characterized by time-of-flight secondary ion mass spectrometry (ToF-SIMS). Spectra were acquired with a reflector-type TOFSIMS IV spectrometer (ION-TOF GmbH, Muenster, Germany) using 25 keV Bismuth primary ions. Static Sims conditions were used (Bi^+ primary ion fluence< 10^{12} ions·cm^{-2}) in order to preserve the molecular information from the surface.

Figure 39 is reports a typical ToF SIMS spectrum obtained for the rhodamine B derivative SAM on ZP-treated quartz substrate, after several careful rinsing steps aimed to remove the eventual excess of physisorbed dye. The spectrum contains some characteristic fragments that are a signature of the successful functionalization of the surface. In particular it is possible molecular fragments related to the presence of rhodamine, including the molecular ion $[C_{31}H_{36}N_2O_5P]^+$(m/z 547) and the molecular fragment $[C_{28}H_{31}N_2O_3]^+$(m/z 443).

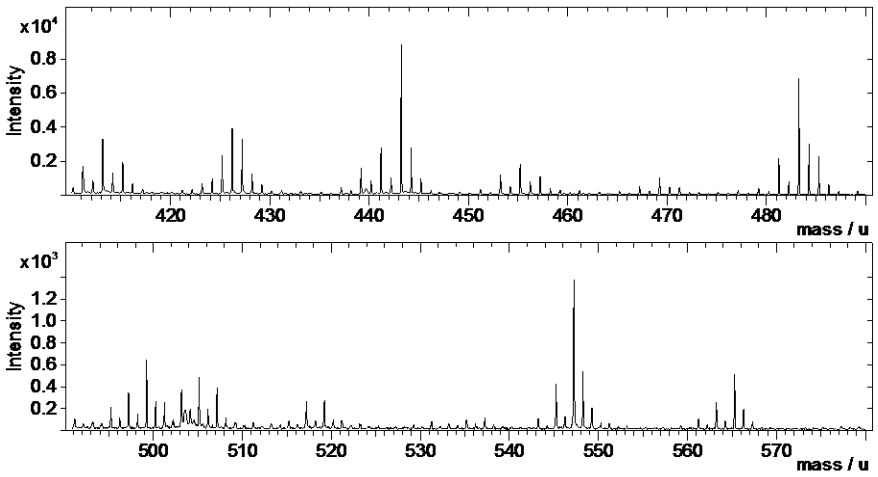

Figure 39. Portion of a typical ToF SIMS spectrum of rhodamine SAM on quartz ZP substrates.

2.2.1.2 Spectroscopic characterization estimation of the surface coverage

As described above, the rhodamine B derivative was chosen because of its excellent optical properties. In fact it has very high ε value and fluorescence yield, and this makes it possible the monitoring of the optical properties even in monolayer form. In Figure 40 UV-visible spectra of the rhodamine B phosphonate derivative are shown, obtained both from a solution and from the anchored system. First of all we notice that the spectrum of the derivative is virtually identical to that of the underivatized molecule, indicating a negligible influence of the alkylphosphonic chain on the optical properties of the molecule. Moreover, the spectrum obtained from the solution and the one obtained from the anchored system appear very similar, with no significant changes in the position of the absorbtion band.

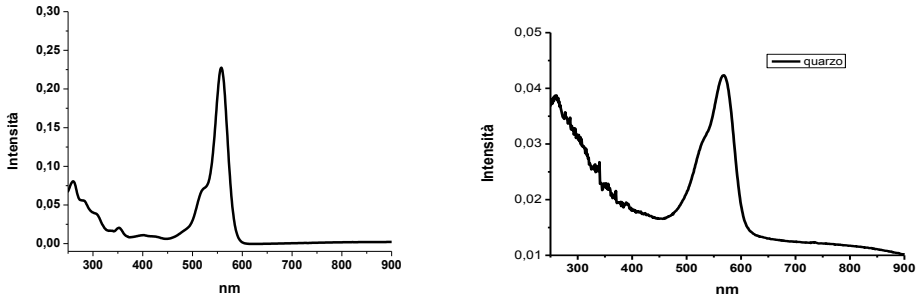

Figure 40. UV-visible spectra of phosphonate rhodamine B in solution (left) and on quartz (right).

Also the emission spectrum of the anchored system remains unchanged with respect to the system in solution, as shown in figure Figure 41 where absorption and emission spectra are reported for both cases. The lack of variation in optical properties indicates that the electronic levels of the molecule are not appreciably affected by the anchoring. Bearing this in mind,

we can assume that the molar absorption coefficient obtained from measurements in solution can be used for quantifying the amount of rhodamine molecules adsorbed on the surface. Such a calculation leads to a coverage of about 10^{14} molecules/$cm^{2.}$ This, in turn, corresponds to an area/molecule of 10^{-14} cm^2 i.e. an average molecular radius of ~1 nm, which is consistent with the molecular dimensions of the rhodamine B that are estimated to be comprised between 0,7 nm and 1,3 nm depending on its geometrical arrangement on the surface. In view of this we can conclude that the coverage obtained is of the same order of the maximum possible number of rhodamine molecules that can be packed at the surface, i.e the measurements suggest that an approximately complete monolayer i is formed.

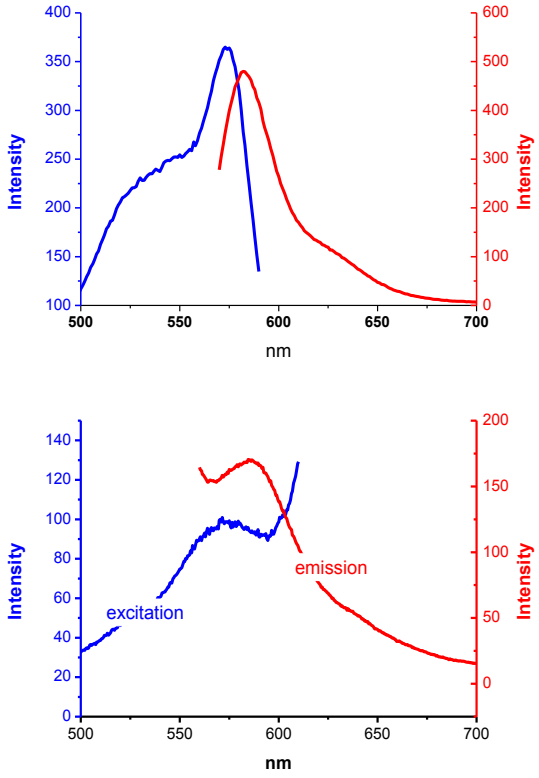

Figure 41. Absorption and emission spectra of phosphonate rhodamine B in solution (upper part) and on quartz (bottom part).

2.2.2 TiO2 functionalization

We have already seen that ZP method allows us to obtain compact dye monolayers on quartz. This part of the PhD thesis work was aimed to the extension of the ZP anchoring method on TiO_2 substrates, also in view of the possible technological applications, especially in solar energy conversion devices. We checked the method by using used different phosphonate-derivatized molecules on variously prepared titania substrates.
In particular three different kinds of substrate were used:

- TiO_2 nanoparticles dispersion (average diameter 20 nm, anatase, Sigma Aldrich)
- TiO_2 thin films grown by hydrolysis of $TiCl_4$ (flat TiO_2) on a transparent conducting substrate (FTO, fluorine-doped tin oxide);
- TiO_2 nanoporous films deposited on FCO using the "doctor blade" technique.

TiO_2 on solid substrates was treated as described for quartz substrates: samples were treated for 15 minutes in UV-O_3, rinsed in pure water, and subsequently msurface modified by means of the ZP.
In the case of titania nanoparticles an analogous treatment was performed, with the only difference that, after each treatment and rinsing stage centrifugation steps are necessary for separating the treated nanoparticles (typical conditions 5000 rpm for 10 min).
In Figure 42 we report the relevant portions of ToF SIMS spectra obtained after the ZP treatment of TiO_2 nanoparticles (deposited on gold from a dispersion in ethanol), TiO_2 thin film ("flat") and TiO_2 nanoporous film respectively. In all the spectra, characteristic peaks diagnostic of the ZP modification are observed, including ZrO^+, ZrO_2H^+, $ZrPO_5H_2^+$. This indicates that the ZP treatment is effective on all the studied samples.
After having established that the ZP treatment is feasible on titania surfaces, anchoring experiments with with molecules bringing phosphonate groups were carried out. In particular, we performed the anchoring of a phosphonic acid-

derivatized ruthenium complex, $[Ru^{II}(bpy)_2(4,4'\text{-}(PO_3H_2)_2bpy)]Cl_2$ (where bpy stands for bipyridyl group, see Figure 43 for the complex structure).
In Figure 44 we report the relevant parts the ToF SIMS spectra obtained after anchoring of the complex on the three above discussed ZP-treated titania surfaces. For all the samples is possible to confirm that the complex is anchored to the substrate on the basis of the presence of ions fragments related with the ruthenium complex structure, including $[Ru(C_{10}H_{14}N_2)]^+$ and $[Ru(C_{10}H_{14}N_2)_2]^+$

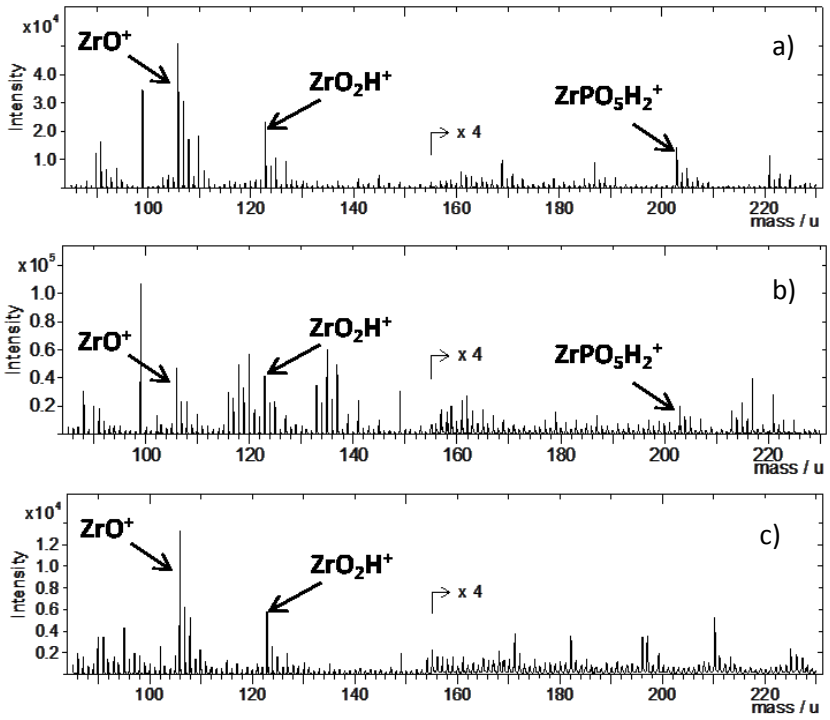

Figure 42. Portions of ToF SIMS spectra of after ZP treatment of TiO_2 samples: (a) flat surface, (b) nanoporous film, (c) nanoparticles deposited on gold.

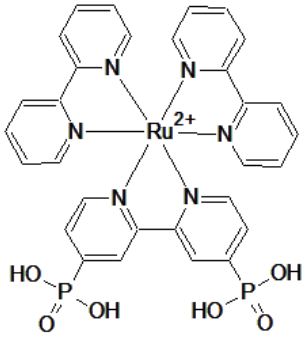

Figure 43. Structure of [Ru (bpy)$_2$(4,4'-(PO$_3$H$_2$)$_2$bpy)]Cl$_2$

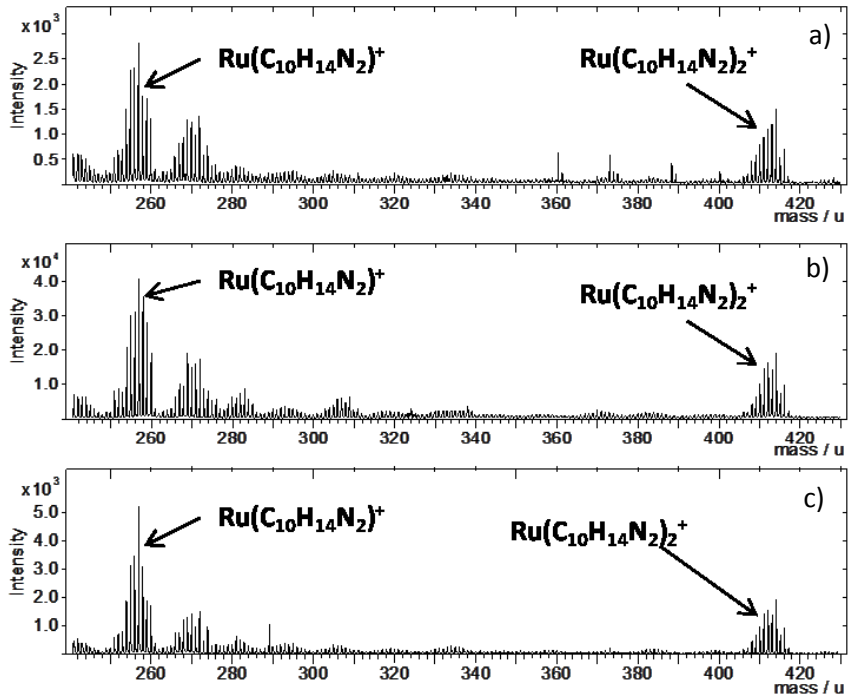

Figure 44. Portions of ToF SIMS spectra of TiO2 ZP (a) flat, (b) nanoporous film, (c) nanoparticles after the immersion in ruthenium complex solution and careful rinsing.

2.2.3 Thermal stability of the layers anchored on TiO_2 *via* ZP procedure

A general problem when a dye is anchored on a substrate, is the stability of the bond. Although it is known from literature that the direct anchoring of phosphonate moieties on titania surfaces is more effective that that obtained by means of the widely used carboxylic function, no data are avalaible that allow to compare the stability of phosphonate anchoring on titania surfaces with that on ZP-treated titania surfaces. For this reason we set-up a simple experiment aimed to this comparison, consisting in prolonged rinsing with boiling ethanol of the layers anchored on bare titania surfaces and ZP-treated ones. Monitoring of the amount of "surviving" anchored molecules was performed via UV-Vis spectroscopy. Among the different types of titania substrates the choice fell on the flat type, because the low roughness (compared with that of the nanoporous substrates or nanoparticles) allows a better reproducibility and comparability of the experimental results. The natural choice for the molecule to anchor was on the derivatized rhodamine B already used for studying the surface coverage on ZP treated quartz surfaces, in view of its favourable optical properties (already outlined in the previous section) and of its high thermal stability (the decomposition temperature of underivatized dye is 570 K).
Self assembled monolayers of the dye were prepared in the already described way, i.e. by immersing substrate samples in an ethanol solution (~10^{-4} M) for 24 hours and then rinsing them with the solvent. We applied the same procedure ZP-treated and bare ("noZP") flat titania samples.
Figure 45 reports the ToF SIMS spectra for both ZP and noZP samples after the formation of the rhodamine SAM. In both spectra the presence of the fingerprint peaks related to rhodamine is observed, qualitatively indicating that both anchoring strategies work correctly.

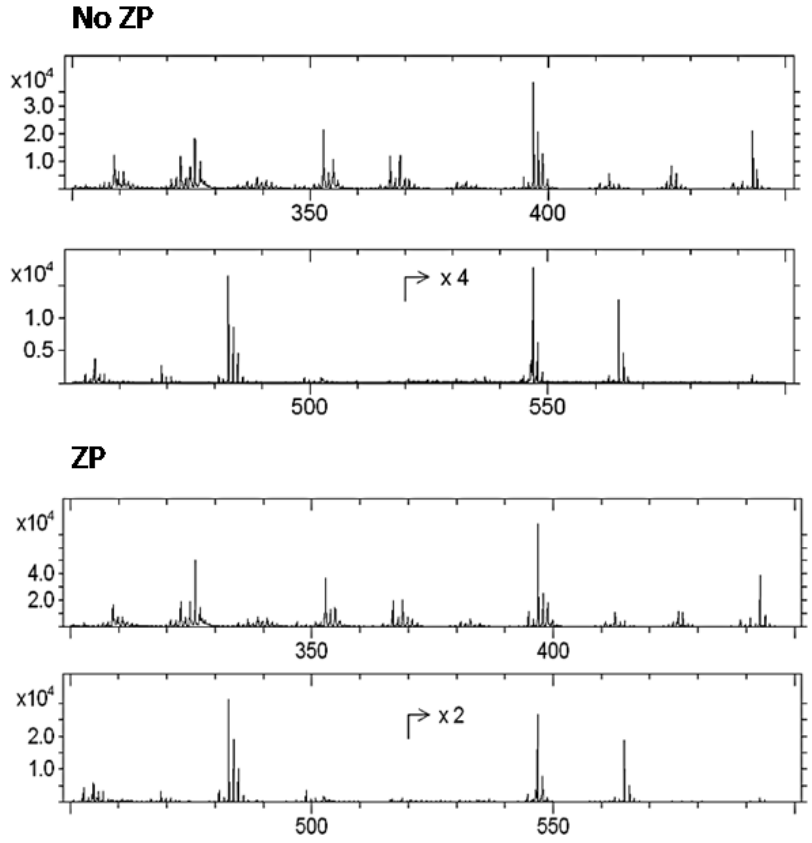

Figure 45. Portions of ToF SIMS spectra of a rhodamine SAM on TiO2 (up) and TiO2 ZP (down).

In Figure 46 UV-visible spectra of rhodamine B SAMs on both ZP and noZP titania surfaces are reported. Noticeably, the intensity of the absorption band is very similar, indicating that the surface coverage on both surfaces is comparable. A small red-shift of the band pertaining to the noZP sample, compared with the ZP-treated one, is observed. This could be related with a slightly different interaction of the molecule with the semiconducting

substrate. At this stage we do not have a clear explanation for this effect, that deserves however future investigation.

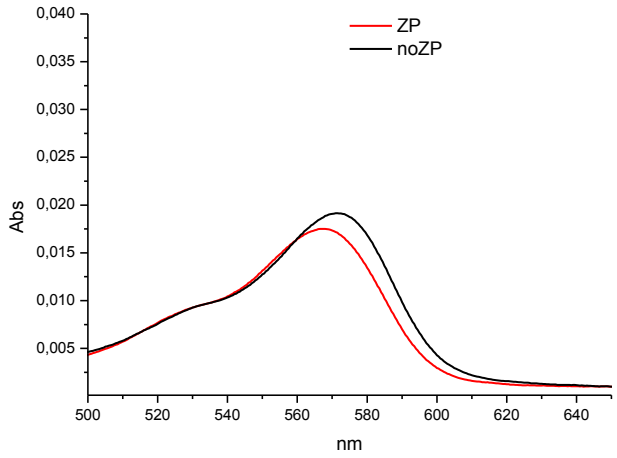

Figure 46. UV-visible spectra of rhodamine SAM on TiO2 flat ZP (red) and noZP(black).

The thermal stability tests of the bonding between dye molecules and substrate surface were carried out by immersing the specimens in boiling ethanol (reflux, 78°C). UV-Vis spectra were recorded after different immersion times, in order to monitor the eventual desorbtion of dye molecules by means of variation of the absorbance. It must be remarked that rhodamine B, *per se*, is very stable up to temperatures much higher to that used in the test (it decomposes at 570K), [72] and this allows us to state that any decrease of surface concentration of the dye can be related to its desorbtion from the surface rather than to its decomposition.
Figure 47 reports the UV-visible spectra recorded after different immersion times in hot ethanol. In the case of the noZP substrate a significant decrease the band intensity is observed, while in the case of the ZP treated samples the decrease appears to be less pronounced. A more quantitative picture of such effect is given by the plots of Figure 48, where absorbance (at the wavelength

of the maximum) is reported as function of immersion time. The different behaviour of the two types of samples is evident: while the intensity of the band of the monolayer anchored on noZP substrates drops of about one order of magnitude (almost to zero) after about 30 minutes, the intensity of the band of the monolayer on ZP-treated titania is reaches a constant value that is about 50% of the original one and is maintained constant also after immersion times as long as 20 hours.

These finding clearly demonstrate a strong stability of the ZP anchoring: the relatively small decrease of surface coverage is probably connected with the desorbtion of molecules that are adsorbed on the surface through weaker interactions, such as – for example – π-stacking interactions.

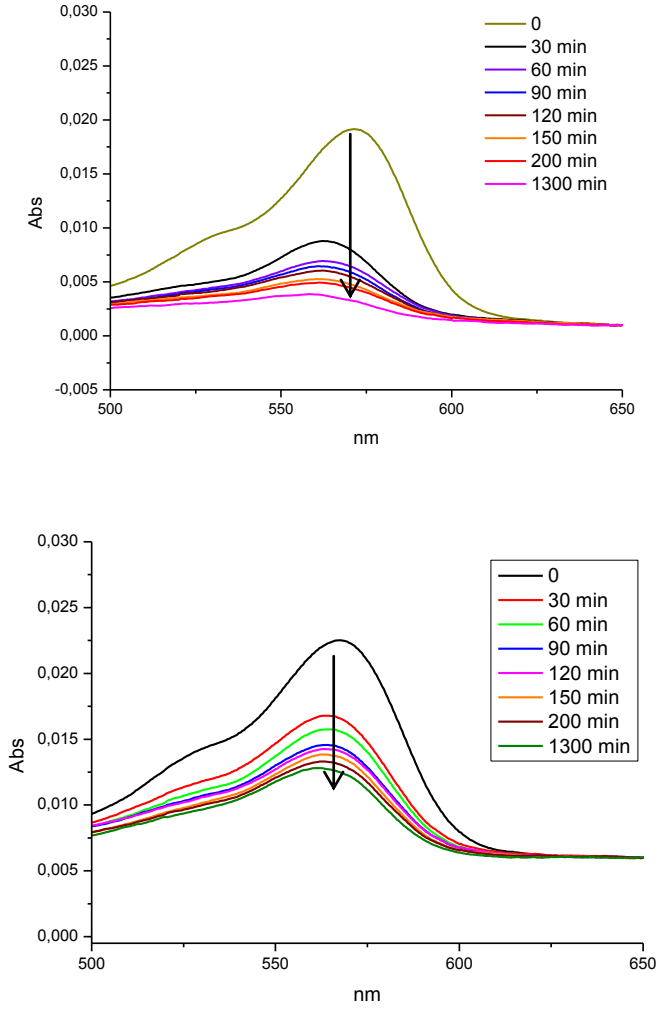

Figure 47. UV-visible spectra of rhodamine on TiO2 ZP (down) and noZP (up) recordered at different time of temperature treatment.

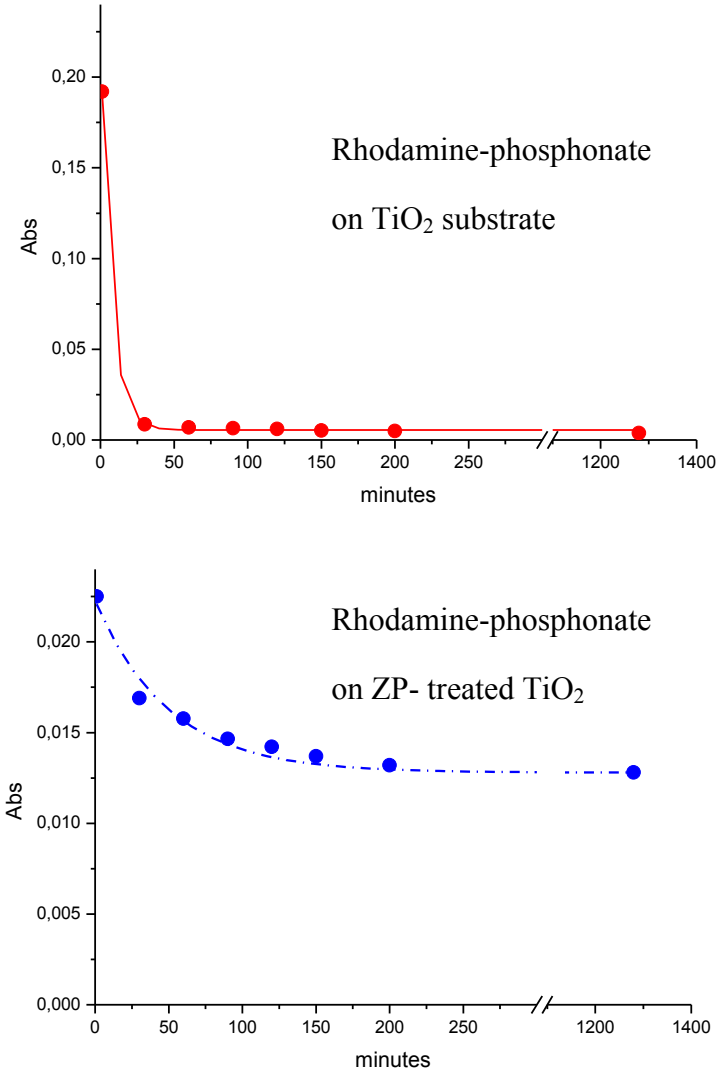

Figure 48. Plot of the absorbance value at λ_{max} as a function of the time in boiling ethanol for the rhodamine dye anchored on bare TiO_2 and on ZP-treated TiO2 surface

2.2.4 Self assembly of a sensitizer/catalyst bi-layer for photo-induced water splitting

Several examples are reported in literature about systems that can perform the photoinduced water oxidation. It is well known that, in order to improve the efficiency of the process, it is necessary to choose an appropriate system of photosensitizer and catalyst. A promising system was shown by Campagna et al; [73] in that paper they show the efficiency in oxygen evolution of the ruthenium complex $[Ru\{(m\text{-}dpp)Ru(bpy)_2\}_3](PF6)_8$ (bpy = 2,2'-bipyridine; dpp = 2,3-bis(2'-pyridyl)pyrazine as photosensitizer and a $[Ru_4(m\text{-}O)_4(m\text{-}OH)_2(H_2O)_4(g\text{-}SiW_{10}O_{36})_2]^{10-}$ as catalyst. They demonstrate that in solution it is possible to obtain a photon-to-oxygen quantum yield Φ=0.3, that is a very high value considering that the maximum value possible for this process is Φ=0.5.

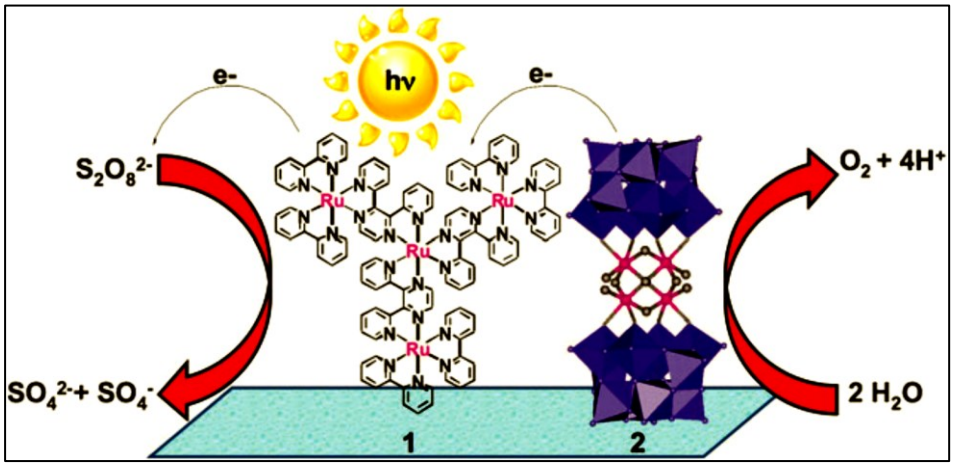

Figure 49. Photocatalytic water oxidation powered by the interplay of tetra-ruthenium sensitizer/catalytic sites of 1 and 2.

The above reported demonstration of feasibility of photoinduced oxidation of water can be exploited in a real device only if the sensitizer and the catalyst are assembled on a semiconductor substrate that will act as the electron acceptor in place of the sacrificial thiosulfate molecules used in the homogeneous phase experiment. For this reason, in the framework of the present PhD thesis, a study was started, with the aim of exploring the possibility of immobilization of both sensitizer and catalyst onto a TiO_2 substrate electrode. We decided to make use of the ZP anchoring strategy, as described in the previous section, turned out to be suitable for stable anchoring of dyes on oxide surfaces and titania in particular. To this aim, a tetranuclear ruthenium complex functionalised with phosphonic groups (synthesized by the group of prof. Campagna) was used. The structure of the complex, very similar to that reported in ref. 73, is shown in Figure 50.

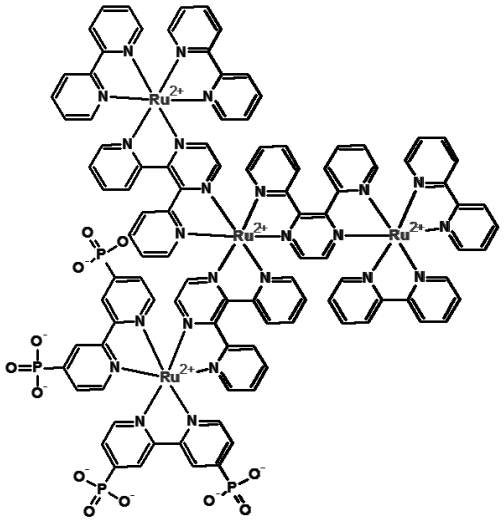

Figure 50. Molecular structure of Ru{[(m-dpp)Ru(bpy)$_2$]$_2$[(m-dpp)Ru(dpb)$_2$]}

The self assembled layer of the complex was obtained by immersing for 24 hours a ZP-treated flat titania substrate in an acetonitrile solution of the complex. The formation of the anchored monolayer was monitored by means of ToF SIMS and UV-visible spectroscopy.

ToF-SIMS spectra, reported in Figure 51, show the presence of several peaks related to the presence – at the sample surface – of the ruthenium complex, including fragments such as $[C_{10}H_8N_2Ru]^+$ (m/z 257, a bipyridyl ligand linked to one ruthenium ion), $[(C_{10}H_8N_2)_2Ru]^+$ (m/z 414, two bipyridyl ligands plus a ruthenium ion), $[C_{14}H_{10}N_4Ru]^+$ (m/z 335, one pyrazine ligand + one ruthenium) and $[(C_{10}H_8N_2)(C_{14}H_{10}N_4)Ru]^+$, a fragment constituted by a pyrazine unit, a bipyridyl unit and a ruthenium ion.

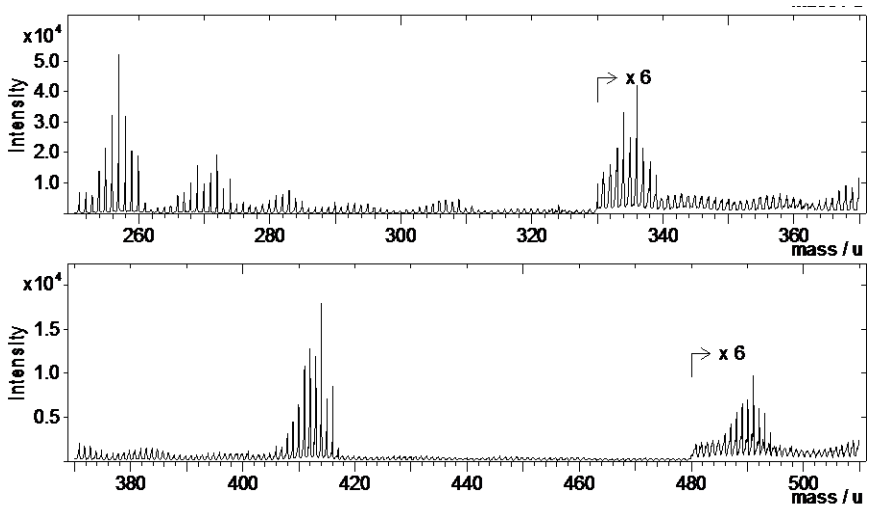

Figure 51. Portion of a typical ToF SIMS spectrum of a TiO2 ZP treated after the formation of the SAM of tetranuclear complex.

The UV-VIS spectrum of the self assembled monolayer of the tetranuclear complex on TiO_2 is reported in Figure 52 together with the spectrum obtained from a solution of the same complex. We note that, similarly to what we observed in the case of rhodamine adsorption, no important changes in the optical properties are observed when comparing the solution with the self assembled dye monolayer.

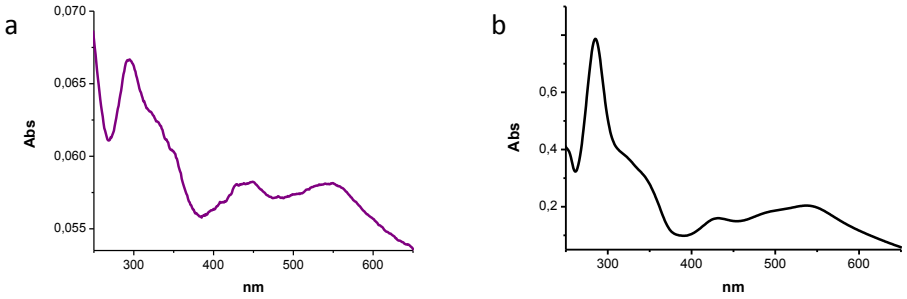

Figure 52. UV-visible spectra of Ru{[(m-dpp)Ru(bpy)$_2$]$_2$[(m-dpp)Ru(dpb)$_2$]} (a) on TiO2 substrate and (b) in solution

For immobilizing the catalyst on the solid electrode it is possible to exploit the electrostatic interaction between the positively charged ruthenium complex and the negatively charged POM. Thus, samples with the anchored ruthenium complex were immersed in an aqueous solution of the POM for 24 hour, and then rinsed with water.

The ToF SIMS negative ions spectra, reported in Figure 53 show some characteristics peaks related to the presence of POM on surface; in particular it is possible to individuate $[W_2O_6]^-$ and $[W_2O_7H]^-$, $[W_2RuO_7]^-$ and $[W_2RuO_8]^-$.

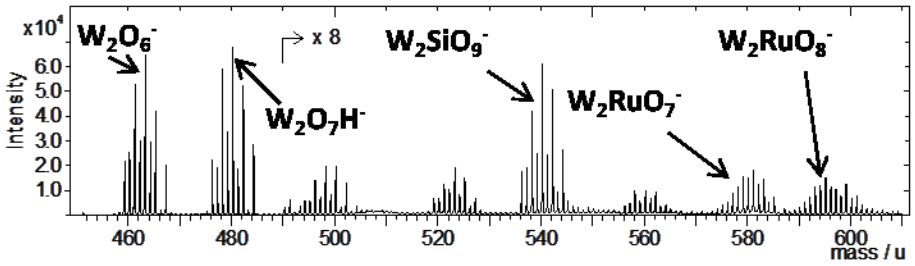

Figure 53. Portion of a typical ToF SIMS spectrum of a TiO2 ZP treated after the formation of the bilayer tetranuclear complex/POM .

2.3 Conclusions

In this part of the thesis we studied the anchoring, on oxide surfaces, of phosphonic-acid-derivatized molecules. The method we used is based on the functionalization of the surface with a zirconium IV monolayer (ZP method) and its subsequent interaction with the phosphonic groups of the molecules to be attached. The method is well suited for efficient anchoring of phosphonic moieties on oxides of different nature (we considered quartz and titanium oxide) and different morphology (flat surfaces, nanostructured films, nanoparticles) and it allows the formation of stable and densely packed monolayers.

Time-of-flight mass spectrometry and electronic spectroscopy were used for characterizing a variety of films formed by self assembly on the oxide surfaces primed with the ZP method. The described methodology is able to produce densely packed monolayers, as shown in experiments were a rhodamine B derivative was used as probe adsorbing molecule. The same dye was exploited for testing the stability of the ZP anchoring onto TiO_2 surfaces, and it turned out that the self-assembled layers produced in this way are by far more stably linked to the surface than the analogous films prepared by direct interaction of the phosphonic groups with the bare TiO_2 surface. This finding could have a relevant impact in the improvement of durability of dye sensitized devices for solar energy conversion, provided that one is able to demonstrate that the presence of the zirconium based monolayers has no (or limited) detrimental effect on the electron transfer process from the dye to the semiconductor oxide.

Once established, the method was used for stable anchoring of ruthenium complexes on titanium oxide, which was demonstrated for a variety of morphologies including flat surfaces, nanoparticles and nanostructured porous films. Finally, we demonstrated the feasibility of preparation of a sensitizer/catalyst bilayer system immobilized onto a TiO_2 electrode, which is of possible interest in photochemical water splitting devices. It consists of a

tetranuclear ruthenium complex monolayer anchored on the substrate via the ZP method, overlaid by a polyoxometalate layer self assembled onto the Ru-complex layer through electrostatic interactions.
In conclusion, the results described in this chapter allow us to propose the ZP anchoring method as a possible valid alternative for anchoring dyes (and more generally functional molecular and supramolecular systems) on oxide surfaces. Although the study was focused on systems of interest for solar energy conversion applications, the used methodologies can be easily extended to other fields where stable anchoring of organic molecules on oxide surfaces is needed.

2.4 References

[1] Nocera D.G. InorgChem 2009, 48, 10001–10017

[2]Cook T.R., Dogutan D.K., Reece S.Y., Surendranath Y., Teets T.S., Nocera D.G. Chem Rev 2010, 110, 6474–6502

[3] Hasan M.A., Sumathy K. Renewable and Sustainable Energy Reviews 2010, 14, 1845–1859.

[4] Meyer T.J. AccChem Res 1989, 22, 163– 170

[5] Dubois D.L. AccChem Res 2009, 42, 1974–1982

[6] Morris A.J., Meyer G.J., Fujita E. AccChem Res 2009, 42, 1983–1994

[7] Concepcion J.J., Jurss J.W., Brennaman M.K., Hoertz P.G., Patrocinio A.O.T., Murakami Iha N, Templeton J.L.and Meyer T.J. AccChem Res 2009, 42, 1954–1965

[8] Walter, M. G.; Warren E. L.; Boettcher S. W.; Mi, Q.; McKone, J. R.; Santori, E. A.; Lewis, N. S. Chem. Rev. 2010, 110, 6446-6473.

[9] Koike K., Naito S., Sato S., Tamaki Y., Ishitani O. J PhotochemPhotobiol A Chem 2009, 207, 109–114

[10] Takeda H., Koike K., Inoue H., and Ishitani O. J Am ChemSoc 2008, 130, 2023–2031

[11] Tributsch H. . PhotochemPhotobiol 1972, 16, 261–269

[12] O'regan B.,Gratzel M. Nature1991, 353,737–40.

[13] Katoh R., Furube A., Barzykin A.V., Arakawa H., Tachiya M. CoordChem Rev 2004, 248, 1195–1213

[14] Gregg B.A. CoordChem Rev 2004, 248, 1215–1224.

[15] Galoppini E. CoordChem Rev 2004, 248,1283–1297.

[16] Anderson N.A., Lian T. CoordChem Rev, 2004, 248, 1231–1246.

[17] Asbury J.B., Anderson N.A., Hao E., Ai X., and Lian T. J. Phys. Chem. B, 2003,107, 7376–7386

[18] J. Nelson, Phys. Rev. B: Condens. Matter Mater. Phys., 1999, 59, 15374–15380

[19] Grätzel M. Nature, 2001, 414, 338–344

[20] Ikeda S., Abe C., Torimoto T.and Ohtani B., J. Photochem. Photobiol.A, 2003, 160, 61–67.

[21] Jiang D.L., Choi C.K., Honda K., Li W.S., Yuzawa T.and Aida T., J. Am. Chem. Soc., 2004, 126, 12084–12089.

[22] Kato C. N., Hara K., Kato M., Amano H., Sato K., Kataoka Y. and Mori W., Materials, 2010, 3, 897–917

[23] Frischmann P.D., Mahata K.and Würthner F. Chem. Soc. Rev., 2013, 42, 1847-1870

[24] de Souza F. L. and. Leite E. R (eds.), Nanomaterials for Solar Energy Conversion, Nanoenergy, Springer-Verlag Berlin Heidelberg 2013

[25] Nazeeruddin, M. K.; Kay, A.; Rodicio, I.; Humphry-Baker, R.; Mueller, E.; Liska, P.; Vlachopoulos, N.; Graetzel, M. J Am ChemSoc 1993,115, 6382–6390

[26] Nazeeruddin M.K., Gratzel M. J PhotochemPhotobiol A Chem 2001, 145, 79–86

[27] Polo A. S., Itokazu M. K. and Murakami Iha N. Y., Coord. Chem. Rev., 2004, 248, 1343–1361.

[28] J. Meyer, Inorg. Chem., 2005, 44, 6852–6864.

[29] Griffith M. J., Sunahara K., Wagner P., Wagner K., Wallace G. G., Officer D. L., Furube A., Katoh R., Mori S. and Mozer A. J., Chem. Commun., 2012, 48, 4145–4162.

[30] Kalyanasundaram, K., Kiwi J.and Graetzel, M., Helv. Chim. Acta, 1978, 61, 2720–2730.

[31] Kalyanasundaram, K. and Graetzel, M., Angew. Chem., Int. Ed. Engl., 1979, 91, 759–760.

[32] Caspar, J. V. and Meyer, T. J., Inorg. Chem., 1983, 22, 2444–2453.

[33] Demas J.and Taylor D., Inorg. Chem., 1979, 18, 3177–3179.

[34] Morris, N.D.; Suzuki M., Mallouk T.E., J. Phys. Chem. A 2004, 108, 9115-9119

[35] Geletii, Y.V.; Botar, B.; Gerler, P.K.; Hillesheim, D.A.; Musaev, D.G.; Hill, C.L., Angew. Chem. Int. Ed.2008, 47, 3896 –3899

[36] Geletii, Y.V.; Huang, Z.; Hou, Y.; Musaev, D.G.; Lian, T.; Hill, C.L, J. Am. Chem. Soc. 2009, 131, 7522–7523

[37] Puntoriero, F.; La Ganga, G.; Sartorel, A.; Carraro, M.; Scorrano G.; Bonchio M.; Campagna S., Chem. Commun., 2010, 46, 4725–4727 | 4725

[38] La Ganga, G.; Francesco Nastasi, F.; Campagna S.; Puntoriero F., Dalton Trans.2009, 9997–9999

[39] Que, L.; Tolman, W. B. Angew. Chem., Int. Ed. 2002, 41, 1114–1137;

[40] DeGrado, W. F.; Di Costanzo, L.; Geremia, S.; Lombardi, A.; Pavone, V.; Randaccio, L. Angew. Chem., Int. Ed. 2003, 42, 417–420.

[41] McEvoy, J. P.; Brudvig, G. W. Chem. ReV.2006, 106, 4455–4483

[42] Long, D.; Burkholder, E., Cronin, L., Chem. Soc. Rev.2007, 36, 105-121

[43] Sartorel, A., Carraro, M., Scorrano, G., Bonchio, M.; Energy Procedia, 2012, 22, 78-87

[44] Howells, A.R, Sankarraj, A., Shannon, C.; J. Am. Chem. Soc.2004, 126, 12258-12259

[45] Sartorel, A.; Carraro, M.; Scorrano, G.; De Zorzi, R.; Geremia, S.; McDaniel, N.D.; Bernhard, S.; Bonchio, J. Am. Chem. Soc.2008, 130, 5006-5007.

[46] Geletii, Y.V., Huang, Z., Hou, Y., Musaev, D.G., Lian, T., and Hill, C.L. J. Am. Chem. Soc. 2009, 131, 7522–7523.

[47]Sartorel, A., Miro´, P., Salvadori, E., Romain, S., Carraro, M., Scorrano, G., Di Valentin, M., Llobet, A., Bo, C., and Bonchio, M. J. Am. Chem. Soc.2009, 131, 16051–16053

[48] Aswal, D. K.; Lenfant, S.; Guerin, D.; Yakhmi, J. V.; Vuillaume, D. AnalyticaChimicaActa, 2006, 568, 84-108.

[49] Janos H. Fendler; Chem. Mater. 2001, 13, 3196-3210.

[50] Brzoska, J. B.; Ben Azouz, I.; Rondelez, F. Langmuir 1994, 10, 4367–4373.

[51] Silberzan, P.; Leger, L.; Ausserre, D.; Benattar, J. J. Langmuir 1991, 7, 1647–1651.

[52] Le Grange, J. D.; Markham, J. L.; Kurkjian, C. R. Langmuir 1993, 9, 1749–1753.

[53] Brzoska, J. B.; Shahidzadeh, N.; Rondelez, F. Nature 1992, 360, 719-721.

[54] Ashkenasy, G.; Cahen, D.; Cohen, R.; Shanzer, A.; Vilan, A. Accounts of Chemical Research 2002, 35, 121-128.

[55] Pe´chy, P.; Rotzinger, F. P., Nazeeruddin, M. K.; Kohle, O.; Zakeeruddin, S. M.; Humphry-Baker, R.; Gra¨tzel, M. J. Chem. Soc., Chem. Commun. 1995, 65.

[56] Trammell, S. A.; Moss, J. A.; Yang, J. C.; Nakhle, B. M.; Slate, C. A.; Odobel, F.; Sykora, M.; Erickson, B. W.; Meyer, T. J. Inorg. Chem. 1999, 38, 3665.

[57] Gillaizeau-Gauthier, I.; Odobel, F.; Alebbi, M.; Argazzi, R.; Costa, E.; Bignozzi, C. A.; Qu, P.; Meyer, G. J. Inorg. Chem. 2001, 40, 6073.

[58] Merrins, A.; Kleverlaan, C.; Will, G.; Rao, S. N.; Scandola, F.; Fitzmaurice, D. J. Phys. Chem. B 2001, 105, 2998

[59] Qu, P.; Meyer, G. J. Langmuir, 2001, 17, 6720.

[60] Bae, E., Choi,W., Park,J., Shin, H.S., Kim,, S.B. and Lee, J.S. J. Phys. Chem. B, 2004, 108, 14093-14101

[61] Taylor, C. E.; Schwartz, D. K. Langmuir, 2003, 19, 2665-2672.

[62] Troup, J. M., Clearfield, A. Inorg. Chern. 1977, 16, 3311-3314.

[63] Kohli, P.; Blanchard, G. J., Langmuir, 2000, 16, 695-701.

[64] Kohli, P.; Blanchard, G. J., Langmuir, 1999, 15, 1418-1422.

[65] Bakiamoh, S.B.; G.J. Blanchard, G. J., Langmuir, 1999, 15, 6379-6385.

[66]Morotti, T.; Calabrese, V.; Cavazzini, M.; Pedron, D.; Cozzuol, M.; Licciardello, A.; Tuccitto, N.; Quici, S. Dalton Trans. 2008, 22, 2974–2982.

[67]Spampinato, V., Tuccitto, N., Quici, S., Calabrese, V., Marletta, G., Torrisi, A., Licciardello, A. Langmuir, 2010, 26, 8400-8406

[68] V. Spampinato, surf interf

[69] Ramette, R.W., Sandell, E.B., J. Am. Chem. Soc, 1956, 78, 4872-4878.

[70] M.Barra, J.J. Cosa, R.H. de Rossi, J. Org. Chem.,1990, 55, 5850-5853.

[71] Ross, D., Gaitan, M., Locascio, L.E., Anal. Chem., 2001, 73, 4117,4123;

[72]Fujii, T., Ishii, A. Journal of Photochem. and Photobiol. A, 1990, 54, 231-237.

[73] Puntoriero, F.; La Ganga, G.; Sartorel, A.; Carraro, M.; Scorrano G.; Bonchio M.; Campagna S., Chem. Commun., 2010, 46, 4725–4727.

3 Molecular depth profiling of organics and polymers

Organic electronics have, at least in principle, several advantages compared to inorganic electronics, including the tunability of chemical properties, compatibility with plastic substrates, and low cost. In particular, semiconductor polymers play an important role due to their applications in optoelectronic devices such as light-emitting diodes (OLEDs), field-effect transistors (FETs), and photovoltaic devices. Polymers can assemble forming ordered structure for efficient transport of charges, preferably along the polymeric conjugated chain. Many studies demonstrate that pentacene derivatives, oligothiophenes, and poly(3-alkyl-thiophenes) (such as poly-3-hexyl-thiophene, P3HT) are good materials for efficient charge transport, and several examples show that is possible to combine different kind of polymers, oligomers, and molecules to improve the efficiency of the device. To understand the mechanism of the charge transport, as well as for improving the performances of the devices, morphological and chemical characterization of these systems is necessary, both at the surface and along the depth.

In particular in this application field it is necessary to have analysis techniques able to give "in depth" information not only about the elementary composition but also about the molecular structure. In other words, in order to characterize layered (or graded composition) organic and polymeric systems, it is necessary to obtain "molecular depth profiles". Although since many decades several techniques are available for obtaining depth profiles of solid samples, such as sputtering-based techniques (SIMS, Auger or XPS depth profiling, plasma based techniques), scattering methods (Rutherford backscattering,) and others (NRA - Nuclear Reaction Analysis, ERDA – Elastic Recoil Detection), the most part of them is well suited for providing only elemental information . This is clearly not sufficient when interested in the study of organic layers, that often display very similar elemental composition in spite of the large differences in chemical structure.

Among the well established depth profiling techniques, those based on mass spectrometry of sputtered material (including secondary ion mass spectrometry

[SIMS], sputtered neutrals mass spectrometry [SNMS], glow discharge mass spectrometry [GD-MS], and others) are widely used mostly because of the unparalleled sensitivity, the depth resolution and the possibility (in the case of SIMS and some SNMS methods) of coupling depth profiling capabilities with high lateral resolution imaging capabilities, so allowing to perform three-dimensional characterization.

However the use of these techniques for in-depth analysis of organic and polymer samples has been unfeasible for many years and the application of sputtering-based techniques (and in particular of the most powerful of them, i.e. SIMS) were in practice limited to the depth profiling of inorganic samples.

This limitation is essentially due to the damage phenomena that occur as a consequence of the interaction between the organic material and the energetic particles, that can modify the organic material in a so large extent (mostly due to ion-beam-induced chemical reactions) to make virtually impossible to recognize its original composition along the depth. For the above reasons for many years the use of secondary ion mass spectrometry in the field of organic and polymer materials was confined to the study of their very outer surface (i.e. the outermost monolayer), thanks to the possibility of performing the measurements in the so-called Static-SIMS mode, that prevents the accumulation of damage but, on the other hand, doesn't give access to the inner layers of the material.

Relatively recently, the introduction of the so-called cluster-SIMS (see next paragraph) made possible, although with some limitations, the in-depth analysis of organics and polymers ("molecular depth profiling").

This part of the thesis was dedicated to the development and application of cluster-SIMS methods to depth profiling of layered polymers, with the aim of applying it to systems of interest in organic electronics.

In particular, since we were interested in studying in-depth inhomogeneities in polimer materials, layered systems were prepared by using polyelectrolites. Once the method was set-up, it was applied for a preliminary study of vertical separation in oligothiophene mixtures suitable for molecular electronics applications.

3.1 Cluster SIMS

As mentioned above, secondary ion mass spectrometry has been used in the past mostly for depth profiling of inorganic materials (dynamic SIMS) or for the study of the surface of both inorganic and organic materials (static SIMS). In static SIMS mode it is possible to obtain molecular information from surfaces since the primary beam fluence during the entire measurement is maintained so low that the accumulation of damage can be considered negligible. In static conditions only a few percent of a monolayer is removed from the surface, so no depth profiling is possible. The static SIMS limit for the analysis of organics and polymers was recently overcame with the introduction of the so called cluster SIMS, [1-2] in which polyatomic ions, such as C_{60}^+, Au_3^+, SF_5^+ e Bi_3^+, Ar_n^+ ($n \approx 400 - 4000$) are used for the erosion of the material. The use of a cluster ion beam has considerable influence on the sputtering yield and damage accumulation. When a cluster ion impacts a surface, it breaks into its *n* constituent atoms, and the initial energy of the cluster is shared to them accordingly with energy and momentum conservation. This causes a lower depth penetration of the ion beam and. as a consequence, the damage effect is confined in a thinner layer of material near the surface. Moreover since the *n* atomic constituents of the cluster impact in the same place of the sample, a space- and time- overlap on *n* collision cascades occurs near the surface, and this cause a non linear increase of the sputter yield (i.e. the amount of material sputtered by a cluster formed by n atoms is usually much larget than n times the amount sputtered by a monoatomic ion). The combination of these two effect makes possible to remove a large amount of the material that was damaged by the ion impact, so ideally leaving unchanged the material layers just below those that have been removed, thus allowing to obtain a molecular depth profile.

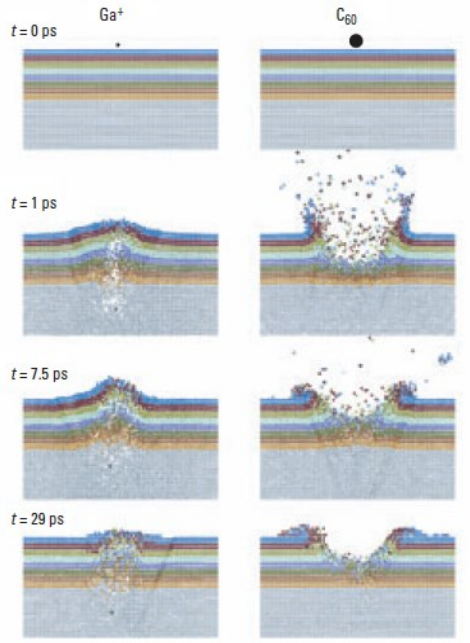

Figure 54. Simulation of molecular dinamics of the bombardment of an Ag substrate with Ga+ e C60+ ions at a 15 keV .

Such a (idealized) description is corroborated by the results of molecular dynamics calculations, an example of which is given in Figure 54.[3]

In the case of polymer systems, the first molecular depth profile (of a PMMA film) was obtained by Gillen et al. [4] by using a SF_5^+. Since this pioneeristic study, many other investigations on the use of cluster ions for depth profiling of polymers were carried out, including many computer simulations attempting to individuate the key parameters influencing the cluster-induced sputtering.[5-10]

In the case of polymeric substrates one of the main issues is that the possibility of obtaining a molecular depth profile (i.e. the "profilability") is strongly influenced by the chemical nature of the polymer. For example, under the same conditions that allow to obtain a "good" molecular depth profile of PMMA, it is impossible to obtain any profile from polystyrene. [11] In fact it is known that when an ion beam impacts a polymer reactive species (including radicals)

are formed as consequence of the energy transfer from the ion to the solid. These reactive species, of course, will give rise to reactions (many of them radical reactions) Reactive species then give rise to further reactions (for example radical reactions) which pathways and final products are different according to the chemical characteristic of the polymer. Generally when polymer is irradiated (with electrons, ions, particles, X ray) it undergoes degradation mainly because of radical reactions, that in many cases give rise to chain-scission or to cross-linking of the material. Chapiro [12] made a classification of polymers according to their different behaviour, distinguishing between type I polymers, in which the prevalent mechanism is the cross-linking, and type II polymers, in which the main mechanism is the main-chain scission that leads to low molecular weight products (in the case of quantitative production of monomeric units this is often referred as "unzipping"). In the context of molecular depth profiling this classification is important because if a mechanism occurs that leads to volatile products due to chain-scission, this makes easier the erosion of the material and on the other hand leaves the remaining solid chemically similar to the original one (although perhaps with a lower molecular weight). On the contrary, in the case of cross-linking new C-C bond are formed, and this leads to the progressive loss (with irradiation) of the original structure of the polymer, that is reflected in the impossibility of obtaining a meaningful molecular depth profile.

A typical example of type II polymer is the PMMA, that under cluster beam irradiation can be eroded (well beyond the "static" limit) thanks to a depolymerization reaction (unzipping) induced by the beam (Figure 55). The depolymerization of PMMA can be generated thermally at a temperature of about 360° C, but it is also known that the energy required to overcome the energy barrier of potential request to trigger the reaction of unzipping can be provided by a polyatomic beam. Therefore, the bombardment of PMMA with a cluster ion beam causes erosion *via* the removal of monomeric units and the progressive disappearance of the polymer. In fact the interaction of the incident ions with the surface of the polymer generates a series of tertiary radicals allowing the break of C-C bonds along the chain and facilitating the erosion process.

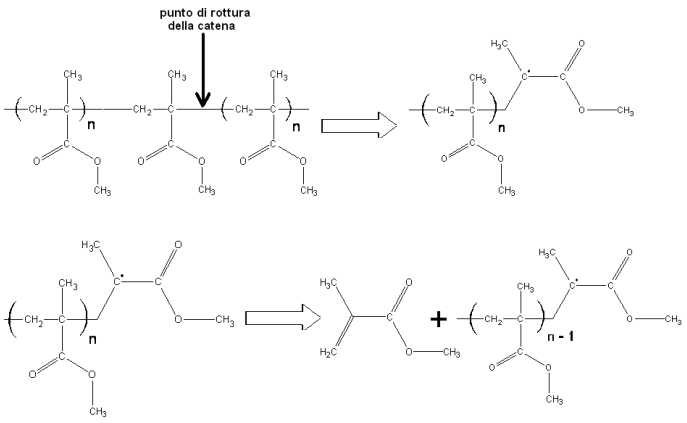

Figure 55. Schematic representation of unzipping mechanism of PMMA.

This kind of mechanism justifies the reason why polymers such as PMMA give rise, under cluster beam irradiation, to depth profiles in which the intensity of structure-related signals remain almost unchanged along the depth of the organic layer, until the interface with the substrate (or with another layer) is reached.

The behavior polymers such as PS, a type I polymer, is quite different due to its different molecular structure. The bombardment with a primary ion beam induces crosslinking reactions to the surface of the polymer, which cause an increase of the molecular weight and of the glass transition temperature of the polymer, along with a progressive amorphization followed by a loss of aromaticity.

Unlike PMMA, the formation of tertiary radicals (made even more stable by the presence of the phenyl group) does not involve the breaking of C-C bonds; such radicals pair up each other with the consequent crosslinking of the surface layer.[13-14]

The decay of the characteristic signals of the PS observed during the acquisition of the depth profile is, therefore, substantially attributed to the exponential increase of the molecular weight of the polymer, due to the coupling of the radical chain (Figure 56) that prevents the erosion of the

polymer since the early stages of irradiation. Moreover, by increasing the irradiation fluence, the formation of new C-C bonds and the progressive depletion of hydrogen from the polymer leads to the formation of an amorphous matrix that is enriched more and more by carbon-like material. Finally, in the case of the widely used fullerene ion beams, an accumulation of amorphous carbon occurs also because of the residues of C_{60}^{+} ions that, depending on the experimental conditions (mainly beam energy), are deposited on the surface.

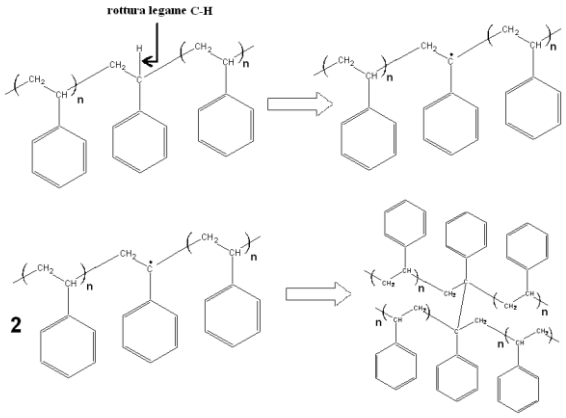

Figure 56. Schematic representation of cross-linking mechanism of PSS

This is the reason why, in the case of polystyrene, it is impossible to obtain molecular depth profiles even by using cluster beams such as SF_5^+ or C_{60}^+

An important innovation in the depth profiling of organic and in particular polymeric systems regards the recent introduction of large clusters primary ion beams consisting in atoms or small gaseous molecules (GCIB , Gas Cluster Ion Beams or Giant Cluster Ion Beams). The GCIB technique was introduced several years ago for non-destructive removal of organic material from inorganic surfaces at the University of Kyoto,[15] but only recently it has been successfully applied to depth profiling of organic layers. [16] The beams from sources GCIB consist of hundreds or thousands of atoms or molecules . Their preparation is done in two steps: the atoms (or small molecules) gas are condensed by cooling in neutral clusters in a supersonic expansion, and

subsequently ionized by electron impact and then accelerated. The CGIB were employed in molecular depth profiling of polymeric materials providing results more promising than those obtained with beams of smaller polyatomic ions, such as C_{60}. Upon impact with the surface, the cluster is fragmented into a considerably higher number of constituent atoms, each retaining a small fraction of the energy of the original ion. This energy is in the order of several eV and is close to the dissociation energies of the chemical bonds of the polymer investigated. This implies a strong limitation of the depth of the damage induced by ion bombardment and at the same time a strong increase in the sputtering yield, for reasons similar to those discussed in introducing polyatomic beams. The combination of these two aspects, namely a low penetration depth of the ions in the material and the consequent superficial location of the damage, combined with a high yield of sputtering, makes the eroded layer thickness comparable to that of the altered one. An interesting work in which molecular depth profiles are obtained with this kind of source was published in 2008 by Toyoda et al.[17] A sample of PMMA was bombarded with 5 keV Ar cluster ions with average size of 700, 1000 and 1350 atoms per cluster. It was observed that the yield of fragment ions of high mass (m / z = 800 for example) emitted from the film of PMMA is higher than the yield obtained in the bombardment with monatomic Ar ions, and increases with size of the projectile . The dependency of the secondary ion yield on the cluster size; can be also discussed from the point of view of the energy per each constituent atom, as a different kinetic energy of the atoms induces a different dissociative behavior of the polymer. These results suggest that the decomposition of the polymer under irradiation is suppressed by decreasing the kinetic energy of the atoms (eV/atom) of the ion cluster.

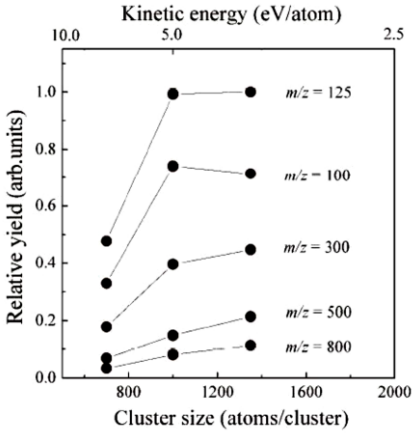

Figure 57. : Dependency of secondary ions yield from the size of the (m/z=100, 125, 300, 500 e 800) in the case of PMMA

In 2009 Moritani, Mochiji and others [18] have shown that it is possible to induce fragmentation at specific sites of a molecular species if bombarded with Ar gas cluster ions of appropriate size. This study was carried out on PS, a polymer non profilable with the widely used fullerene beams, using ions with energy per atom between 1 and 22 eV. The fragment ions emitted by PS under irradiation resulting from the breakup of the phenyl rings and the main alkyl chain can be classified into three groups according to the different relationship between the incident energy per atom (E_{atom}) and the dissociation energy of the site specific binding in the molecule. In fact, to sputter a fragments obtained by the break of the alkyl chain a threshold of about 3 eV/atom is necessary, while for those due to the break of the phenyl rings the threshold is approximately of 5 eV/atom. These results suggest that the break of chemical bonds of a specific surface can be controlled by adjusting E_{atom} of cluster ions by simple selection of their size.

Ninomiya et al [16] reported high quality molecular depth profiles obtained with GCIB on different polymers, including PS and PC, not profilable with polyatomic beams as the C_{60}^{+} or SF_5^{+} .

Rading et al [19] in 2012 compared the potentialities and limitations of C_{60} and GCIB Ar clusters in molecular depth profiling of polymeric materials. For this

purpose beams of different energy were employed, in a range between 2 and 10 eV/atom in the case of Ar_n, and between 167 and 667 eV/atom in the case of C_{60}. The polymeric samples used in this study are PS, PMMA and PC. In all cases an improvement of the stability and the intensity of the characteristic signals was observed during the entire depth profile. Furthermore, variations of the beam energy and the size of the cluster showed a linear relationship between sputtered volume and energy per atom. It was also observed that at a given energy per atom, the sputtered volume increases with the size of the cluster, while with a constant energy it decreases with the increasing of the cluster size.

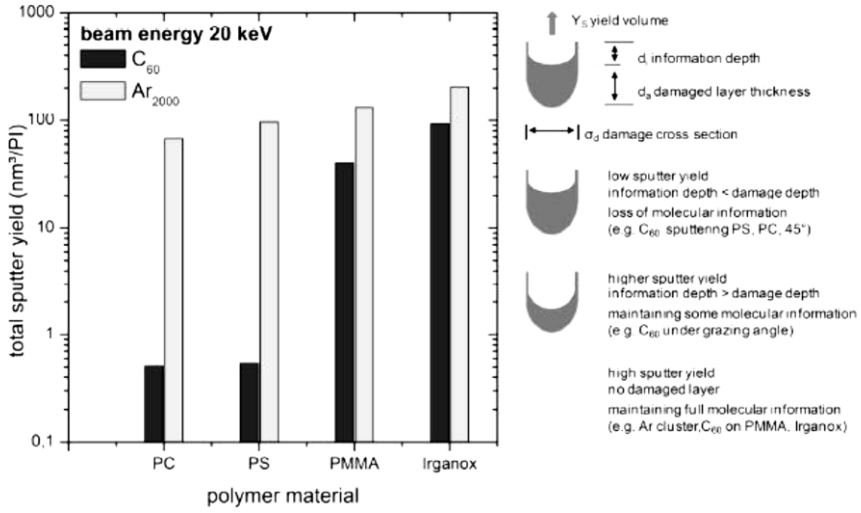

Figure 58. Total volume per primary ion for different polymeric materials (left) and schematic representation of corresponding sputtering process (right).

From these experiments it is possible to conclude that limitations of sputtering of polymers performed with C_{60} can be overcame through the use of clusters of Ar, which thus appear to constitute a more universal in depth profiling of organic systems.

It should however be noted that, under the experimental conditions in which the GCIB produce good depth profiles of molecular polymers, the yield of

sputtering of inorganic materials is practically negligible, and this is probably the most serious limitation to the universality of this type primary ion .
This is the reason why other kind of approach have to be developed. A possibility can be to intervene in the radical mechanisms, that have adverse effect in the sputtering of the material, by introducing a radical scavenger in the main chamber. The reaction between NO and the radicals formed by the interaction radiation/polymer was studied by Wilken et al; [20] in a completely different context, where they wanted to quantify, by XPS measurements, the surface radicals formed on plasma treated or UV irradiated PE and PP.

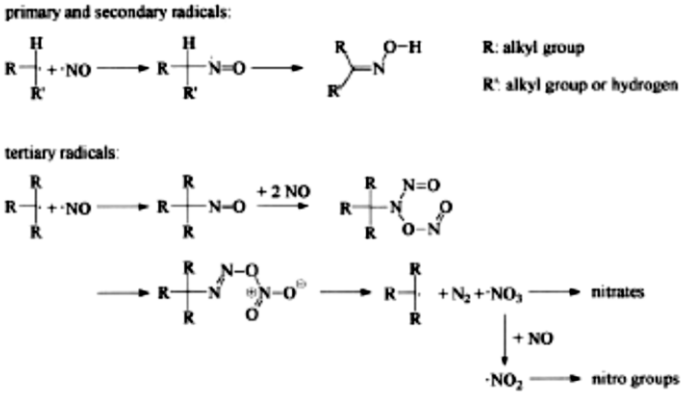

Figure 59. Reaction scheme of quenching of radical with NO [20]

According to the diagram shown above primary and secondary alkyl radicals react with NO becoming oximes, while tertiary alkyls give rise to nitrous groups, which can further react with nitric oxide giving nitrates and nitro groups. Recently, Licciardello and co-workers [21] proposed to perform molecular depth profiling of polymers such as polystyrene with C_{60} in the presence of NO. In fact, the NO would inhibit the recombination processes of free radicals that are responsible of the cross-linking, and it could hence favour the competitive processe giving rise to chain scission, thus allowing the obtaining of molecular depth profiles . In fact, they noted that the use of NO

during the bombardment with ions fullerene makes PS profilable, while it has not a significant effect on the depth profile of the PMMA, which, as a type II polymer, is already profilable with polyatomic beams without the intervention of the radical scavenger.

The ability to affect radical reactions induced by the ion beam during depth profiling of polymers has also been highlighted in other experimental conditions. Houssiau and co-workers observed that it is possible to obtain molecular depth profiles of polymers (PMMA, PS and PC) by using monoatomic Cs^+ ions at very low energy (250 eV).[22-23] In positive mode the emission of characteristic ions of the type MCs_n^+ is observed, where M indicates a fragment of the polymer useful for its recognition, while in negative mode analogous M^- ions are obtained. The intensity of these characteristic fragments persists well beyond the static limit, allowing the obtaining of molecular depth profiles. The factors that determine the success are the following:

i) the low energy of the primary ion (similar to the low energy of the fragments of polyatomic ions in cluster SIMS) determines the deposition of a high energy density near the surface,
ii) the charge exchange between the alkali metal and polymer fragments increases the probability of formation of negative ions M^- (or positive ions MCs^+) allowing the detection of the non-damaged polymer fraction;
iii) in the case of polystyrene a mechanism of inhibition of crosslinking by radical recombination occurs, since the radicals produced upon irradiation are blocked by the reaction with the implanted cesium atoms, with the formation of stable species R-Cs. This inhibition mechanism is very similar to that which is thought to operate when using nitric oxide.

1.1.1.1 Dual beam mode

In order to obtain depth profiles in SIMS instruments initially designed for static SIMS applications (such as the ToF-SIMS instrument used in this thesis work) the so-called dual-beam mode [24-26] is used. It consists in using,

alternatively, two different pulsed ion beams (as shown schematically in Figure 4), one with a high beam intensity (ion current of the order of some nA) suitable for efficient etching of the surface (the “sputter beam”), and the other (the “analysis beam”) with a negligible current (~ pA) compared to the previous one, optimized for the analysis of the bottom of the "crater" produced by the sputter beam.

Typically, the sputter beam is scanned over an area in the range between 100 x 100 μm^2 and 1000 x 1000 μm^2, while the analysis is carried out in much smaller area (concentric to the previous one) a much more restricted area (between 10% and 1% of the crater formed by the sputter beam) in order to avoid crater edge effects.

Figure 60 and Figure 61 report, respectively, a sketch of the dual beam mode and the timing scheme applied for the measurement.

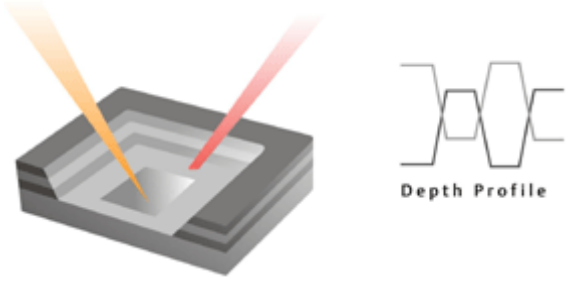

Figure 60. Scheme of the "dual beam" mode.

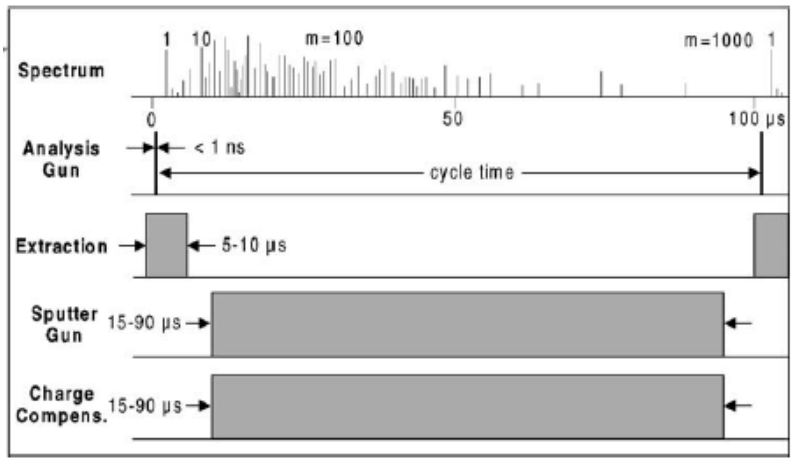

Figure 61. Scheme of timing generally used in "dual beam" mode.

3.2 Polyelectrolyte multilayers as model systems for molecular depth profiling.

Polimeric multilayers play an important role in a lot of technological applications, including molecular capsules, [27] immobilization of enzymes, [28] patterning of surfaces, [29] preparation of light-emitting diodes, [30] fotoelettrochemically active electrodes, [31] membranes, [32] microporous [33] and erodible [34] films. Among several method to obtain multilayers, a simple and versatile approach is the layer-by-layer (LbL) deposition, that was used for the first time by Iler [35] in 1966 in the case of colloidal particles, and that was extended in the case of polymers (polyelectrolytes in particular) by Decher [36] in 1990. This strategy has become one of the most used methods for surface functionalization [37] because it allows to obtain uniform films with a well-defined thickness.

Using the LbL technique, it is possible to grow polyelectrolyte multilayers (PEM), in a versatile and economic way, and to obtain well-defined interfaces,

with a definite structure, thanks to the alternating absorption of polyanions and polycations in aqueous solution. [38]
The formation of polyelectrolyte multilayers can be explained considering an overcompensation mechanism: if a surface is positively charges (for example) a negative polyelectrolyte can be easily adsorbed on it, making the surface negatively charged and allowing the subsequent absorption of a positive polyelectrolyte. [39]

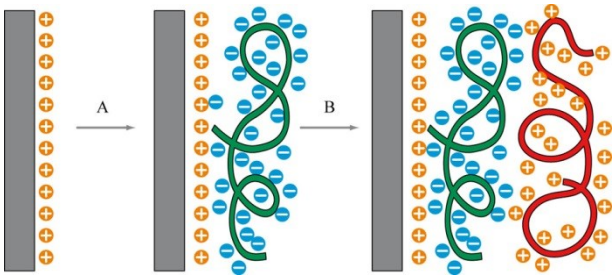

Figure 62. Schematic representation of the formation of a polyelctrolyte bilayer.

There are two different effects that allow the PEM growth: the first is due to the electrostatic forces with short-range (van der Waals forces, hydrophobic forces) that occur between polyelectrolytes having different charge, and the second is a favourable entropic contribution due to the release of counterions during absorption process both from the surface and from polyelectrolyte chains.
It is known that the conformation of chains plays an important role in multilayer growth, [40] and it is generally determined not only by intrinsic properties such us chain length [41], but also by other factor such us pH and ionic force of solution. [42-44]

3.2.1 Polyelectrolyte multilayers preparation

The first part of this section is aimed to study the effect of the nature of polymers and their thickness on the profilability of a polymeric multilayered sample. We used polyelectrolyte multilayes in order to obtain samples with a well defined composition and thickness.
With the aim to obtain a LbL deposition of polyelectrolyte, different strategies have been developed. The most common is the dipping technique: the substrate is (i) immersed into a polyelectrolyte solution for a certain time, rinsed with water and then (ii) dipped into the opposite-charged polyelectrolyte solution. The result is a bilayer of the two polyelectrolytes: in order to obtain a multilayer steps (i) and (ii) are repeated iteratively until the desired number of layersis reached.
Although dipping is a well know procedure, a drawback in using this approach is the long time requested for obtaining a thick multilayer. For this reason other strategies were developed and in particular the polyelectrolyte spin-assembly (PSA) approach is nowadays frequently used. It exploits the same principles of the spin coating technique, in which a substrate is covered with a solution and then rotated at high speed in order to spread the coating material by centrifugal force and evaporate the solvent.

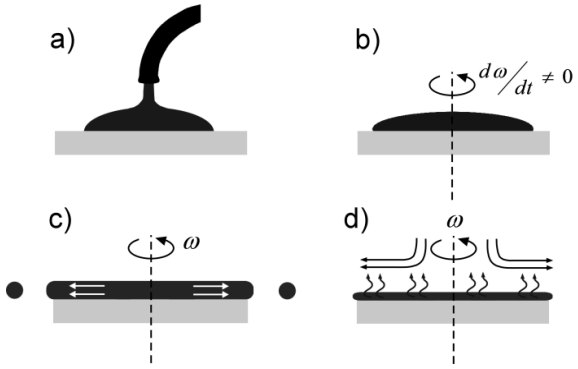

Figure 63. Spin coating mechanism.

In the case of polyelectrolites it is possible to apply this technique by alternatively spin casting a polyanion and a polycation, interposing rinsing

steps between each polymer deposition. It has been demonstrated that this method allows obtaining uniform films, [45] and a comparison between PSA and dipping showed that films obtained with PSA are thicker. [46] This difference is due to the different mechanism that occur in the two processes: in the case of dipping (that involves several minutes of immersion per single step) an equilibrium condition is reached, while in the case of PSA the time of the process is of the order of a few seconds, so polymer chains do not have time enough to stretch completely on the substrate: the adsorption is a non-equilibrium process and is due to the centrifugal force produced by the high rotation speed of the substrate that eliminates the water and makes the polymer chains to be weakly linked weakly to the substrate. Furthermore hydrodynamic stress due to centrifugal force, which distorts the polymer chains, combined with the electrostatic attraction between the polyelectrolyte and the opposite charged substrate, allow the irreversible formation of the bilayer.
To prepare polyelectrolyte multilayers three different polyelectrolytes were used, poly diallyldimethylammonium (PDDA), polyacrylic acid (PAA) and polystyrene sulfonate (PSS). In particular these polymers were chosen because of their different behaviour under ionic bombardment. In fact it is known that PAA and PDDA under cluster irradiation act as type II polymers (main chain scission) while PSS has the tendency to cross-link. Silicon and quartz substrates were treated in UV-O_3 for 15 minutes and then immersed in water. This procedure is used for two reason: it allows i) to clean surface from organic contamination and ii) to form hydroxyl groups that make the surface negatively charged, allowing the absorption of a first layer of polycation. The multilayers were obtained by means of the PSA technique, applying the following steps:

1. *Spin casting* of the polycation solution;
2. Two rinsing *steps* with water;
3. *Spin casting* of the polyanion solution;
4. Two rinsing *steps* with water;
5. Repetition of 1-4 until the wanted number of layers is reached.

Spin coating parameters are reported in Table 2.

RAMP	1	2	3
RPM (turn/min)	100	100	3000
TIME (s)	1	1	15

Table 2. Spin coating parameters

In order to monitor the growth of the multilayer it is possible to follow the UV-visible absorption of one of the two polyelectrolytes, and quartz as substrate. Among the chosen polymers, it is known that PSS has an absorption band centered at 225nm: Figure 64 reports the plot of the area of such band as a function of the number of bilayers in the case of the PSS/PDDA multilayer. A linear dependency is observed, indicating that the film growth is regular.

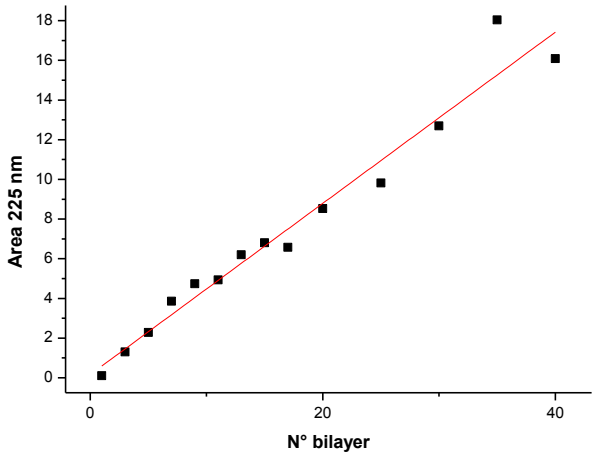

Figure 64. Plot of the area of the peak at 225 nm as a function of the number of bilayers.

In the case of the bilayer PAA/PDDA both polymer do no absorb in the UV-visible range, so we assumed that the growth is similar to the couple

PSS/PDDA. This assumption turned out to be realistic in view of the thickness measurements made by AFM and reported in the next paragraph.
Polyelectrolytes were combined in order to form multilayers with different sequences of the blocks PSS/PDDA and PAA/PDDA. In particular the following samples were prepared:

i. $Si/(PDDA/PAA)_{30}/(PDDA/PSS)_{\mathbf{5}}/(PDDA/PAA)_{30}$
ii. $Si/(PDDA/PAA)_{30}/(PDDA/PSS)_{\mathbf{15}}/(PDDA/PAA)_{30}$
iii. $Si/(PDDA/PAA)_{30}/(PDDA/PSS)_{\mathbf{30}}/(PDDA/PAA)_{30}$
iv. $Si/(PDDA/PSS)_{30}/(PDDA/PAA)_{\mathbf{30}}/(PDDA/PSS)_{30}$

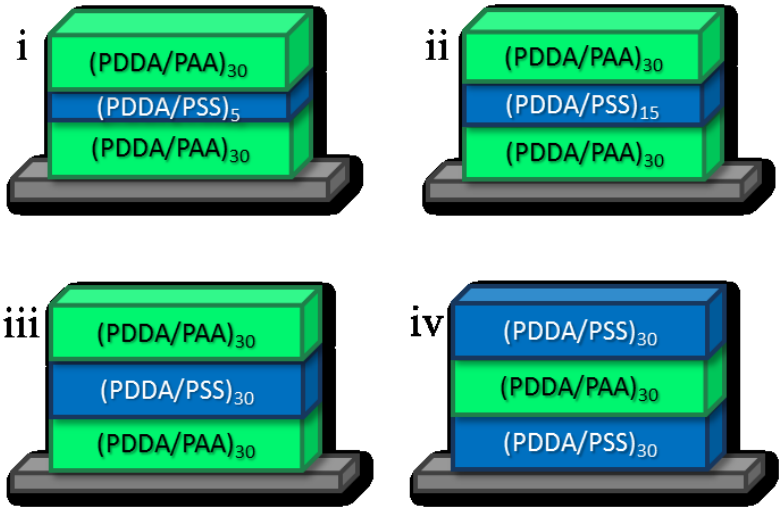

Figure 65. Schematic representation of the stucture of prepared multilayers.

The above samples were designed in order to have, in a constant PDDA polycation "matrix" blocks of desired thickness differing each other for the polyanion. In particular, in samples (i), (ii), and (iii) we changed the thickness of the central PSS-containing block which is sandwiched between PAA-containing blocks of constant thickness, while in sample (iv) a PAA_based block is deposited between two PSS-containing blocks.

3.2.1.1 Thickness measurements

Atomic Force Microscopy (AFM) was used for measuring the thickness of samples. The following strategy was adopted: [47] some incisions were done on the sample by means of a sharp blade, leading to the removal of the polymer layer and leaving unchanged the substrate (Figure 66 a). Then an AFM image over an area crossing the edge was obtained, and the thickness of the film was measured as the height of the step at the edge of the scratch. (Figure 66b).

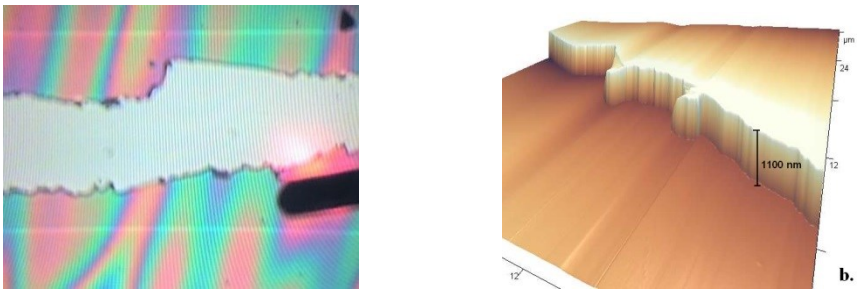

Figure 66. example of an incision on a polymeric sample: (a) optical image; (b) 3D AFM image.

One of the limitation of this technique is that the data are related to a specific area of the sample, and a single measure cannot take into account possible thickness inhomogeneities of the film. For this the reason we collected several measurements for each sample and averaged the results, that are reported in

Table 3.

Sample	Thickness
Si-$B_{30}A_{30}B_{30}$	~922 nm
Si-$B_{30}A_{15}B_{30}$	~799 nm
Si-$B_{30}A_{5}B_{30}$	~715 nm

Table 3. Average thickness obtained from AFM measurements

As expected the thickness increases with the increase of the number of layers of the PSS based block. Moreover, by a linear fit of the data it is possible to obtain a slope value (8.4 ±0.2 nm) that corresponds the the thickness of a single bilayer PSS/PDDA and to extrapolate an intercept value (672.9 ±3.9 nm) that is the thickness of 60 bilayers of PAA/PDDA, resulting in an average thickness of about 11.2 nm for a single bilayer.

3.2.2 SIMS Molecular depth profiling

SIMS depth profiles were acquired using a ToF−SIMS IV (ION−TOF GmbH, Münster, Germany). The instrument is equipped with a C_{60}^{n+} ion beam for sputtering and a liquid metal ion beam with a Bi_n^+ emitter for analysis. A pulsed 20 keV C_{60}^{2+} ion beam was raster scanned for sputtering of the samples over an area of 200 μm × 200 μm. In between sputtering pulses, a Bi_3^+ ion pulse (25 keV, 0.2 pA) was used for SIMS analysis in the central 130 μm × 130 μm of the sputter crater.

Sample *i* to *iii* were prepared in order to verify the effect of the thickness of the PSS-based block in "profilability" (Figure 67-10). We observe that in all cases it is always possible to profile the external PAA-based block, as evidenced by the presence of a plateau in the structure related signals, that drops down when the interface with the PSS-containing film is reached. The presence of the intermediate PSS-based layer is detected from the presence of characteristic sulfur-containing fragments, but a good profile through the layer is obtained only for the narrower one (50 nm-thick). The quality of the profile in such a layer degrades with its thickness, due to the accumulation of ion-beam-induced damage. It must be noted that this damage accumulation affects also the "profilability" of the underlying PAA-based block. Also the latter effect appears to depend on the thickness of the PSS-based film: in the case of 5 layers (about 50 nm) the damage accumulation is low and it makes possible to profile the entire sample with a good depth resolution for each block. In the case of 30 PSS layers (about 250 nm), on the contrary, it not possible to etch

the PSS-based block: it is worth to note that the effect does not consist just in the loss of the structure-related signals of PSS, but it is reflected also on the profilability of the underlying PAA-based layer, in such an extent that it is not possible to reach the interface in a reasonable time due to the drop of the sputtering yield caused by damage accumulation. The sample with 15 PSS-based layers (about 130 nm) shows an intermediate behaviour, in the sense that it is possible to obtain a profile down to the silicon substrate, but with a worse depth resolution than in the case of the sample i. All above is a clear indication that the accumulation of damage along the PSS-containig film increases with thickness and it is propagated (possibly via radical migration) into the underlying PAA-based layer which, in the same experimental conditions but in the absence of the PSS overlayer is instead easily profiled.

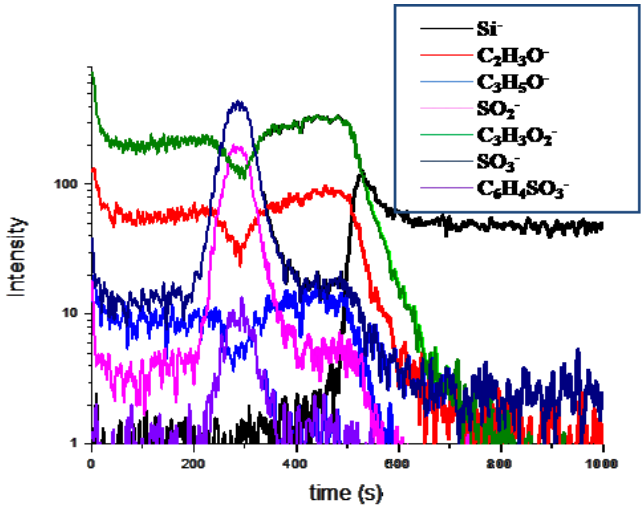

Figure 67. ToF SIMS depth profile of the silicon/ (PDDA/PAA)30 (PDDA/PSS)5 (PDDA/PAA)30 sample.

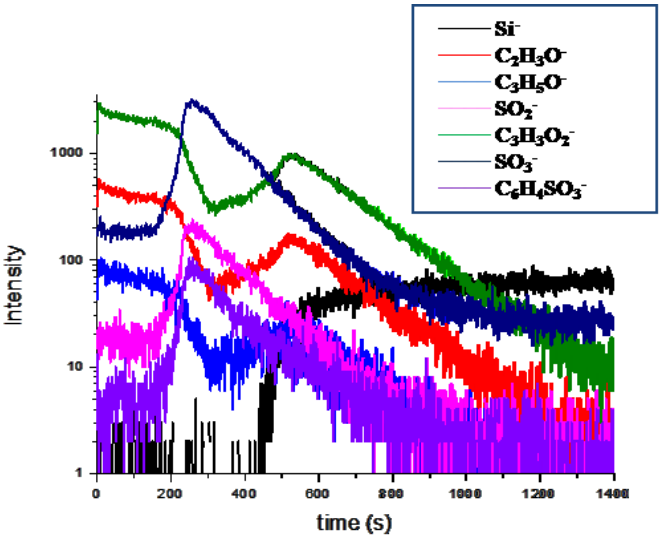

Figure 68. ToF SIMS depth profile of the silicon/ (PDDA/PAA)30 (PDDA/PSS)15 (PDDA/PAA)30 sample.

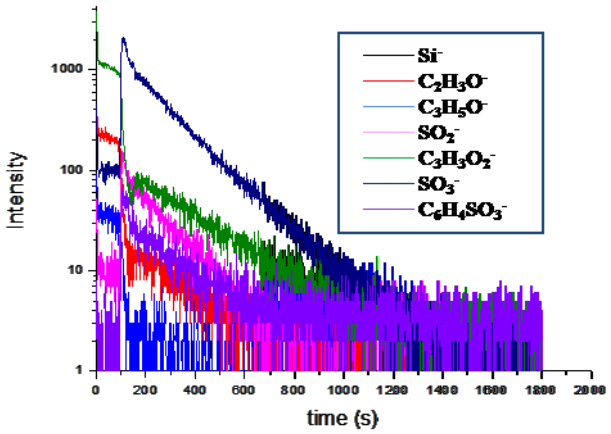

Figure 69. ToF SIMS depth profile of the silicon/ (PDDA/PAA)30 (PDDA/PSS)30 (PDDA/PAA)30 sample

As said before the different profiling behavior of PAA- and PSS-based layers is due to the different nature of the chosen polymers. In particular, due to the

interaction with the beam, radicals are formed in both system but they produce different effects into the two system, according with their reactivity that places them in the two different radiochemical classes proposed by Chapiro and cited above. In particular, in the case of PSS (and also in tha case of PAA suffering injection of damage from the PSS overlayer) it is the formation of highly crosslinked material that causes the lack of emission of structure-related fragments as well as a strong decrease of sputtering yield. This effect, not unexpectedly, is also evident in the case of sample *iv*, in which the presence of an upper PSS based film totally hinders the possibility of obtaining a reasonable depth profile.

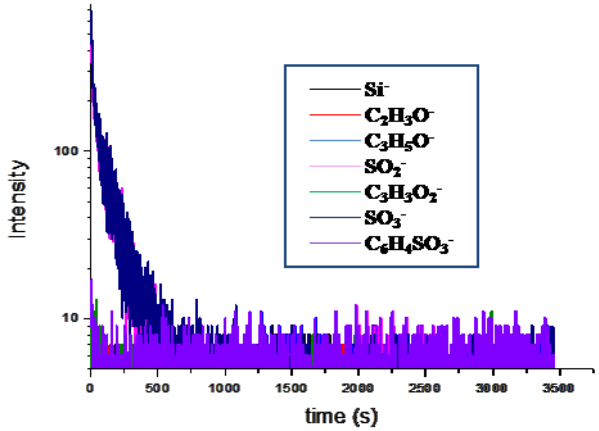

Figure 70. ToF SIMS depth profile of the silicon/ (PDDA/PSS)30 (PDDA/PAA)30 (PDDA/PSS)30 sample.

To overcome this limitation we decided to apply the approach based on the use nitric oxide, that, as mentioned before, acting as a radical scavenger, should be able to can quench the cross-linking reactions, thus allowing to obtain molecular depth profiles from polymers such as PS and PSS. In our experiments NO was feed in the analysis chamber of the SIMS instrument in the proximity of the sample surface and the pressure was adjusted to a value of 1.5 $x10^{-5}$ mbar. This pressure value can be regarded as the partial pressure of

NO, considering that the base pressure in the analysis chamber is in the range 10^{-8}-10^{-9} mbar.

An effect of the NO-dosing is observed in all the samples. From the depth profile (Figure 71) of sample *i* (the one obtained with good quality also without NO-dosing) it is possible to observe that, upon introduction of the NO, i) the overall shape of the profile remains unchanged, ii) intensity of structure-related signals is increased by about one order of magnitude and iii) sputtering rate is increased by a factor ~2.5 as demonstrated by the corresponding decrease of the time needed for reaching the interface with substrate.

In the case of sample sample *ii*, the one in which the damage accumulation degraded the resolution of the profile especially on the trailing edge of the PSS-based layer (see Figure 68), the introduction of NO induces a well visible improvement in the quality of the profile (Figure 72). In particular, a striking improvement of depth resolution is observed, as witnessed by the presence of a flat-top shape in the profile of the intermediate PSS-based block.

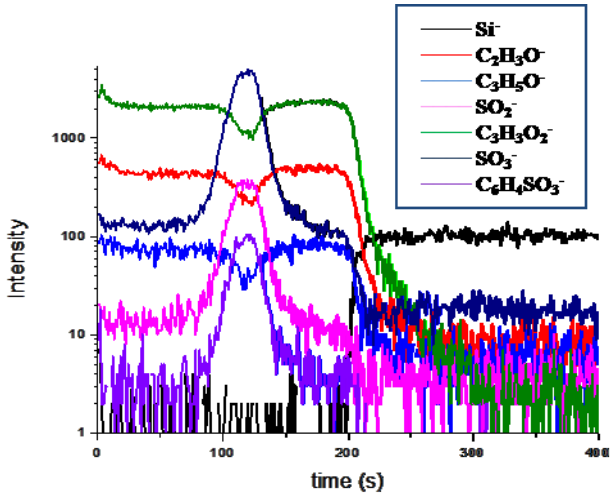

Figure 71. ToF SIMS depth profile of the silicon/ (PDDA/PAA)30 (PDDA/PSS)5 (PDDA/PAA)30 sample in precence of NO.

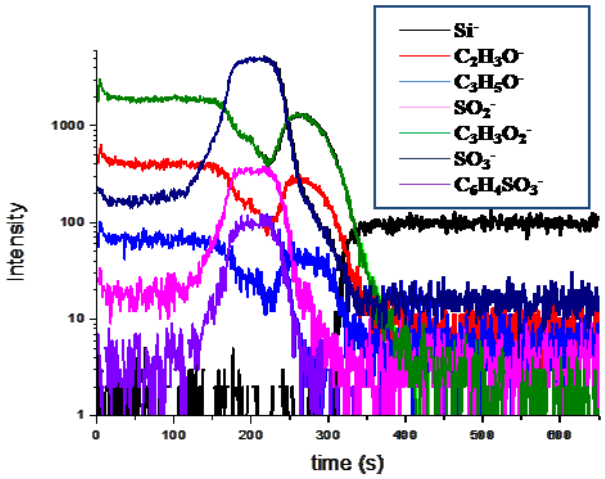

Figure 72. ToF SIMS depth profile of the silicon/ (PDDA/PAA)30 (PDDA/PSS)15 (PDDA/PAA)30 sample in presence of NO.

Nevertheless, the most surprising results concern samples *iii* e *iv*. As shown in Figure 69 and Figure 70, without NO-dosing it is not possible to reach the interface in a reasonable time and to distinguish the second layer (PSS-based) from the third one (PAA layer). By contrast, the introduction of NO allows to obtain in both cases good molecular depth profiles and to discriminate, on the basis of the intensity of structure-related fragments, among all the layers, with satisfactory depth resolution and sputter yield (Figure 73 and Figure 74).

The above findings confirm the ability of nitric oxide to inhibit radical reactions leading to cross-linking and damage accumulation during C_{60} SIMS depth profiling of polymers and prompt NO-dosing method as a valuable one for the SIMS characterization of polymer multilayers whith C_{60} primary beams. Although similar and even better results have been recently obtained by means of large polyatomic argon clusters (GCIB), NO-dosing has the advantage of allowing to continue to use the widespread C60 sources and, moreover, it is probably useful when profiling hybrid organic/inorganic multilayers. Indeed GCIBs are not able to profile inorganic materials at the low energies per constituent atom that are suitable for organic depth profiling,

while a fullerene beam with the aid of NO-dosing should be suitable for this purpose.

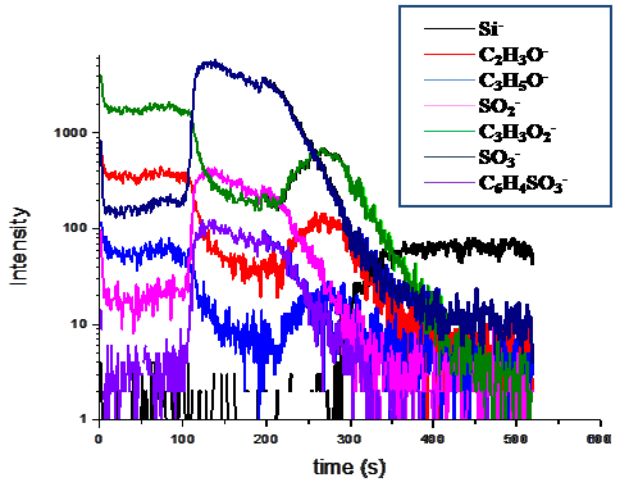

Figure 73. ToF SIMS depth profile of the silicon/ (PDDA/PAA)30 (PDDA/PSS)30 (PDDA/PAA)30 sample in presence of NO.

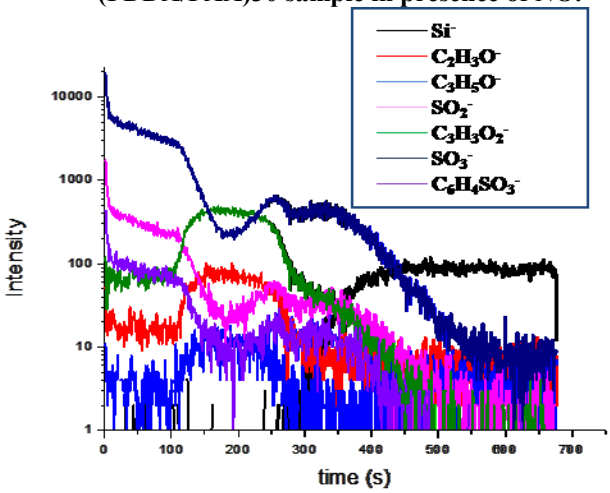

Figure 74. ToF SIMS depth profile of the silicon/ (PDDA/PSS)30 (PDDA/PAA)30 (PDDA/PSS)30 sample in presence of NO.

3.3 Molecular depth profiling of oligothiophenes

As organic semiconductors, conjugated polymers have been considered attractive, and, among them oligomers appeared of particular interest, as the electronic properties of these molecular materials can be easily tailored by subtle chemical modifications performed on the oligomer molecules. In particular it was shown, already in 1990, that using oligothiophenes it is possible to observe a significant increase, by two orders of magnitude, of the field-effect mobility. [48-49]

Oligo and polythiophenes are conjugated organic semiconductors obtained from polymerization of thiophene. These materials show a good electrical conductivity that is due to the delocalization of electrons along the polymer backbone, usually through overlap of π-orbitals, resultingin in an extended π-system with a filled valence band. By removing electrons from the π-system ("p-doping"), or adding electrons into the π-system ("n-doping"), it is possible to form a charged unit called a bipolaron, which makes possible the conduction.

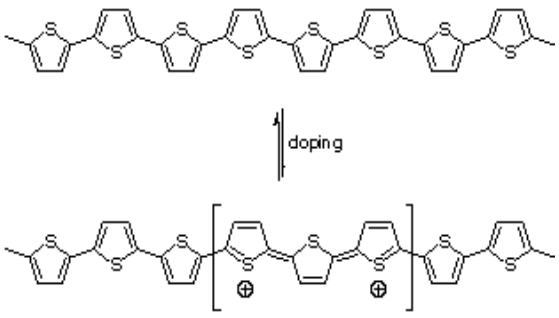

Figure 75. Example of p doping of a polythiophene.

During this thesis, blends containing oligothiophenes in different percentage were studied. In particular, the aim of the study, conducted in the framework of a collaboration with a group interested in correlating the effect of the composition of the blends with their electrical behavior, was that of studying

the compositional homogeneity of such blends along the depth of the film and of identifying eventual compositional gradients and/or segregation phenomena. Here we report some preliminary results, that however are sufficient for showing the applicability of cluster-SIMS in molecular depth profiling to this kind of materials, relevant for organic electronics. The used oligomers are the 5,5‴-Dihexyl-2,2′:5′,2″:5″,2‴-bithiophene(DH2T), 5,5‴-Dihexyl-2,2′:5′,2″:5″,2‴-quaterthiophene (DH4T) and the 5,5‴-Dihexyl-2,2′:5′,2″:5″,2‴-sexithiophene (DH6T) (Figure 76).

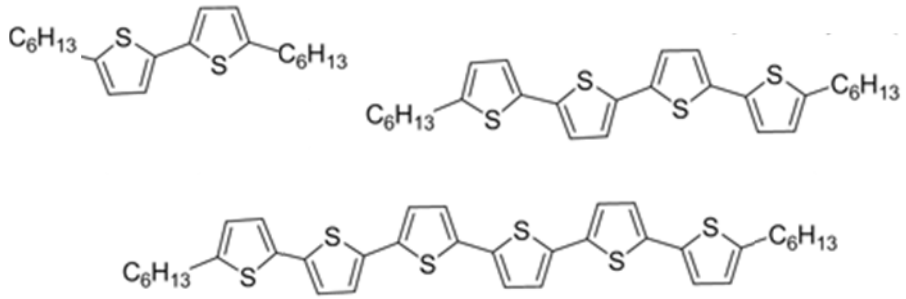

Figure 76. Molecular structure of (a) DH2T, (b) DH4T and (c) DH6T.

In particular we focused our attention on films made out of binary blends containing a large majority of one of the components (98%) and a minority concentration of a second oligomer (2%). The films were cast on silicon substrates from solutions containing the desired molar ratio of the two oligomers.

The first example of C_{60} depth profile, shown in Figure 77, pertains to a DH4T film additivated with 2% D2HT. The traces reported in the profile pertain to the molecular ions of the two oligomers.

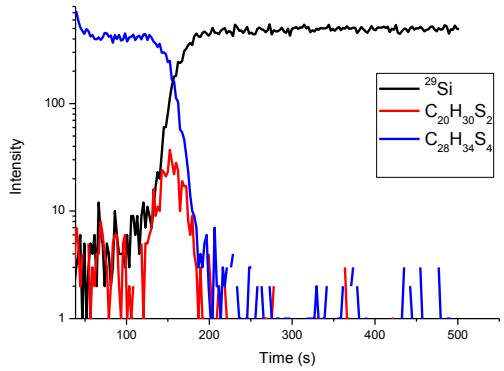

Figure 77. ToF-SIMS molecular depth profile of a blend DH4T/DH2T 98/2 %

A clear indication of segregation of the lower molecular weight component at the interface with substrate is given by this profile.

Analogous results were found in the case of a D6HT film with a minority content of D4HT (Figure 78). Also in this case it appears, although less clearly than in the previous one, that the system displays compositional inhomogeneity along the depth, with a higher concentration of the low molecular weight component towards the interface with the substrate.

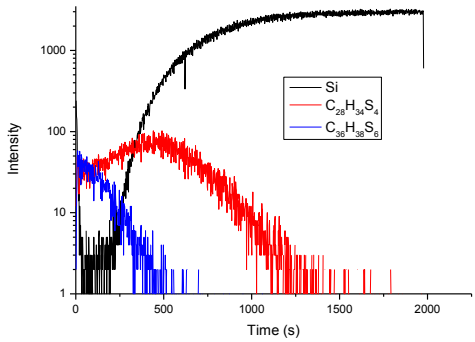

Figure 78. ToF-SIMS molecular depth profile of a blend DH6T/DH4T 98/2 %

Although quite preliminary, the above results clearly show that cluster SIMS is able to detect in-depth compositional inhomogeneities in blends constituted by very similar components. It is worth to stress that such an information would be virtually impossible to achieve without the use of or cluster-SIMS. Indeed the elemental composition of the two oligomers is very similar and they can be clearly discriminated only by using a technique that is able to provide molecular information.

3.4 Conclusions

In this section the general problem of obtaining molecular depth profiling of organic materials has been outlined, and the depth profiling results obtained on some selected polymer system with in-depth compositional heterogeneity were presented. This research is currently of great interest, from the point of view of applications as well as for the fundamental implications related to the understanding of the phenomenology involved in the interaction between polymers and cluster ions, that are strongly influencing the practical capability of sputtering-based techniques, such as SIMS, in achieving molecular depth profiles from organic and polymer systems. In particular, we prepared polyelectrolyte-based multilayers *via* a layer by layer (LBL) technique, in order to modulate both their thickness and the composition. C_{60} SIMS depth

profiling of these systems highlighted the fact that the possibility of obtaining a good profile depends heavily on the order in which layers with different radiochemical behaviour are deposited. In particular, it turned out that the presence of a layer that tends to accumulate ion-beam damage has a detrimental effect also on the profilability of underlying layers, even if such layers, *per se*, are amenable of molecular depth profiling. Moreover, it was showed that it is possible to overcome this problem by introducing a radical scavenger, such as NO, into the analysis chamber during SIMS depth profiling with fullerene ions. NO-dosing has the effect of strongly reducing ion-beam induced damage, thus improving the molecular depth profiling capabilities of the technique by making amenable of molecular depth profiling systems that otherwise could not be profiled, and by improving the profiles in terms of depth resolution, signal intensity and sputtering rate.
Finally, as an application of the cluster SIMS in molecular depth profiling of materials of interest in molecular electronics, it was shown that C_{60}-SIMS can provide molecular information in oligothiophene-based thin films, being able to detect in-depth inhomogeneous distributions of oligomers of different molecular weight.

3.5 References

[1] Mahoney, C. M., *Mass Spectrom. Rev*., **2010**, *29*, 247-293

[2]Nicholas Winograd, *Surf. Interface Anal.* **2012**, *45*, 3-8

[3] http://galilei.chem.psu.edu/sputtering-animations.html

[4] Gillen, G., Roberson ,S., *Rapid Commun. Mass Spectrom*., **1998**, *12*, 1303–1312

[5] Delcorte, A., Garrison, B. J., *J. Phys. Chem B*., **2000**, *104,* 6785–6800.

[6] Delcorte, A., *Nucl. Instr. Meth. Phys. Res B.*, **2005**, *236,* 1–10

[7] Delcorte A., Poleunis, C., Bertrand, P., *Appl. Surf. Sci*., **2006**, *252*, 6542–6546 .

[8] Delcorte, A., Garrison, B. J., *Nucl. Instr. Meth. Phys. Res B.*, **2007**, *255,* 223–228 .

[9] Delcorte, A., Yunis, S., Wehbe, N., Nieuwjaer, N., Poleunis, C., Felten, A., Houssiau, L., Pireaux ,J.J., Bertrand, P., *Anal. Chem*., **2007**, *79*, 3673–3689.

[10] Czerwinski B., Samson R.,Garrison B. J., Winograd N., Postawa Z., *Vacuum*, **2006,** *81***,** 167-173.

[11] R. Moellers, N. Tuccitto, V. Torrisi, E. Niehuis, A. Licciardello, Appl. Surf. Sci., 252 **2006** 6509 –6512

[12] Chapiro A., *Radiation chemistry of polymeric systems,* New York & London: John Wiley & Sons, **1962**, 712

[13] Zekonyte, J., Erichsen, J., Zaporojtchenko, V., Faupel, F., *Surf. Sci.* , **2003**, *532-535*, 1040-1044.

[14] Calcagno, L., Compagnini, G., Foti, G. *Phys Rev B,* **1992** , *46,* 10573-10578.

[15] I. Yamada, J. Matsuo, N.Toyoda, A. Kirkpatrick, Materials Science & Engineering, **2001**, R34, 231-295

[16] Ninomiya, S., Ichiki, K., Yamada, H., Nakata, Y., Seki, T., Aoki, T., Matsuo, J., *Rapid Commun. Mass Spectrom*., **2009**, *23*, 1601-1606.

[17] Hashinokuchi, M., Moritani, K., Nakagawa, J., Kashiwagi, T., Toyoda, N., *Journal of surface analysis*, **2008**, 14, 387-390

[18] Moritani, K., Mukai, G., Hashinokuchi, M., Mochiji, K., *Applied Physics Express 2,* **2009**, 046001

[19] Rading, D., Moellers, R., Cramer, H. G., Niehuis, E., *Surface and Interface Analysis*, **2012,** *45*, 171-174.

[20] Wilken, R., Holländer, A., Behnisch, J., *Surface and Coatings Technology*, **1999**, *116-119*, 991-995

[21] Havelund R., Licciardello, A., Bailey, b J., Tuccitto, N., Sapuppo, D., Gilmore, I. S., Sharp, J. S., Lee, J. L. S., Mouhib, T. and Delcorte, A. *Anal. Chem***. 2013**, *85*, 5064−5070

[22] Mine N., Douhard B., Houssiau L., *Applied Surface Science*, **2008**, *255*, 973–976

[23] Houssiau L., Mine N., *Surf. Interface Anal*., **2010**, *42*, 1402-1408

[24] Iltgen, K., Bendel, C., Benninghoven, A., Niehuis, E., *Proceeding of the SIMS X*, *Wiley*, **1996**, 375.

[25] Iltgen K., Bendel C., Benninghoven, A., Niehuis, E., *Journal of Vacuum Science and Technology B*, **1997**, *15*, 460-469.

[26]Niehuis, E., Grehl, T., *ToF SIMS- Surf. Anal. by Mass Spectrometry*, *IM Publications*, **2001**, 753.

[27] Lvov, Y.; Antipov, A. A.; Mamedov, A.; Möhwald, H.; Sukhorukov, G. B. *Nano Lett.* **2001**, *3*, 125−128

[28] Y. Lvov, Ed: Y. Lvov and H. Möhwald, In book: *Protein Architecture: Interfacial Molecular Assembly and Immobilization Biotechnology*, **2000**, M. Dekker Publ., NY, p. 125-167.

[29] Shi, F. Wang, Z. Q. Zhao, N. Zhang, X. *Langmuir* **2005**, *21*, 1599−1602

[30] Rogach, A. L. Koktysh, D. S. Harrison, M. Kotov, N. A. *Chem. Mater.* **2000**, 12, 1526−1528

[31] Xu, J. P. Weizmann, Y. Kriekhely, N. Baron, R. Willner, I. *Small* **2006**, *2*, 1178− 1182

[32] Harris, J. J., DeRose, P. M., Bruening, M. L. *J. Am. Chem. Soc.* **1999**, *121*, 1978−1979

[33] Roy, X., Sarazin, P., Favis, B. D. *Adv. Mater.* **2006**, *18*, 1015−1019

[34] Vázquez, E. Dewitt, D. M. Hammond, P. T. Lynn, D. M. *J. Am. Chem. Soc.* **2002**, *124*, 13992−13993

[35] Iler, R. K. J. *Colloid Interface Sci.* **1966**, *21*, 569−594

[36] Decher, G. Fuzzy *Science.* **1997**, *277*, 1232−1237

[37] Hammond, P. T. *AIChE J.* **2011**, *57*, 2928− 2940

[38] Hammond, P. T. *Adv. Mater.* **2004**, *16*, 1271−1293

[39] Patel, P. A., Jeon, J., Mather, P. T., Dobrynin, A. V. *Langmuir* **2006**, *22*, 9994−10002

[40] Schoeler, B., Kumaraswamy, G., Caruso, F. *Macromolecules* **2002**, 35, 889−897

[41] Dobrynin, A. V., Rubinstein, M. Prog. *Polym. Sci.* **2005**, *30*, 1049−1118

[42] Liu, G. M., Zou, S. R., Fu, L., Zhang, G. Z. *J. Phys. Chem. B* **2008**, *112*, 4167−4171

[43] Liu, G., M. Hou, Y., Xiao, X., Zhang, G. Z. J. *Phys. Chem. B* **2010**, *114*, 9987−9993

[44] Decher, G. Schmitt, J. Prog. *Colloid Polym. Sci.* **1992**, *89*, 160-164.

[45] Lee, S.S., Hong, J.D., Kim, C. H., Kim, K., Koo, J. P., Lee, K.B. *Macromolecules*, **2001**, *34*, 5358-5360.

[46] Cho, J., Char, K., Hong, J.D. *Adv Mater* , **2001**, *13*, 1076-1078

[47] Lobo, R.F.M., Pereira da Silva, M.A., Raposo, M., Faria, R.M., Oliveira Jr O.N. *Nanotechnology,* **1999***, 10,* 389-393 .

[48] Horowitz, G., Peng, **X.Z.,** D. Fichou , D. and Gamier, F., *J. Appl. Phys.* **1990,** *67*, 528-532.

[49] Gamier, F., Horowitz, G., Peng, X.Z. and Fichou, D., *Adv. Mater***., 1990**, *2*, 592-594

4 Conclusions

This thesis was focused on the preparation and on the characterization, of functional thin films for molecular electronics and energetics.
In the first part of this work a nanoscale electrical investigation of molecular wires was discussed. Molecular wires were prepared as a self assembled array on gold by means of a bottom up approach that exploits the coordination of metal with terpyridine-based ligands. These molecular wires were characterized by using different techniques. The formation and growth of the molecular films has been demonstrated by ToF-SIMS, XPS and UV-Vis spectroscopy. Structural information was obtained from NEXAFS measurements, that demonstrated that wires grow vertically to the surface and that the orientation doesn't change during the growth. The electrical characterization was performed by using the conductive atomic force microscopy (C-AFM) technique, that allowed to determine the molecular conduction mechanisms of these systems. It has been shown that wires are chatacterized by β decay values as low as the ones measured by using macroscopic Hg-drop junctions, providing unambiguous evidence for the existence of a hopping charge transport mechanism. In the case of short wires, less that 3.5 nm long, the electrical data indicate an ohmic conduction mechanism. On the contrary longer wires (4 nm or longer) exhibit, at certain voltages, a transition in the charge transport mechanism, to a regime in which the current is roughly following a quadratic dependence on the bias, indicative of a space charge limited current (SCLC) regime.
The theoretical calculations performed on different models of the wire rule out the existence of resonant tunnelling mechanisms while fully support a charge transport mechanism dominated by charge hopping.
The second part of the work was focused on the development of methodologies for functionalization of oxide substrates, suitable for applications in the field of dye sensitized solar cells. The "ZP" methodology has been applied, and the amount of surface coverage as well as the stability of the formed layers has been studied by using a phosphonate derivative of rhodamine B. Then the ZP

method was applied to the preparation of different systems of interest in solar energy conversion, including a self assembled bilayer on TiO_2 made out a dendrimeric complex of Ru (II) (the sensitizer) and a polyoxometallate (the catalyst) that can act as an electrode for photo -induced water splitting.
Finally, the general problem of obtaining molecular depth profiling of organic materials has been discussed. In particular, a SIMS method (NO-assisted cluster-SIMS) has been studied, that gives promising results in this direction. With the aim of studying the applicability of the method to polymer-based multilayers, well-controlled layered systems have been prepared by means of layer-by-layer polyelectrolyte deposition. C_{60}-SIMS depth profiling of these systems highlighted the possibility of obtaining a good profile depends heavily on the order in which layers with different radiochemical behavior are deposited. In particular, it turned out that the presence of a layer that tends to accumulate ion-beam damage has a detrimental effect also on the profilability of underlying layers, even if such layers, *per se*, are amenable of molecular depth profiling. This problem can be overcome by introducing a radical scavenger (nitric oxide) into the analysis chamber during SIMS depth profiling with fullerene ions. Finally, the cluster-SIMS technique was applied to the study of a system of interest in molecular electronics. In particular the measured C_{60}-SIMS profiles provided evidence of in-depth inhomogeneous distribution of oligothiophenes in binary blends formed by oligomers with different molecular weight.

5 Appendix: materials and methods

Benzenethiol (≥ 99%, MB), iron(II) sulfate heptahydrate (≥ 99%, $FeSO_4 \bullet 7H_2O$), and 4',4''''-(1,4-Phenylene)bis(2,2':6',2''-terpyridine) (TPT), chloroform ($CHCl_3$) and ethanol (EtOH) were purchased by Sigma Aldrich and used without further purification. 4-[2,2':6',2''-terpyridin]-4'-yl-benzenethiol (MPTP) was synthesized as previously reported. Ultrapure milliQ water with resistivity of 18 MΩ·cm was used when required.

Polymer solutions of polystyrene sulfonate (PSS, Mw = 70000, Aldrich), poly acrylic acid (PAA, Mw= 1000000, Aldrich), and Polydiallyldimethylammonium chloride (PDDA, MWav = 200000-350000, 20wt% in water, Aldrich) were prepared in Millipore water 1mg/mL.

Synthesis of Rodamine B- phosphonate derivative.

The synthesis of rhodamine B phosphonate derivative was performd by prof. Amato. It was synthesized starting from RhB (1) and diethyl-3-bromopropil-phosphonate (2). These species, in presence of a non-nucleophilic base, such as N, N-diisopropyl-ethyl-amine (DIPEA), and of a polar aprotic solvent, such as dimethyl-formamide (DMF), react via an esterification reaction, known such as O-alkylation of the carboxylate [66-69], to form the RodaminaB-propyl-(diethyl) phosphonate, RhB-phosphonate-protected (3). It is necessary to start from bromo-propyl-phosphonic in which hydroxyl groups of phosphonic are protected (in the form of ethyl phospho-esteri), in order to avoid autocondensation reactions of the 3bromopropil-phosphonic acid. From the deprotection of the compound-RhB-protected phosphonate (3) through the hydrolysis reaction of the phosphodiesteric bond with bromo-trimethyl-silane (TMBS), the derivative RhB-phosphonate (4) was obtained. The entire synthetic scheme is shown in Figure 79

1H-NMR spectra and the mass spectrum of ToF-SIMS showed that the yield of the product 4 was not quantitative, and it was mixed with the protected derivative 3. It was not, however, considered necessary to employ any chromatographic technique for the purification of the product (4), as has been previously observed, that only the derivative with the deprotected phosphonic group is capable of anchoring at the surface of TiO2.

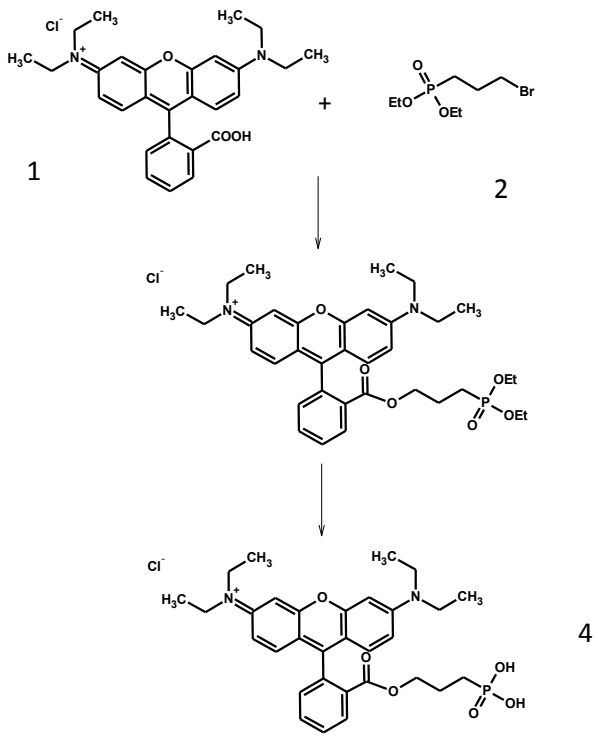

Figure 79. Scheme of the syntesis of RhB-fosfonato.

Samples preparation

Gold was thermally evaporated (100 nm) on silicon oxide employing 5 nm of Cr adhesion layer for NEXAFS and XPS analysis.
Semitransparent ultrathin gold substrates for UV-Vis characterization were prepared by thermal evaporation of 10 nm of gold on Fused Silica Plates (UQG Optics Ltd, Cambridge). C-AFM measurements were performed on ultraflat gold substrates on mica prepared by thermal evaporation of 100 nm Au at 0.01 nm/s and 450°C.

The gold substrates were cleaned by 15 min UV-Ozone treatment immediately prior to the incubation in a 0.5 mM mixed solution of MB and MPTP in EtOH in a 1:1 ratio. After 24 hours incubation the MB/MPTP samples were washed with EtOH and dried in a stream of nitrogen.
To fabricate the layers, MB/MPTP samples were immersed for 90 sec in a saturated solution of the Fe(II) salt in water/ethanol (1:1) and rinsed with water, ethanol and chloroform (i), then immersed for 15 min in a 0.5 mM solution of TPT in chloroform and rinsed with warm chloroform, ethanol and water (ii). Stages (i) and (ii) were repeated iteratively, until the desired length was reached.

TiO_2 flat samples were prepared on FTO on glass substrates. They were cleaned using $CHCl_3$, ethanol and Millipore water. TiO2 was deposited on substrates using titanium tetrachloride ($TiCl_4$, purity >99.9% Aldrich) as a precursor. It was slowly added to pre-cooled millipore water in an ice bath. Then substrates were dipped into 40 mM $TiCl_4$ aqueous solution at 70 °C, and washed with deionized water to remove the remaining neutral washing solution.Titanium tetrachloride. Substrates were finally post-annealed at 450 °C for 30 min and cooled down.
Nanoporous TiO2 films were prepared on FTO substrates by a doctor blade method. The electrodes were post-annealed at 450 °C for 30 min.
TiO_2 nanopowder (21 nm particle size) was purchased by Sigma Aldrich and dispersed in reactants for each step under stirring using the same procedures of planar samples. Centrifugation was carried out using 5000 rpm for 10 minutes for each step of reaction and of rinsing.
Self-assembled monolayers were formed immersing samples in a 5x10-4 M solution for 24 hours, then samples were washed with solvent and dried in a stream of nitrogen.

Measurements parameters

C-AFM measurements were performed on ultraflat gold substrates on mica prepared by thermal evaporation of 100 nm Au at 0.01 nm/s and 450°C.
UV-Vis measurements were performed on a Jasco V-650 UV-VIS spectrophotometer in transmission mode.

ToF-SIMS spectra were acquired in a TOFSIMS IV (IONTOF GmbH) using a 25 keV Bi^+ primary beam rastered over a 200μm×200μm and the primary ion fluence was kept $<10^{12}$ ions/cm^{-2} in order to assure static-SIMS conditions. SIMS depth profiles were acquired using a ToF−SIMS IV

(ION−TOF GmbH, Münster, Germany). The instrument is equipped with a C_{60}^{n+} ion beam for sputtering and a liquid metal ion beam with a Bi_n^+ emitter for analysis. A pulsed 20 keV C_{60}^{2+} ion beam was raster scanned for sputtering of the samples over an area of 200 μm × 200 μm. In between sputtering pulses, a Bi_3^+ ion pulse (25 keV, 0.2 pA) was used for SIMS analysis in the central 130 μm × 130 μm of the sputter crater.

XPS and NEXAFS measurements were carried out at the HE-SGM beamline (bending magnet) of the synchrotron storage ring BESSY II in Berlin, Germany, using a custom designed experimental station. All experiments were performed at room temperature and UHV conditions at a base pressure lower than $1x10^{-9}$ mbar. The spectrum acquisition time was selected in such a way that no noticeable damage by the primary X-rays occurred during the experiments. The XP spectra were measured using a Scienta R3000 spectrometer. The X-ray energy was set to either 350 or 580 eV. The spectrum acquisition was carried out in normal emission geometry with an energy resolution of ~0.3-0.4 eV, depending on the photon energy. The energy scale of the XP spectra was referenced to the Au 4f7/2 peak at a binding energy (BE) of 84.0 eV.

AFM and C-AFM measurements were carried out in air in a Dimension 3100 microscope with a NanoScope IV controller (Digital Instrument). Commercial silicon cantilevers with a nominal spring constant of 40 N/m were used for morphological characterization in tapping mode while Pt/Ir coated silicon probes with a nominal spring constant of 0.2 N/m were used to perform the current-voltage measurement in contact mode by applying a constant load force of 5 nN. For each sample about 100 current-voltage characteristics in the range -1 to 1V were measured on different points of the surface.